INTERNATIONAL JOURNAL OF AVIATION SCIENCE AND TECHNOLOGY

IJAST

International Journal of Aviation Science and Technology

Volume 5, Issue 1, June 2024

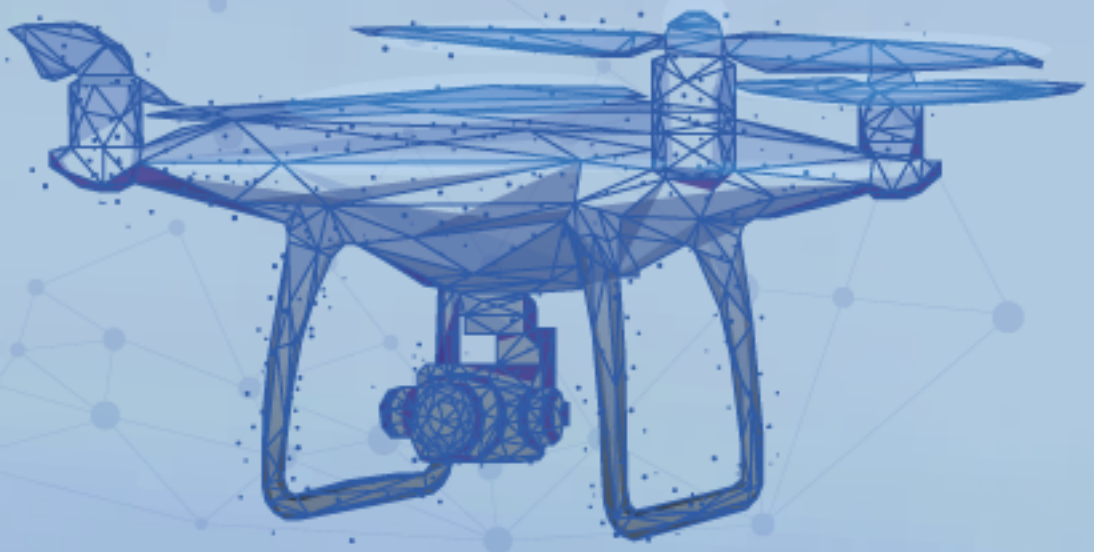

e-ISSN: 2687-525X

SARES

www.sares.org

International Journal of Aviation Science and Technology

Owner

International Sustainable Aviation and Energy Society (SARES)

Privilege Owner

T. Hikmet Karakoç
Eskisehir Technical University, Turkiye
hkarakoc@eskisehir.edu.tr

Honorary Editor in Chief

Max F. Platzer
University of California, USA
maximilian.platzer@gmail.com

Editor in Chief

T. Hikmet Karakoç
Eskisehir Technical University, Turkiye
hkarakoc@eskisehir.edu.tr

Co-Editor

Alper Dalkıran
Suleyman Demirel University, Turkiye
alperdalkiran@sdu.edu.tr

Section – Editors

Pouria Ahmedi
University of Illinois, USA pouryaahmadi81@gmail.com

Patti J. Clark
Embry-Riddle Ae. University. USA clark092@erau.edu

Raj Das
RMIT University, Australia raj.das@rmit.edu.au

Chingiz Hajiyev
Istanbul Technical University, Turkiye cingiz@itu.edu.tr

Soledad Le Clainche
Universidad Politécnica de Mad., Spain soledad.leclainche@upm.es

Ionna Pagoni
University of Aegean, Greece ipagoni@aegean.gr

Publisher	: SARES International Sustainable Aviation and Energy Research Society	e-ISSN	: 2687-525X
Licence holder	: Prof. Dr. T. Hikmet Karakoç (President, SARES)	DOI	: 10.23890/IJAST
Address	: Research and Application Center of Civil Aviation, Research Centers Building, Eskisehir Technical University, Eskisehir, Turkiye	web	: www.ijast.org
		submission	: DergiPark-IJAST
		e-mail	: ijast@sares.org
		Copyright	: SARES Society

IJAST is published with the contribution of "Research and Application Center of Civil Aviation, Eskisehir Technical University"

CC BY SA

Language Editor

Utku Kale
Budapest University of Techology and Economy, Hungary
kale.utku@kjk.bme.hu

Editorial Board

Ramesh K. Agarwal
Washington University, USA rka@wustl.edu

Pouria Ahmedi
University of Illinois, USA pouryaahmadi81@gmail.com

Hikmat Asadov
National Aerospace Agency, Azerbaijan asadzade@rambler.ru

Ruxandra Mihaela Botéz
Université du Québec, Canada ruxandra.botez@etsmtl.ca

Elbrus Caferov
Istanbul Technical University, Turkiye cafer@itu.edu.tr

Patti J. Clark
Embry-Riddle Ae. University. USA clark092@erau.edu

Raj Das
RMIT University, Australia raj.das@rmit.edu.au

Rao Korrai Deergha
Vasavi College of Engineering, India korraidrao@yahoo.com

Umut Durak
German Aerospace Center, Germany umut.durak@dlr.de

Marina Efthymiou
Dublin City University, Ireland marina.efthymiou@dcu.ie

Vincenzo Fasone
Universita Kore di Enna, Italy vincenzo.fasone@unikore.it

Akhil Garg
Huazhong University of Sci. and Tech. garg.mechanical@gmail.com

Chingiz Hajiyev
Istanbul Technical University, Turkiye cingiz@itu.edu.tr

Jae-Hung Han
Institution:Korea Advanced Institute of Sci. Tech., Korea jaehunghan@kaist.edu

Gopalan Jagadeesh
Indian Institute of Science, India jagadeeshgopalan@gmail.com

John Kian
Northumbria University, England k.tan@northumbria.ac.uk

Kyriakos I. Kourousis
University of Limerick, Ireland Kyriakos.Kourousis@ul.ie

Soledad Le Clainche
Universidad Politécnica de Mad., Spain soledad.leclainche@upm.es

Luiz A Horta Nogueira
Federal University of Itajubá, Brasil lahortanog@gmail.com

Ionna Pagoni
University of Aegean, Greece ipagoni@aegean.gr

Marco Raiola
University Carlos III de Madrid, Spain mraiola@ing.uc3m.es

Mohammad Mehdi Rashidi
Tongji University, China mm_rashidi@yahoo.com

Ethirajan Rathakrishnan
Indian Institute of Technology, India erath@iitk.ac.in

Daniel Rohacs
University of Tech. & Econ., Hungary drohacs@vrht.bme.hu

Yevgeny Somov
Samara State Technical University, Russia e_somov@mail.ru

Jelena Svorcan
University of Belgrade, Serbia jsvorcan@mas.bg.ac.rs

Kateryna Synylo
National Aviation University, Ukraine synyka@googlemail.com

David Sziroczak
University of Tech. & Econ., Hungary dsziroczak@gmail.com

Nadir Yilmaz
Howard University, USA nadir.yilmaz@howard.edu

Oleksander Zaporozhets
National Aviation University, Ukraine zap@nau.edu.ua

Editorial Office

Mustafa Azer
Eskişehir Technical University, Türkiye mustafaazerr@gmail.com

Benginur Kaplan
Eskişehir Technical University, Türkiye benginurkaplan@gmail.com

Elif Karakılıç
Eskişehir Technical University, Türkiye ekarakilic26@gmail.com

Özge Küçükkör
Cappadocia University, Türkiye ozgekucukkor123@gmail.com

Ezgi Begüm Akıncı
Gumushane University, Türkiye ezgibegum.ondes@gumushane.edu.tr

Murathan Pekacar
Eskişehir Technical University, Türkiye murathanpekacar@gmail.com

Index

International Journal of Aviation Science and Technology

Research Article

Design and Simulation of Seats for Emergency Landing Conditions in Electrical VTOLs

Hasan Totoş[1*], Çağlar Üçler[2]

[1] *Istanbul Technical University, Aviation Institute, Department of Defense Technologies, Istanbul, Turkiye*
hasantotos53@gmail.com - 0009-0001-1829-3046
[2] *Ozyegin University, Faculty of Aviation and Aeronautical Sciences, Istanbul, Turkiye*
caglar.ucler@ozyegin.edu.tr - 0000-0003-4209-7915

Abstract

Emerging electrification technologies in aviation and recent advances drive the increased usage of electrical vertical take-off and landing (VTOL) air vehicles. Weight considerations are predominant due to the weaker powertrain and lower payload capacity. Moreover, most systems are automated, and there is no distinction between pilot and passenger seats anymore. Conventional aircraft seating typically exhibits excessive weight, necessitating the development of lightweight troop seats with simple designs and textile seat pans and backrests. This research focuses primarily on the design aspects of these lightweight troop seats. There are already guiding military standards and civilian codes for physical tests for passenger or pilot seats. Nevertheless, there needs to be a comprehensive document combining all of these and explaining how simulation tools can be practically used for the same purpose. Consequently, a generic design was generated based on the troop seat of military helicopters, which was then tested and simulated virtually by finite element analysis according to MIL-S-85510, CS27, and CS29 standards. After finalizing the static tests for forward, rearward, lateral, downward, and upward g forces on a 10-degree floor deformation in the longitudinal axis, implicit dynamic tests were conducted with loading in longitudinal and vertical directions as specified by the MIL-S-85510 standards. Then, hotspot analysis is made for stress interpretation. As a result, a near-optimum design was achieved with stresses 10% lower than the yield stress of the materials, which can be used on board an electrical VTOL.

Keywords

VTOL
Seat
Design
Analysis
MIL-S-85510
CS27
CS29

Time Scale of Article

Received 14 February 2024
Revised until 15 May 2024
Accepted 17 May 2024
Online date 21 June 2024

1. Introduction

The aviation sector is rapidly growing (Alharasees et. al., 2023) and electrification technologies in transportation are rapidly transforming aviation. Vertical take-off and landing (VTOL) air vehicles are becoming popular, and their penetration is further boosted by the mission flexibility provided (Aldemir and Ucler, 2022). Since VTOLs can take off and land vertically, they are an ideal candidate for military usage and civil applications when no runway is available (Zhou et al, 2020). In some missions, VTOLs are necessary to track objects or make stationary measurements when hovering (Ozdemir et al., 2014). Moreover, there is a broad application of VTOLs in observation for military purposes, transport of cargo, and rescuing soldiers and victims (Intwala and Parikh, 2015). In addition to these, they can be used for security

*: Corresponding Author Hasan Totoş, hasantotos53@gmail.com
DOI: 10.23890/IJAST.vm05is01.0101

operations, climate examination, and forest fire detection (Dinç, A., 2020).

Nevertheless, the structural requirements for VTOLs are very high. There are two distinct ways of designing them; either military or civilian codes can be used. In civil aviation, helicopter standards must be respected. For military VTOL cockpit seats, the MIL-S-58095 standard is used (DoD, 1981). For cabin seats, MIL-S-85510 is used (DoD, 1981). Nevertheless, the new generation VTOLs are highly automated, and there is no distinction between passenger and pilot seats anymore. Considering that the g levels for cabin seats are lower than cockpit seats (Demircan, 2020), but regular pilot seats are too heavy for a weaker electrical powertrain, troop seats can be used for electrical VTOLs. Moreover, civil aviation codes CS27 and CS29 standards must be respected as well (EASA, 2018; EASA 2018).

Historically, there have been some accidents in which humans get injured because of troop seat's insufficient strength (Reilly, 1977). The structural strength of the seats is a vital factor for protecting the occupant in crash events. Aviation standards contain various guidelines and criteria to ensure that seats meet specific minimum structural strength requirements, where static loads and peak acceleration values are defined for physical tests.

This study aims to improve the structural strength of the troop seat for electrical VTOLs by utilizing simulation technologies. In a crash, the design must be strong enough to withstand the loads without breaking, and the permanent deformation must absorb the energy. This requires an optimum design with appropriate materials selected. Current seat designs need to be improved to increase their impact-damping capabilities and optimized to protect inmates in the event of a crash.

Consequently, the research questions are:

- RQ 1: Which boundary conditions and loads can be used to develop a cheap, lightweight, and strong troop seat for electrical VTOLs?
- RQ 2: What is a near-optimum design for a certification-ready electrical VTOL?

This research investigates different material selections and structural design variations made by the SolidWorks program with virtual simulations by the ANSYS program. First, a literature review was leveraged to isolate the calculation, i.e., simulation basis. Then, the method is explained in detail, where the initial design was made according to MIL-S-85510 standard with a mixed model of shell and solid elements to reduce the computational time, which was optimized after applying g loads with the maximum values across MIL-S-85510, CS27, and CS29 standards. The discussion uses mesh sensitivity analysis and successive hotspot analysis for high-stress regions in an iterative manner.

It has been shown that the structural strength of the troop seat can be increased by using different material combinations, and it was seen that some parts' thickness can be reduced to decrease the weight. This research has provided new design recommendations to increase the structural strength of seats and offered practical application recommendations for the aviation industry and troop seat manufacturers. Suggestions have been made as to what material combinations or design changes could increase the strength of troop seats without increasing the weight and manufacturing costs.

2. Literature review

Amaze et. Al. (2024) studied commercial aircraft seat support structure analysis and topology optimization. Design and analysis conducted by the Solidworks program. Al6061-TS6(SS), Al7075-T6(SN),1023Carbon steel sheet (SS) and KYDEX®T materials were used. After topology optimization, the maximum stress observed was 189 MPa, and weight was reduced by 30% to 1.89 kg. Weight reduction achieved without loss of necessary strength.

Trivers et al. (2020) studied business aircraft seat design by topology optimization. In this study, Canadian Aviation Regulations 525.561 and 525.562 parts were used for making static and dynamic tests. Two topology optimizations were made for decreasing the manufacturing costs and decreasing the weight. They use explicit dynamic models to determine the response of the seat under 14g and 16g. 77.11 kg is used as an occupant. The static ultimate load factors are 9 g for forward, 4 g for sideward, 3 g for upward, 6 g for downward, and 1.5 g for rearward. 2024 T351 aluminum was used for the preliminary design. Buckling and complete fractures were unacceptable. But, the small amount of harm and yielding is not considered a problem for the design. However, there are some limitations of that study, the floor deformation was not considered in the analysis, and due to the limited density of meshes, results are approximately close to real cases. The results showed that the weight of the seat must be 32% lighter and the manufacturing costs decreased by 24%.

Tzanakis et al. (2023) researched composite aircraft seat structural analysis. In this study, Part 25.561 and 25.562 guidelines were used. According to the 25.562 guidelines, two dynamic tests are made. One with 14g and the other one with 16 g. Economy class 3 people seat is used. Von Misses' stress evaluation showed that the front seat rows were subjected to more loadings than the back rows due to the passenger's impact. Results showed that there is no significant material damage or critical loads on the structure. Injury criteria were also investigated with LS-DYNA software.

Özturk and Kayran (2018) studied crash analysis and the energy absorption mechanism of helicopter seats. EASA standards are used. The ABAQUS program is used for analysis. In this study, the seat hit a fixed wall, and the seat deformation was investigated. The tests were made with and without absorbers. The seat legs were aluminum. The g loads of seat and EASA standards compared to conclude that the seat is crashworthy. The effectiveness of the energy absorption mechanism is investigated.

3. Method

In crash events, the fuselage and cabin will be deformed (Trivers et al, 2020). The aircraft floor should be deformed so that this floor warpage conditions are also considered before and throughout tests (DoD,1981). One of the floor attachments of the floor-connected seats should be misaligned 10 degrees in pitch, and the other floor attachment of the seat should be misaligned 10 degrees in roll (Wiggenraad,1997). For tests, the maximum g values of the CS27/29 and MIL-S-85510 standards were used in the analysis. For the forward static test, 30 g, rearward test, 12 g, lateral test, 23 g, and upward test, 8 g load was applied according to MIL-S-85510 standards. For the downward test, 20 g was applied. CS 27/29 standards were considered in the downward test because the load requirement was higher for the downward test in CS 27/29 standards. According to the CS 27/29 standards, the test should be 3 seconds. For other static tests, the time was taken as 1 second. For the vertical dynamic test, the minimum peak deceleration was 32 g at 0,087th second, and the maximum peak deceleration was 37 g at 0,059th second. For the longitudinal dynamic test, the minimum peak deceleration was 22 g at 0,127th second, and the maximum peak deceleration was 27 g at 0,0811th second.

The directions were considered for dynamic tests as shown in Figure 1 according to MIL-S-85510 standards. Test 1 configuration is for the vertical dynamic test, and test 2 configuration is for the longitudinal dynamic test in Figure 1. The dummy was taken as 110 kg for all tests except for downward static and vertical dynamic tests. For the downward static test dummy was taken as 75 kg according to the CS 27/29 standards and for the vertical dynamic test dummy was taken as 89 kg according to MIL-S-85510 standards.

Solidworks program was used for the CAD design. For analysis, Ansys software was used. The static structural module of the Ansys software was used for static tests. The transient structural module of the Ansys software was used for dynamic tests.

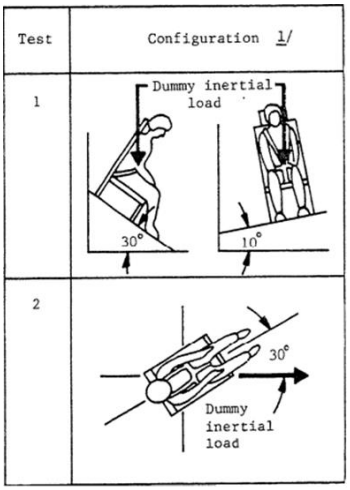

Fig. 1: Dynamic test conditions (DoD, 1981).

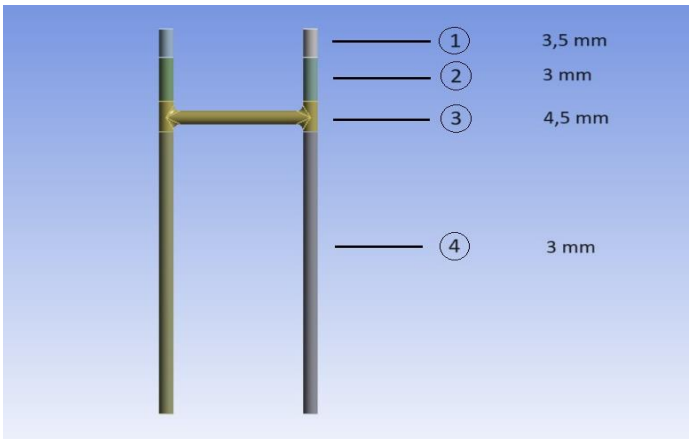

Fig. 2: Seat Pole design.

The seat pan, seat pole, seat belt, and fabrics were converted to shell models in SpaceClaim software for better mesh quality and faster analysis. The seat pole design is shown in Figure 2. For the upper leg of the seat pole, a thickness of 3,5 mm was used, labeled as 1 in Figure 2. High stress was observed on the upper leg of the seat pole. To reduce this, thickness increased. For the middle tube of the seat pole, a thickness of 4,5 mm was used, labeled as 3 in Figure 2. It was also because high stress was observed in the middle tube. For the rest of the seat pole, 3 mm thickness was appropriate, labeled as 2 and 4 in Figure 2.

The seat pan design is shown in Figure 3. Initially, the seat pan was 3 mm thick, but the thickness decreased to reduce the weight. For the 1st section, 2,5 mm thickness and for the 2nd section, 2 mm thickness was used as shown in Figure 3. A generic dummy model made of wood includes the passenger's weight, which is used in simplified real tests. The design is shown in Figure 4.

Different designs were tried to decrease the stress on the junction part. The flat junction part decreased the stresses, but a flat surfaced junction part would not be weldable; therefore, it could not be used. Increasing the area of the junction part was also tried, but the stresses were not changed.

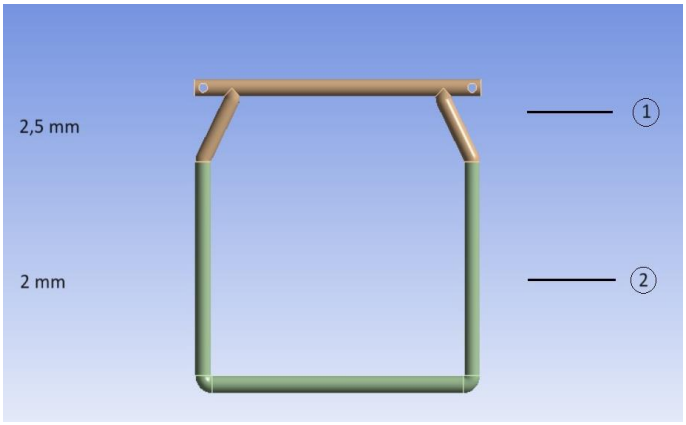

Fig. 3: Seat Pan design.

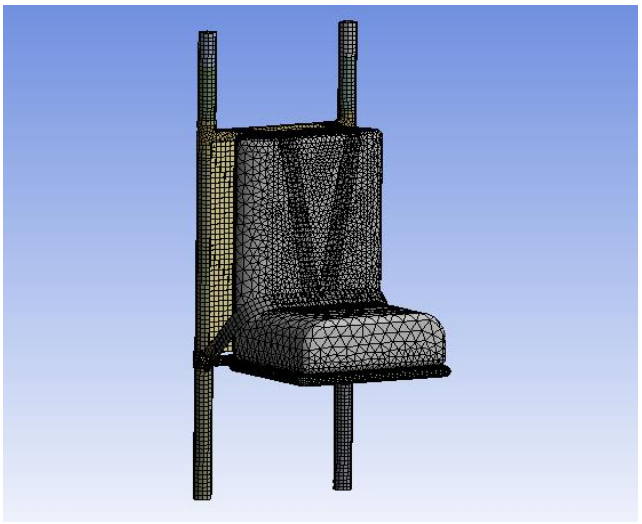

Fig. 4: Seat design.

Aluminum (Al) 7068 was used for the seat pole. For the seat pan, bolts, washers, and seatbelt buckle Al 7075 was used. For washers inside the junction part, copper alloy material was used, and for the junction part, solution-treated and aged Ti-8V-5Fe-1Al material was used. Seatbelts, seatbelt buckles, and fabrics were taken readily from ETSO standards, and the stress values on these parts were not investigated in this study. The weight limit was 6.8 kg according to MIL-S-85510 standards. The total weight of our design was 6,72 kg.

Finite element analysis (FEA) is a popular program used worldwide. Very complex problems can be solved by FEA (Roylance, 2001). FEA can make dynamic and static analyses. Static analysis is made to examine the fixed system's limits of force in the elastic region. Static analysis is a linear analysis method. Dynamic analysis is a nonlinear analysis type.

Dynamic analysis is a time-dependent analysis, and it considers the inertia effect (Balaban and Penekli, 2020). Dynamic analysis finds the dynamic behavior of the system. It is a widely known method; hence it is not explained in detail. Books written by Bhavikatti (2005) and Balaban and Penekli (2020) are good sources for further information.

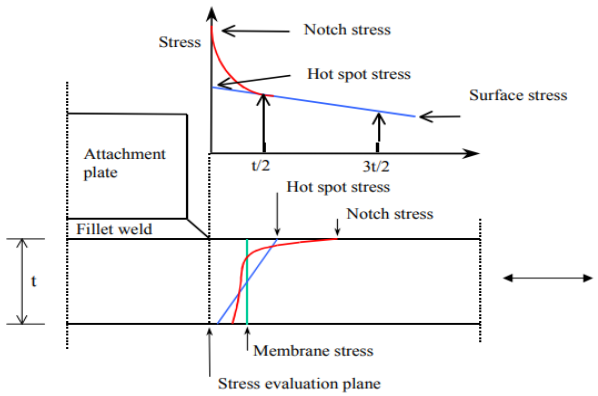

Fig. 5: Schematic stress distribution at a hotspot (DNV, 2011).

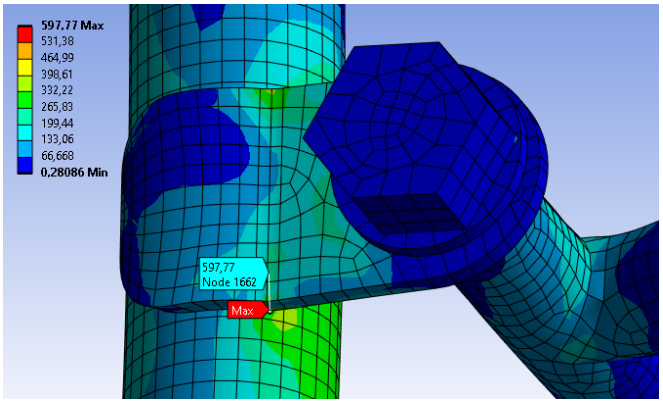

Fig. 6: Mesh sensitivity analysis for forward test.

Hotspot analyses were performed for high-stress values. This method is usually used for fatigue tests and determining actual stresses. It is used to find the actual stresses of the singularities and discontinuities. This stress is calculated with specific locations around the hotspot point (Caccese, 2010). The points with distances 0.5 t and 1.5 t from the hotspot point are used for extrapolation, where t represents the object's thickness (DNV, 2011). Stress distribution for hot spot analysis is shown in Figure 5.

4. Results and Discussion

Test 1: 30 g forward static test

The maximum stress was observed on the junction part for the forward static test. There was 577,22 MPa stress on the junction part. With a 5 mm element size, this stress increased to 597,77 MPa as shown in Figure 6. Then, hotspot analysis was made to investigate the real stress value. The stress at the point 2.5 mm away from the hotspot point was 386,4 MPa, and 7.5 mm away from the hotspot point was 214,65 MPa, as shown in Figure 7. With interpolation, hotspot analysis 1 showed that this stress was 472,275 MPa. Therefore, this stress value was considered as a singularity point.

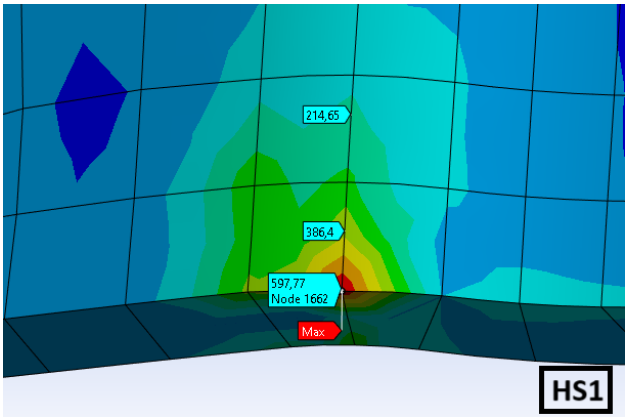

Fig. 7: Hotspot analysis 1 for forward test.

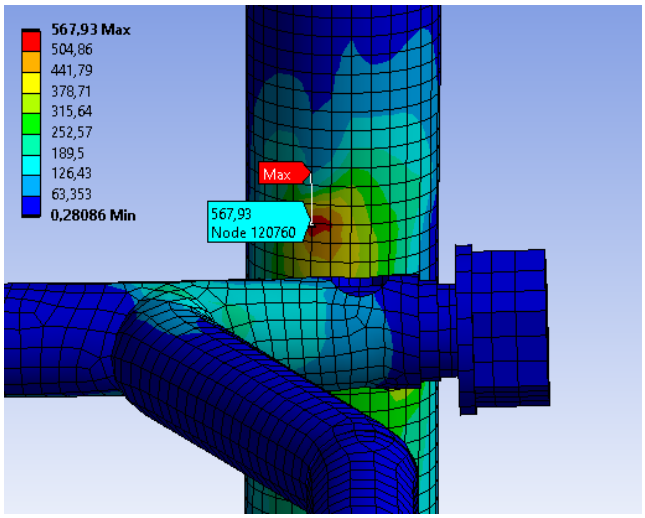

Fig. 8: Mesh sensitivity analysis for the main structure except the junction part.

Except for the junction part, the maximum stress was observed on the seat pole as 476,59 MPa. This stress increased to 567,93 MPa with mesh sensitivity analysis, as shown in Figure 8. Then, hotspot analysis 2 was made. At 0,5t away from the hotspot, the stress was 552,62 MPa; at 1,5t away from the hotspot, the stress was 522,11 MPa, as shown in Figure 9. By extrapolation, hotspot stress was found to be 567,875 MPa, almost the same as the stress value found by Ansys analysis. This means that this stress was not a singularity.

For the seat pan, the maximum stress observed was 259,84 MPa. This stress value decreased to 246,77 MPa with mesh sensitivity analysis, as shown in Figure 10. For the seat pan, 2,5 mm and 2 mm tubes were used. The maximum stress for copper alloy washers was 46,87 MPa, for bolts 118,83 MPa, and for washers 61,885 MPa. Hotspot analysis was not required for seat pans, bolts, washers, and copper alloy washers because the stresses were low.

All stresses on the forward static test were 10% lower than the yield strength of the materials, therefore this design was considered safe for the forward static test. The stresses observed on the forward static test are shown in Table 1.

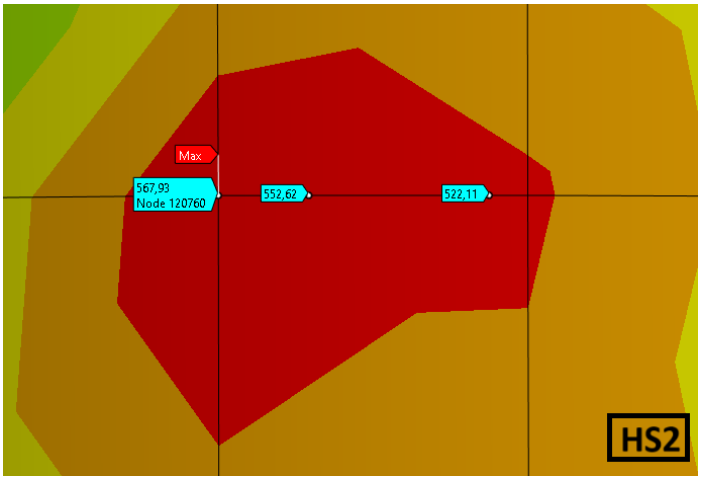

Fig. 9: Hotspot analysis HS2 for the forward test.

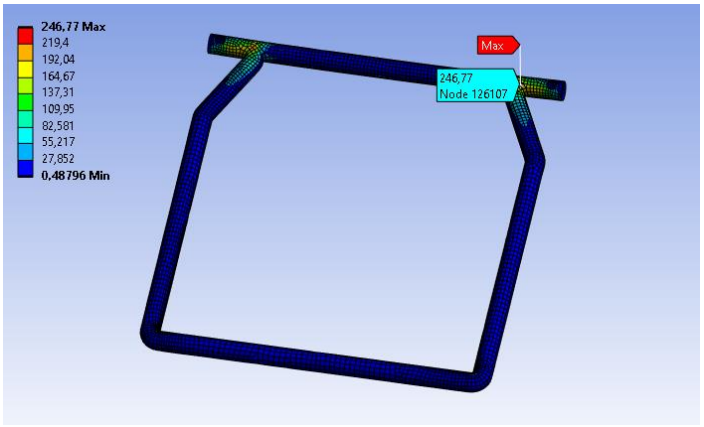

Fig. 10: Mesh sensitivity analysis for the seat pan.

Test 2: 12 g rearward static test

The maximum stress observed for the rearward static test was 226,81 MPa on the seat pole. With mesh sensitivity analysis, this stress increased to 314,65 MPa, as shown in Figure 11. Initially, Al 7034 material was used on the seat pole. But Al 7034 was not produced as a tube commonly. Therefore, Al 7068 was used on the seat pole, and it was seen that this material has enough strength for this part.

For the seat pan, the maximum stress observed was 95,258 MPa, as shown in Figure 12. Al 7075 was used on the seat pan, and Al 7075 material's yield stress was 503 MPa. 10% below the yield strength of Al 7075 was 452,7 MPa. 95,258 MPa was lower than 452,7 MPa. Therefore, mesh sensitivity analysis and hotspot analysis were not required.

The maximum stress observed for copper alloy washers was 6,6565 MPa, for bolts 38,6844 MPa, and for washers 9,7124 MPa. These stresses were 10% below the yield strength of the materials. Thus, this test passed the requirements without plastic deformation. The stress values observed on the rearward static test are shown in Table 2.

Table 1: Stress values for forward static test.

Forward Static Test	Materials	Stress (MPa)	Hotspot Analysis (MPa)	10% below the yield strength of the materials (MPa)
Junction Part	Ti-8V-5Fe-1Al (STA)	597,77	472,275	1242
Seat Pole	Al 7068	567,93	567,875	614,7
Seat Pan	Al 7075	246,77	NA*	452,7
Bolt	Al 7075	118,83	NA*	452,7
Copper Alloy Washer	Copper Alloy	46,87	NA*	252
Washer	Al 7075	61,885	NA*	452,7

NA*: Not available

Table 2: Stress values for rearward static test.

Rearward Static Test	Materials	Stress (MPa)	Hotspot Analysis (MPa)	10% below the yield strength of the materials (MPa)
Junction Part	Ti-8V-5Fe-1Al (STA)	130,47	NA*	1242
Seat Pole	Al 7068	314,65	NA*	614,7
Seat Pan	Al 7075	95,258	NA*	452,7
Bolt	Al 7075	38,684	NA*	452,7
Copper Alloy Washer	Copper Alloy	6,6565	NA*	252
Washer	Al 7075	9,7124	NA*	452,7

NA*: Not available

Test 3: 23 g lateral static test

The maximum stress observed for the 23 g lateral static test was 556,55 MPa on the junction part. This stress increased to 632,23 MPa with mesh sensitivity analysis, as shown in Figure 13. Then, hotspot analysis 3 was conducted to assess this stress. 0,5t away from the hotspot, there was 578,43 MPa stress; 1,5t away from the hotspot, there was 457,19 MPa stress, as shown in Figure 14. Extrapolated stress was 639,05 MPa. The hotspot stress increased from 632,23 MPa to 639,05 MPa. Therefore, 632,23 MPa was considered as a true stress.

Except for the junction part, the maximum stress was 432,48 MPa observed on the seat pole, as shown in Figure 15. Initially, 3 mm thick tubes were used on the seat pole's upper legs. However, it was seen that 3 mm tubes do not have enough strength. Thus, to decrease the stresses on the seat pole's upper legs, 3,5 mm thick tubes were used. Then, mesh sensitivity analysis was made with a 5 mm element size for this region. The 432,48 MPa stress increased to 493,65 MPa with mesh sensitivity analysis on the seat pole's upper leg, as shown in Figure 16. Hotspot analysis 4 made to this stress. With hotspot analysis, this stress was found to be 493,625 MPa, almost the same as that found by the analysis. Therefore, this stress value was a real stress.

On the seat pole's middle tube, 4,5 mm thickness was used. In the earlier design, 3 mm thickness was used. It was seen that there were high-stress values with 3 mm thickness. Hence thickness increased to 4,5 mm. Thus, stress values decreased. Making a mesh sensitivity analysis with a 5 mm element size to that region to get a more accurate stress value. It is obtained that 482,94 MPa stress occurred in this region with mesh sensitivity analysis as shown in Figure 17.

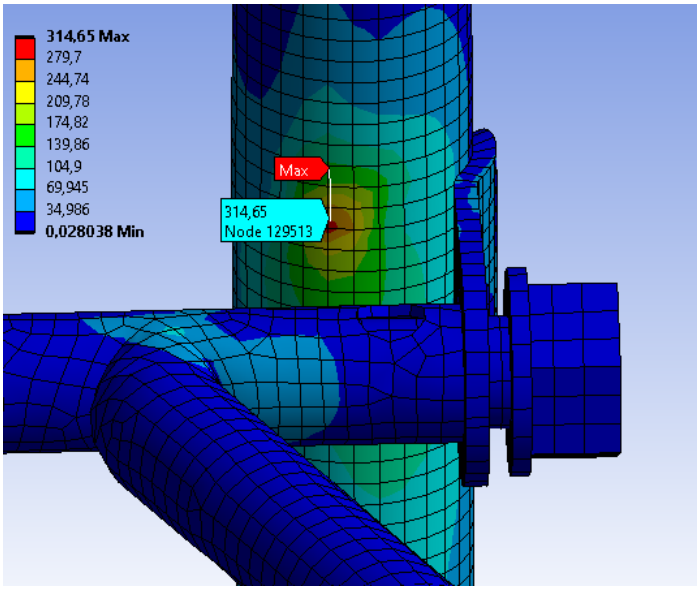

Fig. 11: Mesh sensitivity analysis for rearward test.

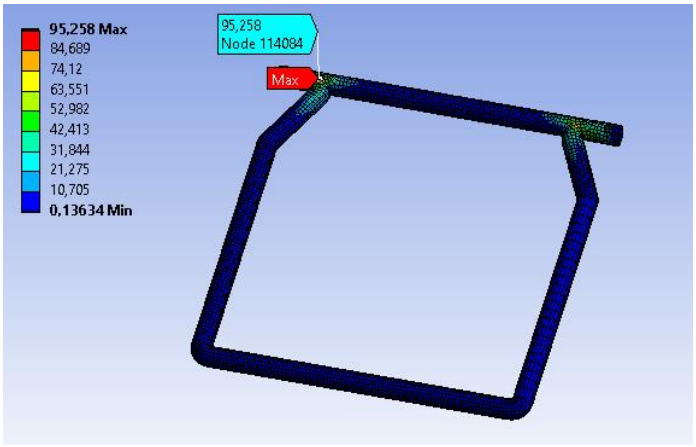

Fig. 12: Seat Pan analysis for rearward test.

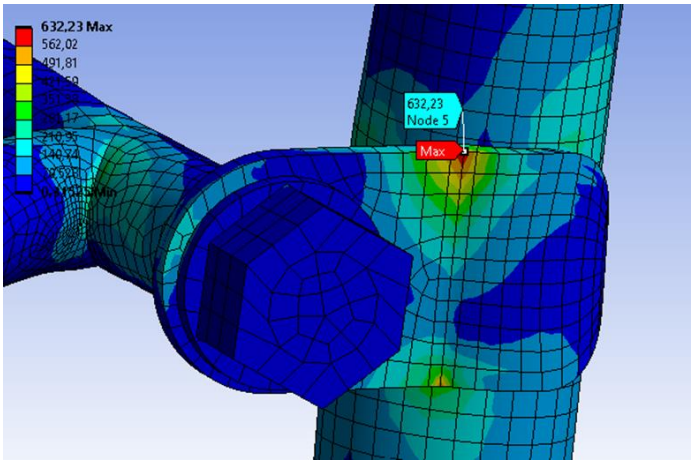

Fig. 13: Mesh sensitivity analysis for the lateral test.

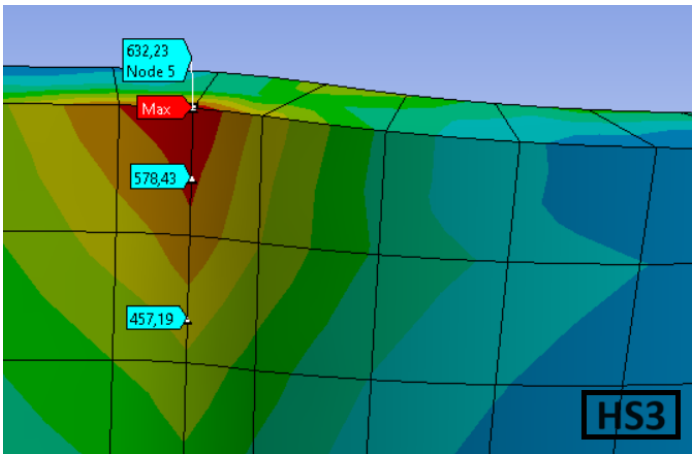

Fig. 14: Hotspot analysis 3 (HS3) for the lateral test.

Hotspot analysis 5 was made to find the actual stress for 482,94 MPa stress. The hotspot stress increased from 482,94 MPa to 499,725 MPa. These stresses were still lower than the 614,7 MPa critical stress value for the Al 7068 material. Therefore, this stress value was not dangerous.

The maximum stress on the seat pan observed was 357,76 MPa. To investigate it better a mesh sensitivity analysis was made with a 5 mm element size and the stress increased to 416,98 MPa as shown in Figure 18.

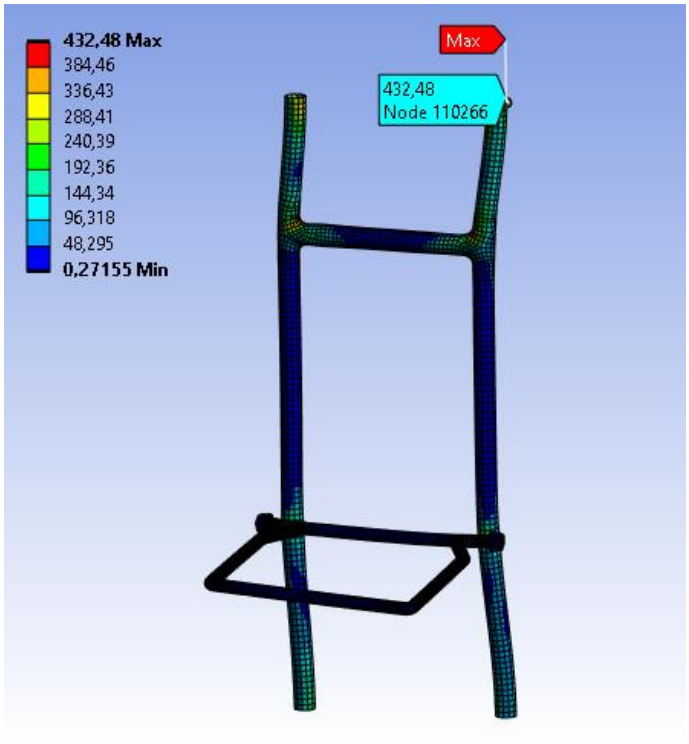

Fig. 15: Maximum stress on the main structure except the junction part for the lateral test.

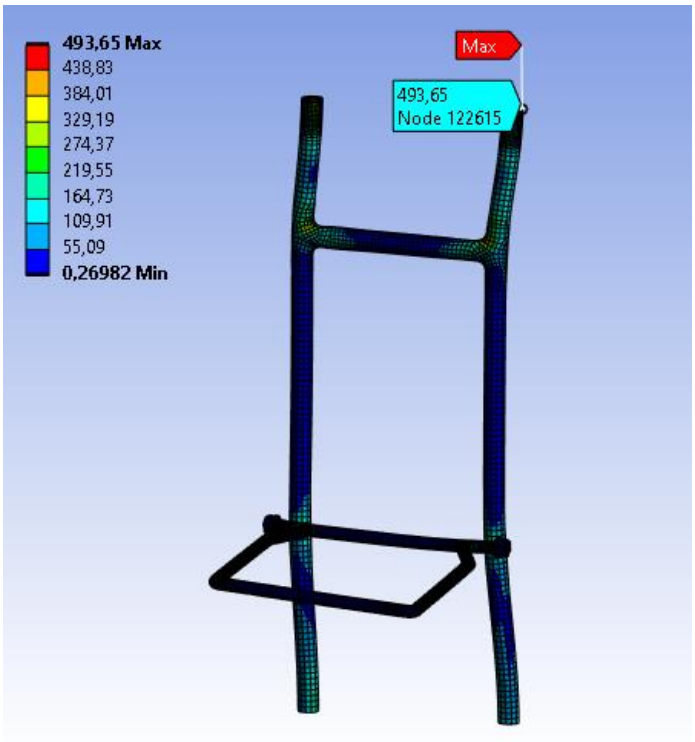

Fig. 16: Mesh sensitivity analysis of seat pole upper legs for the lateral test.

Since this stress was high, hotspot analysis 6 was performed on this stress. With hotspot analysis, this stress value was found to be 413,435 MPa. It was very close to the stress found by the analysis. 413,435 MPa was very low from the Al 7075 material's yield strength.

Table 3: Stress values for lateral static test.

Lateral Static Test	Materials	Stress (MPa)	Hotspot Analysis (MPa)	10% below the yield strength of the materials (MPa)
Junction Part	Ti-8V-5Fe-1Al (STA)	632,23	639,05	657
Seat Pole	Al 7068	493,65	493,625	614,7
Seat Pan	Al 7075	416,98	413,435	452,7
Bolt	Al 7075	176,32	NA*	452,7
Copper Alloy Washer	Copper Alloy	80,313	NA*	252
Washer	Al 7075	95,286	NA*	452,7

NA*: Not available

For the copper alloy washer, the maximum stress observed was 80,313 MPa. The maximum stress observed for the bolts was 176,32 MPa; for the washers, the maximum stress observed was 95,286 MPa. For the lateral test, it is concluded that these values are very below the material's yield strength. Therefore, there will be no plastic deformation in the structure. The stress results observed for the lateral static test are given in Table 3.

Test 4: 20 g downward static test

CS 27/29 standards were used for the downward static test because the load was higher in CS 27/29 standards and the analysis was made for 3 seconds according to the CS 27/29 standards. The maximum stress observed for the downward static test was 590,43 MPa on the junction part. Then, mesh sensitivity analysis was made, and this stress increased to 674,33 MPa, as shown in Figure 19.

For the junction part, hotspot analysis 7 was made. The hotspot stress was calculated as 626,975. Hotspot analysis showed that true stress decreased from 674,63 MPa to 626,975 MPa. This stress was a singularity stress. For the junction part, Ti-8V-5Fe-1Al (STA) material was used. The 10% below the yield strength value of the Ti-8V-5Fe-1Al (STA) material was 1242 MPa. Therefore 626,975 MPa was in the safe region.

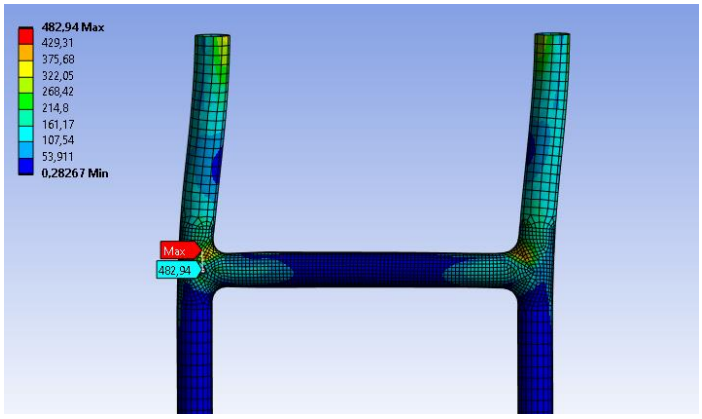

Fig. 17: Mesh sensitivity analysis for the middle tube for the lateral test.

If the stresses were investigated except the junction part, the maximum stress observed was 290,24 MPa on the seat pan. This stress decreased to 257,04 MPa with mesh sensitivity analysis, as shown in Figure 20.

Then to ensure that this stress value was real hotspot analysis 8 was made. The hotspot stress was calculated as 256,16 MPa. Hotspot analysis resulted in as same as the analysis made by Ansys. Thus, this stress value was real. This stress value was low for the Al 7075 material's yield strength. Therefore, no dangerous situation was observed.

The maximum stress for copper alloy washers was 59,754 MPa. For the bolt, the maximum stress was 109,22 MPa and for the washer, it was 59,048 MPa. Those stress values were very low. There won't be any plastic deformation occurrence on those parts. In summary, with analysis, it is ensured that there were no high-stress values for the downward test. This test passed the requirements of the CS27/CS29 standards. The stress results for the downward static test are shown in Table 4.

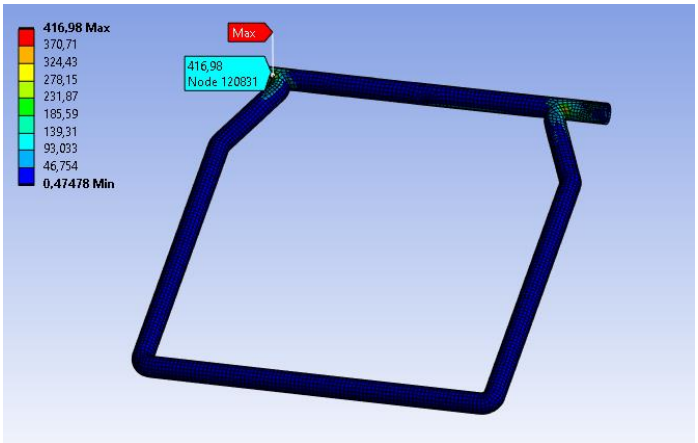

Fig. 18: Mesh sensitivity analysis for seat pan.

Table 4: Stress values for downward static test.

Downward Static Test	Materials	Stress (MPa)	Hotspot Analysis (MPa)	10% below the yield strength of the materials (MPa)
Junction Part	Ti-8V-5Fe-1Al (STA)	674,63	626,975	657
Seat Pole	Al 7068	220,64	NA*	614,7
Seat Pan	Al 7075	257,04	256,16	452,7
Bolt	Al 7075	109,22	NA*	452,7
Copper Alloy Washer	Copper Alloy	59,754	NA*	252
Washer	Al 7075	59,048	NA*	452,7

NA*: Not available

Test 5: 8 g upward static test

The maximum stress observed for the upward static test was 415,59 MPa on the junction part. With mesh sensitivity analysis, this stress decreased to 385,35 MPa. Hotspot analysis 9 made to this stress. With hotspot analysis, the stress was found to be 350,625 MPa. Hence, this stress value was a singularity stress.

The rest of the structure, except the junction part, was investigated, and the maximum stress was 112,58 MPa on the seat pole, as shown in Figure 21. This part of the seat pole was 3 mm thick. With 5 mm element size mesh sensitivity analysis, the 112,58 MPa stress increased to 206,09 MPa stress, as shown in Figure 22. Since Al 7068 material's yield strength was very high from this value. There was nothing to worry about. Hence, hotspot analysis wasn't required.

For the seat pan, the maximum stress observed was 81,002 MPa. To investigate the stress on the seat pan better, a mesh sensitivity analysis was performed on the seat pan with a 5 mm element size. With mesh sensitivity analysis, the maximum stress decreased to 74,682 MPa as shown in Figure 23. Al 7075 material was used on the seat pan. Since Al 7075 material's yield strength was 503 MPa and 10% below the yield strength was 452,7 MPa. 74,682 MPa stress value was low.

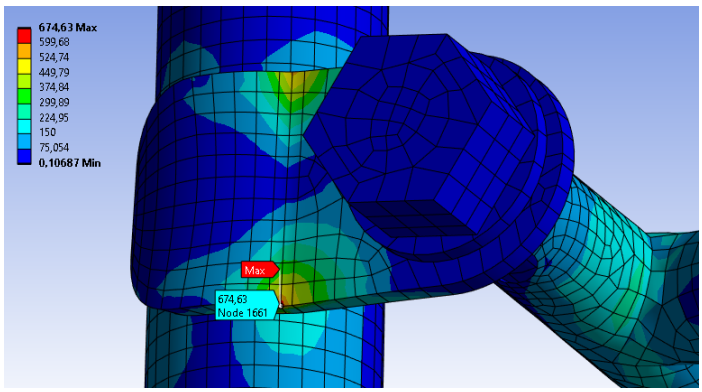

Fig. 19: Mesh sensitivity analysis for junction part.

For copper alloy washers, the maximum stress observed was 26,53 MPa. The maximum stress observed for the bolt was 34,773 MPa; for the washer, the maximum stress observed was 23,856 MPa. Since Al 7075 and copper alloy material's yield strength is very high from these stress values. There was no serious stress observation. In conclusion, stress values were low for the upward test, and it was ensured that this design is safe for the upward test without plastic deformation. The stress values observed for the upward static test are given in Table 5.

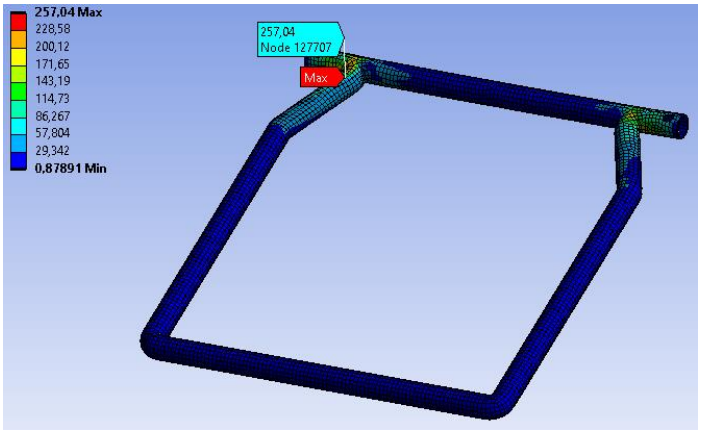

Fig. 20: Maximum stress on seat pan.

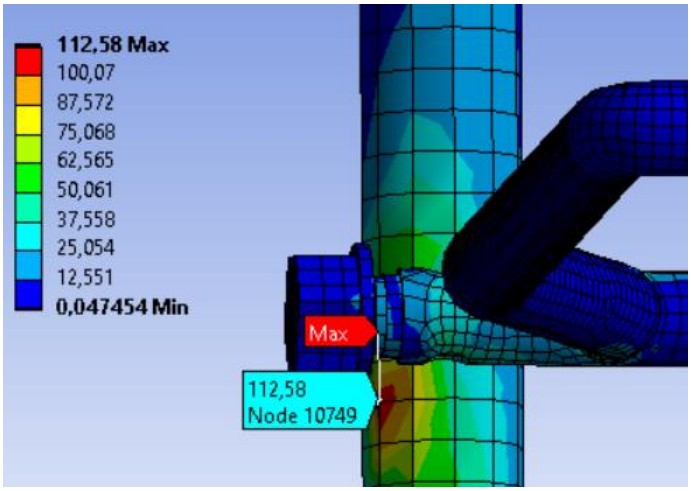

Fig. 21: Maximum stress except the junction part.

Table 5: Stress values for upward static test.

Upward Static Test	Materials	Stress (MPa)	Hotspot Analysis (MPa)	10% below the yield strength of the materials (MPa)
Junction Part	Ti-8V-5Fe-1Al (STA)	385,35	350,625	657
Seat Pole	Al 7068	206,09	NA*	614,7
Seat Pan	Al 7075	74,682	NA*	452,7
Bolt	Al 7075	34,773	NA*	452,7
Copper Alloy Washer	Copper Alloy	26,53	NA*	252
Washer	Al 7075	23,856	NA*	452,7

NA*: Not available

Test 6: 37g/32g vertical dynamic test

The maximum stress observed was 1331,8 MPa on the junction part for the vertical dynamic test at 0,05934th second. With mesh sensitivity analysis, this stress decreased to 1230 MPa at 0,05934th second. Hotspot analysis 10 was made for this stress region, and the stress was found to be 850,715 MPa with hotspot analysis. Hence this stress value was a singularity stress point. For the junction part, Ti-8V-5Fe-1Al (STA) material was used. 10% below this material's yield strength was 1242 MPa. 850,715 MPa was below the critical stress value.

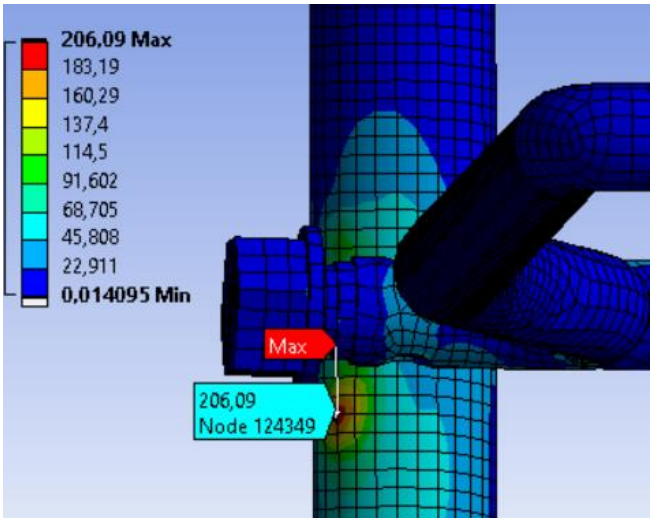

Fig. 22: Mesh sensitivity analysis of seat pole.

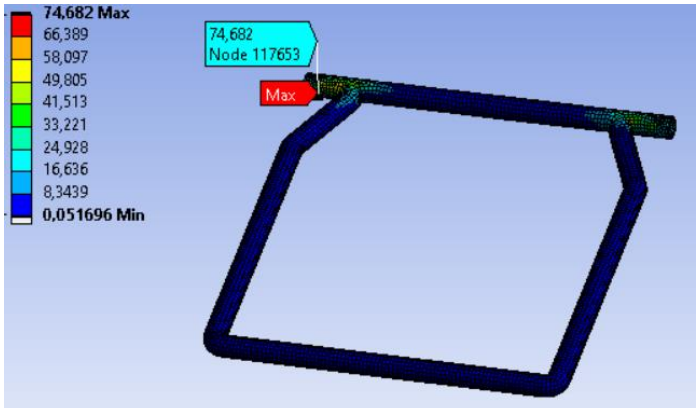

Fig. 23: Mesh sensitivity analysis of seat pan.

If we investigate the maximum stress except for the junction part. On the seat pole, 315,32 MPa stress was observed, as shown in Figure 24. With a 5 mm element size, mesh sensitivity analysis was made, and this stress increased to 520,29 MPa, as shown in Figure 25.

Hotspot analysis 11 made. This part of the seat pole was 3 mm. By making hotspot analysis, 520,135 MPa stress was observed. This stress was almost the same stress found by analysis.

The maximum stress on the seat pan observed was 226,55 MPa with a 5 mm element size, as shown in Figure 26. Initially, 3 mm tubes were used on the seat pan. Then, it was converted to 2,5 mm and 2 mm tubes for weight reduction. 226,55 MPa was a low stress; therefore, hotspot analysis was not required.

The maximum stress observed on the copper alloy washer was 71,847 MPa. For bolts, the maximum stress observed was 143,71 MPa; for washers, the maximum stress was 74,214 MPa. These were very low stresses. In conclusion, there were no stresses higher than 10 percent of the material's yield strengths for the vertical dynamic test. It is ensured that this design was safe for the vertical dynamic test. Stress results for vertical dynamic tests are shown in Table 6.

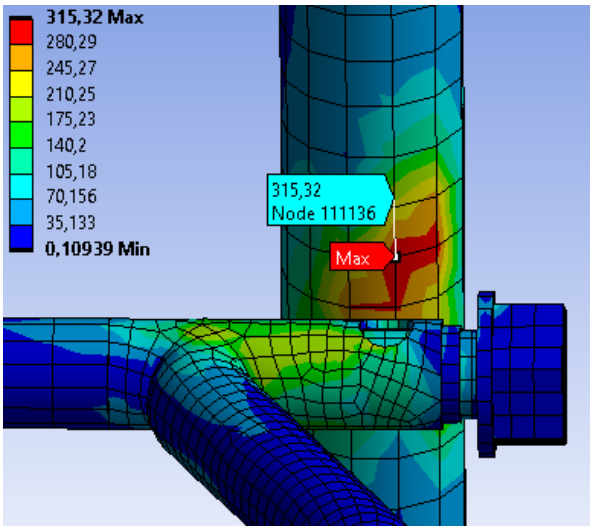

Fig. 24: Maximum stress except the junction part.

Table 6: Stress values for vertical dynamic test.

Vertical Dynamic Test	Materials	Stress (MPa)	Hotspot Analysis (MPa)	10% below the yield strength of the materials (MPa)
Junction Part	Ti-8V-5Fe-1Al (STA)	1230	850,715	657
Seat Pole	Al 7068	520,29	520,135	614,7
Seat Pan	Al 7075	226,55	NA*	452,7
Bolt	Al 7075	143,71	NA*	452,7
Copper Alloy Washer	Copper Alloy	71,847	NA*	252
Washer	Al 7075	74,214	NA*	452,7

NA*: Not available

Test 7: 27g/22g longitudinal dynamic test

For the longitudinal dynamic test, the maximum stress observed was 1008,8 MPa on the junction part at 0,081781th second. With mesh sensitivity analysis this stress decreased to 850,27 MPa at 0,087531th second as shown in Figure 27.

For the longitudinal dynamic test, hotspot analysis 12 was made for maximum stress on the junction part. The maximum stress was 850,27 MPa. The hotspot stress was calculated as 727,97 MPa. 850,27 MPa stress was found to be 727,97 MPa with hotspot analysis. It means that this stress was a singularity stress. Since 727,97 MPa was lower than the 1242 MPa, which was 10% below the Ti-8V-5Fe-1Al (STA) material's yield strength value. This stress was considered as safe.

If we investigate the maximum stress except for the junction part, high stress was observed on the seat pole. On that part of the seat pole, 3 mm thickness was used. 513,39 MPa stress was observed on the seat pole at 0,081781st second, as shown in Figure 28.

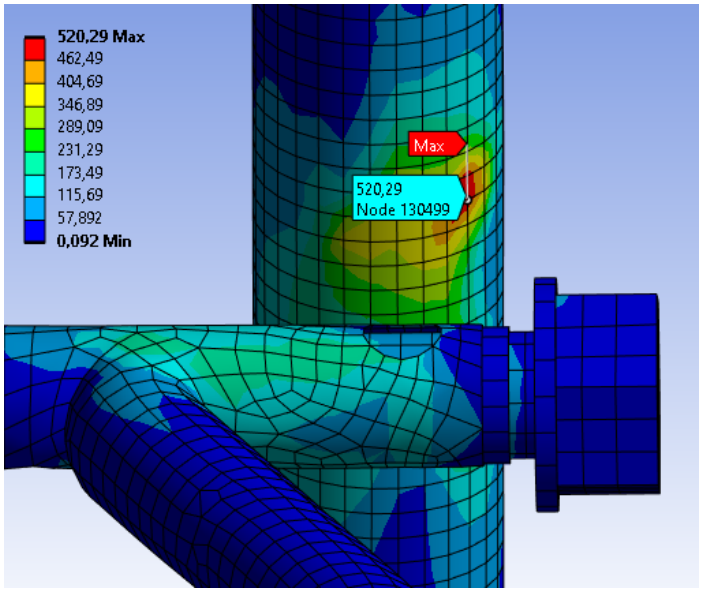

Fig. 25: Mesh sensitivity analysis of seat pole.

To investigate this stress better, a mesh sensitivity analysis was made with a 5 mm element size to this upper part of the seat leg. When a mesh sensitivity analysis was made. The 513,39 MPa stress value increased to 559,73 MPa at 0,087531st second, as shown in Figure 29.

559,73 MPa was a high-stress value. Therefore, hotspot analysis was performed to assess this stress. The hotspot stress was calculated as 559,65 MPa. Which was almost the same as 559,73 MPa stress. It was concluded that this stress was real stress.

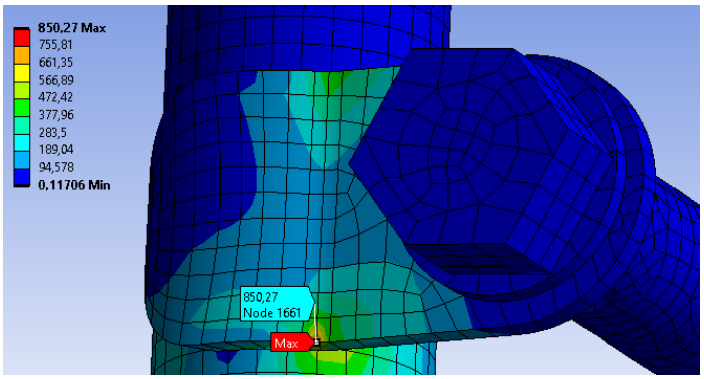

Fig. 26: Mesh sensitivity analysis for junction part.

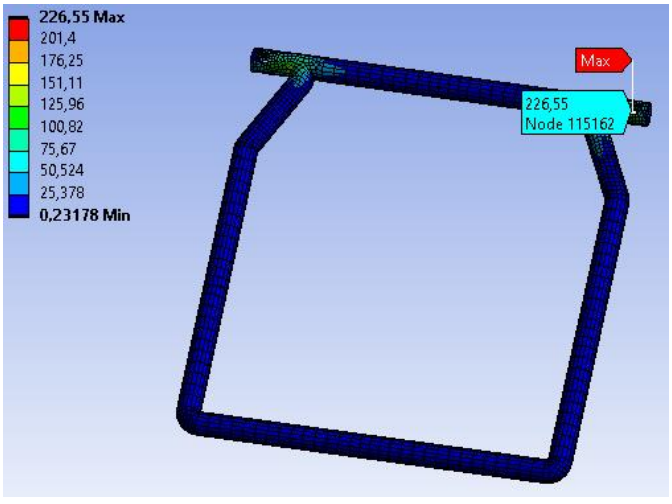

Fig. 27: Maximum stress on seat pan.

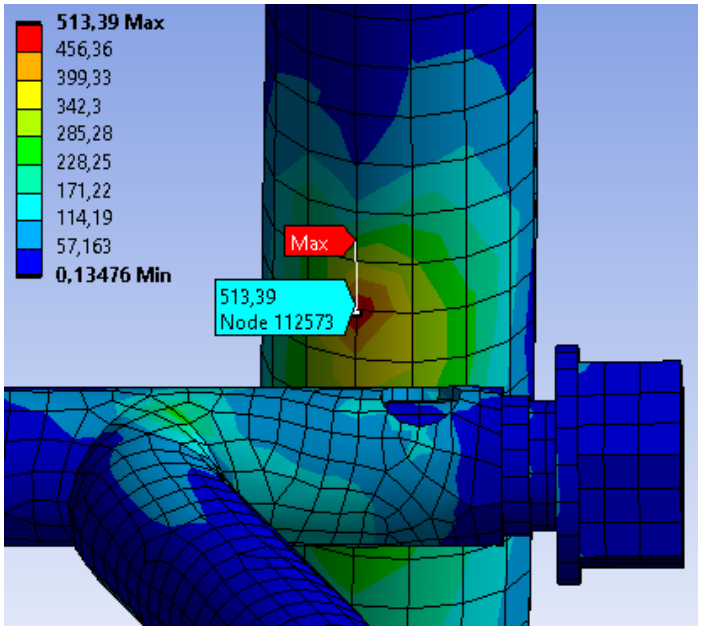

Fig. 28: Maximum stress except junction part.

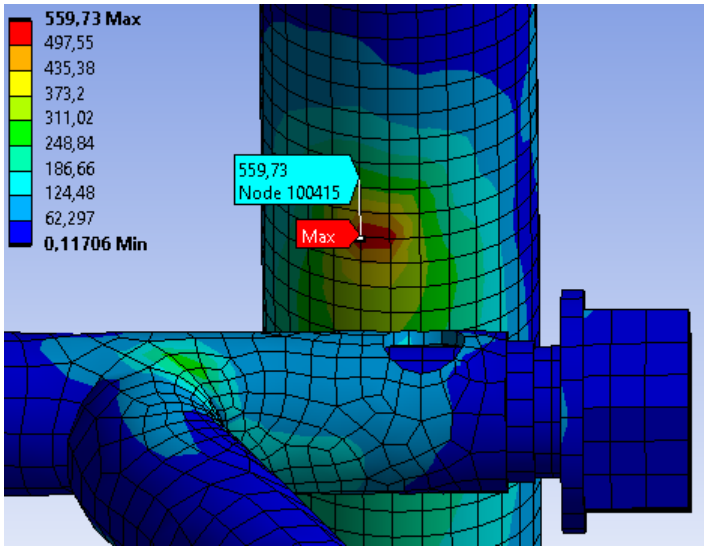

Fig. 29: Mesh sensitivity analysis of the seat pole.

Also, the upper legs of the seat pole were investigated for the longitudinal dynamic test with a 5 mm element size. A maximum of 522,31 MPa stress was observed on the upper leg of the seat pole, as shown in Figure 30. With hotspot analysis, this stress was found to be 522,075 MPa; it was ensured that this stress was real.

The maximum stress observed was 256,37 MPa on the seat pan at 0,085156th second with mesh sensitivity analysis as shown in Figure 31. The maximum stress observed on the copper alloy washer was 55,381 MPa at 0,081781th second. The maximum stress observed on bolts was 122,71 MPa, and the maximum stress observed for washers was 95,57 MPa. The stress results for the longitudinal static test are shown in Table 7.

Those findings show that instead of 3 mm, 2 and 2,5 mm parts can be used in the seat pan for weight reduction.

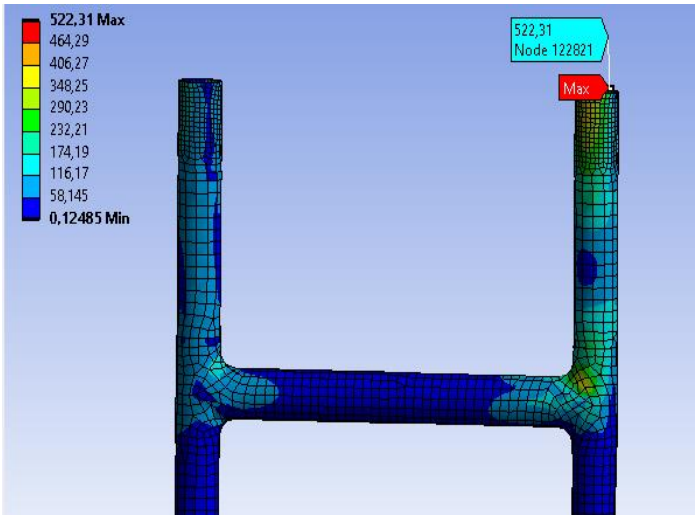

Fig. 30: Maximum stress on the upper legs.

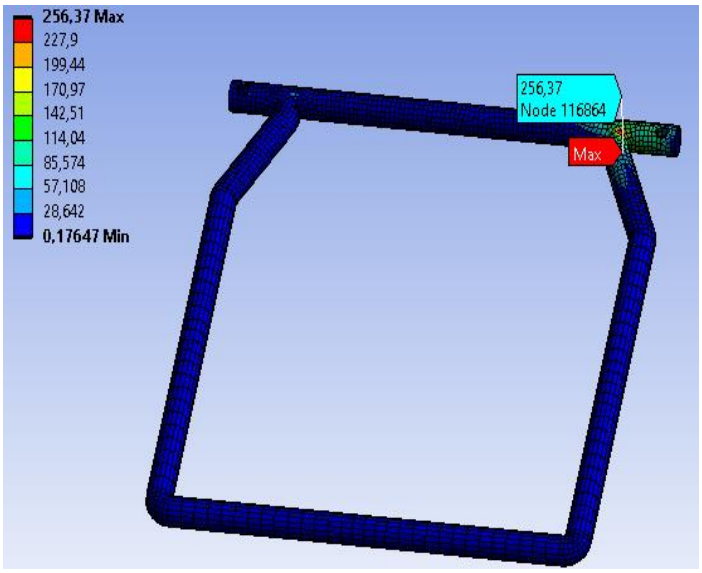

Fig. 31: Mesh sensitivity analysis of seat pan.

For the seat pole's middle tube, it was found that the 3 mm thickness was insufficient because high stress was observed in that part, especially in the lateral static test. Therefore, the thickness of the middle tube of the seat pole increased to 4,5 mm. For the upper leg of the seat pole, high stress was observed in the longitudinal dynamic test, and the thickness of this part increased to 3,5 mm. For the rest of the seat pole, 3 mm thickness was appropriate. In addition, in most tests, there was a singularity stress, which is an exaggerated stress result for the junction part. With hotspot analysis, it is shown that these stress results were lower.

Hotspot analysis showed that only 3 stress values occurred because of singularity in static tests. These singularities were on the junction part. For the junction part to decrease these singularity stresses, a flat junction part design was created, but since it was not weldable, it wasn't used. The hotspot analysis results are shown in Table 8.

Table 7: Stress values for longitudinal dynamic test.

Longitudinal Dynamic Test	Materials	Stress (MPa)	Hotspot Analysis (MPa)	10% below the yield strength of the materials (MPa)
Junction Part	Ti-8V-5Fe-1Al (STA)	850,27	727,97	657
Seat Pole	Al 7068	559,73	559,65	614,7
Seat Pan	Al 7075	256,37	NA*	452,7
Bolt	Al 7075	122,71	NA*	452,7
Copper Alloy Washer	Copper Alloy	55,381	NA*	252
Washer	Al 7075	95,57	NA*	452,7

NA*: Not available

Table 8: Hotspot analysis results for static tests.

Test	Hotspot	Maximum Stress (MPa)	Stress at t/2 (MPa)	Stress at 3t/2 (MPa)	Adjusted Hotspot Stress (MPa)
Forward static test	HS1	597,77	386,4	214,65	472,275 (Singularity)
	HS2	567,93	552,62	522,11	567,875
Lateral static test	HS3	632,23	578,43	457,19	639,05
	HS4	493,65	490,38	483,89	493,625
	HS5	482,94	475,38	426,69	499,725
	HS6	416,98	371,5	287,63	413,435
Downward static test	HS7	674,63	537,95	359,9	626,975 (Singularity)
	HS8	257,04	253,11	247,01	256,16
Upward static test	HS9	385,35	298,16	193,23	350,625 (Singularity)

Table 9: Hotspot analysis results for dynamic tests.

Test	Hotspot	Maximum Stress (MPa)	Stress at t/2 (MPa)	Stress at 3t/2 (MPa)	Adjusted Hotspot Stress (MPa)
Vertical dynamic test	HS10	1230	711,51	433,1	850,715 (Singularity)
	HS11	520,29	515,67	506,74	520,135
Longitudinal dynamic test	HS12	850,27	595,69	331,13	727,97 (Singularity)
	HS13	559,73	553,61	541,53	559,65
	HS14	522,31	518,95	512,7	522,075

In dynamic tests, all the stresses were below 10% of the yield stress of the materials. Hence, it was a safe design. 2 singularities were observed with hotspot analysis for dynamic tests. These 2 singularities were on the junction part. Nevertheless, the reaction forces were looked at, and all were within acceptable limits. Hotspot results can be found in Table 9.

The restriction is that generic models are used for the textile seatbelts, and the calculations were implicitly made using a simplified generic dummy model representing the human body. While this is acceptable due to the low deformation level and the reaction loads, which are in line with the general loading, a comparison with explicit dynamics, including an actual dummy model, is not necessarily required. Nevertheless, this can be done in future work.

5. Conclusions

The lack of suitable lightweight seats for electrical VTOLs in civil and military applications necessitated this work, where passenger and pilot seats are not distinct. Hence, a troop seat with a textile backrest and seat pan was developed to be safe for emergency landing conditions. The design was made according to military and civilian standards and codes. Loads and boundary

conditions were taken from the maximum values across MIL-S-85510, CS27, and CS29 standards.

There is no distinction between passenger and pilot seats because of the automated systems. Regular pilot seats are too heavy for a weaker electrical powertrain. There are already guiding military standards and civilian codes for physical tests for passenger or pilot seats. Nevertheless, there is no comprehensive document combining all of these. Hence, a generic design was generated based on the troop seat of military helicopters, which was then tested and simulated virtually by finite element analysis according to MIL-S-85510, CS27, and CS29 standards.

In this study, 5 static and 2 dynamic tests were conducted. Mesh sensitivity and hot spot analyses were used to decide whether a design change was required. In the end, all stresses were kept below 10% of the yield strength of the materials. At the same time, targeted weight limitations weren't exceeded. Hence, a near-optimum solution was achieved for electrical VTOL seats after iterations.

To the authors' best knowledge, there were no comparable electrical VTOL seat development examples available in the literature, which is a novel contribution. Existing literature is either for passenger seats or for pilot seats. There is no double-purpose seat proposal for electrical VTOLs. Moreover, the research outlines the simulation methodology and load cases required to develop these VTOL seats by explaining how the results must be interpreted. This is the second contribution to literature, which practitioners can also benefit from.

It has been shown that the structural strength of the troop seat can be increased by using different material combinations, and it was seen that some parts can be thinner to decrease the weight. Also, this research has provided new design recommendations to increase the structural strength of seats. This research offered practical application recommendations for the aviation industry and troop seat manufacturers. Suggestions have been made as to what material combinations or design changes could increase the strength of troop seats without increasing the weight and manufacturing costs. Light weight will also be beneficial for less fuel consumption.

In conclusion, aluminum alloys were appropriate for seat poles and seat pans. Because it was lightweight with high strength. Since high-stress results were observed for the junction part, titanium alloys were more appropriate for use. Because there were no high-stress results for the seat pan, the thickness of the seat pan can be reduced for weight reduction. Instead of using a uniform thickness, the seat pole can be divided into parts with different thicknesses. Because on the middle tube and upper legs of the seat pole, 3 mm thickness was insufficient. Singularity stresses were observed only on the junction part. A detailed joint design and a more detailed dummy model may be used in future studies.

Another future work is conducting accurate tests to verify the analysis results. These simulations can be performed using the Ls-Dyna program, and the results can be compared. In addition to that, the occupant's survivability may be inspected. Fatigue analysis could be conducted as a future study.

CRediT Author Statement

Hasan Totoş: Methodology, Investigation, Data curation, Visualization, Writing-Original Draft, Formal Analysis. **Çağlar Üçler**: Supervision, Conceptualization, Writing – Review and Editing.

Nomenclature

AISI	: American Iron and Steel Institute
Al	: Aluminum
APTA	: American Public Transportation Association
CS27	: Certification Specifications for Small Rotorcraft
CS29	: Certification Specifications for Large Rotorcraft
EASA	: European Aviation Safety Agency
ECE	: European Economic Commission
ETSO	: European Technical Standard Order
eVTOL	: Electrical vertical takeoff and landing
Fe	: Iron
FMVSS	: Federal Motor Vehicle Safety Standards
HS	: Hotspot
MIL-S-85510	: Military specifications for seats, helicopter cabin, crashworthy
MIL-S-58095	: Military specifications for seat system: crash resistant, non-ejection, aircrew
STA	: Solution Treated and Aged
Ti	: Titanium
UAV	: Unmanned air vehicle
USA	: United States of America
V	: Vanadium
VTOL	: Vertical take-off and landing

References

Aldemir, H. O., & Ucler, C. (2022). Airspace deregulation for UAM: Self-organizing VTOLs in metropoles. *The Collegiate Aviation Review International*, 40(1).

Alharasees, O., Jazzar, A., Kale, U., & Rohacs, D. (2023). Aviation communication: the effect of critical factors on the rate of misunderstandings. *Aircraft engineering and aerospace technology*, 95(3), 379-388.

Amaze, C., Kuharat, S., Bég, O. A., Kadir, A., Jouri, W., & Bég, T. A. (2024). Finite element stress analysis and topological optimization of a commercial aircraft seat structure. *European Mechanical Science*, 8(2), 1-17.

Balaban, H. and Penekli, U. (2020). Sonlu elemanlar yöntemlerinin tasarım süreçlerine yararlı etkileri, *Mühendis ve Makina*, 47, 17-22.

Bhavikatti, S. S. (2005). *Finite element analysis*. New Age International.

Bhonge, P. S. (2008). A *methodology for aircraft seat certification by dynamic finite element analysis* (Doctoral dissertation, Wichita State University).

Caccese, V. (2010). Fatigue in laser welds. In *Failure Mechanisms of Advanced Welding Processes* (pp. 218-257). Woodhead Publishing.

Demircan, M. (2020). *Energy Absorber Design and Analysis for Military Utility Helicopter Troop Seats* (Master's thesis, Hacettepe University).

Dinç, A. (2020). Sizing of a Turboprop Engine Powered High Altitude Unmanned Aerial Vehicle and Its Propulsion System for an Assumed Mission Profile in Turkey. *International Journal of Aviation Science and Technology*, 01(01), 9-13.

DoD (1981). MIL-S-85510 (AS) Military Specification Seats, Helicopter Cabin, Crashworthy, General Specification for.

DNV (2011). Fatigue design of offshore steel structures. *Rev.* 3.

EASA (2018). Certification Specifications CS-27: Large Small Rotorcrafts, Amendment 10.

EASA (2018). Certification Specifications CS-29: Large Rotorcrafts, Amendment 11.

Intwala, A., & Parikh, Y. (2015). A review on vertical take off and landing (vtol) vehicles. *International Journal of Innovative Research in Advanced Engineering (IJIRAE)*, 2(2), 187-191.

Ozdemir, U., Aktas, Y. O., Vuruskan, A., Dereli, Y., Tarhan, A. F., Demirbag, K., ... & Inalhan, G. (2014). Design of a commercial hybrid VTOL UAV system. *Journal of Intelligent & Robotic Systems*, 74, 371-393.

Özturk, G., & Kayran, A. (2018). Energy absorption mechanisms and crash analysis of helicopter seats. In ASME *International Mechanical Engineering Congress and Exposition* (Vol. 52040, p. V04BT06A046). American Society of Mechanical Engineers.

Reilly, M. J., & ARMY AIR MOBILITY RESEARCH AND DEVELOPMENT LAB FORT EUSTIS VA EUSTIS DIRECTORATE. (1977). *Crashworthy troop seat testing program* (p. 0206). USAAMRDL-TR-77-13, US Army Research and Technology Laboratories, Ft. Eustis, VA.

Roylance, D. (2001). Finite element analysis. *Department of Materials Science and Engineering, Massachusetts Institute of Technology, Cambridge*.

Trivers, N. C., Carrick, C. A., & Kim, I. Y. (2020). Design optimization of a business aircraft seat considering static and dynamic certification loading and manufacturability. *Structural and Multidisciplinary Optimization*, 62(6), 3457-3476.

Tzanakis, G., Kotzakolios, A., Giannaros, E., & Kostopoulos, V. (2023). Structural Analysis of a Composite Passenger Seat for the Case of an Aircraft Emergency Landing. *Applied Mechanics*, 4(1), 1-19.

Wiggenraad, J. F. M. (1997). Design, Fabrication, Test and Analysis of a Crashworthy Troop Seat, European Rotorcraft Forum.

Zhou, Y., Zhao, H., & Liu, Y. (2020). An evaluative review of the VTOL technologies for unmanned and manned aerial vehicles. *Computer Communications*, 149, 356-369.

International Journal of Aviation Science and Technology

Research Article

Numerical Aerodynamic and Aeroacoustic Analysis of Toroidal Propeller Designs

Xuan-Duc Vu[1], Anh-Tuan Nguyen[2], Tuong-Linh Nha[3], Hoang-Quan Chu[4], Cong-Truong Dinh[5]*

[1] *School of Mechanical Engineering, Hanoi University of Science and Technology, Hanoi 11615, Vietnam*
duc.vx196848@sis.hust.edu.vn - 0009-0003-5788-5233
[2] *School of Mechanical Engineering, Hanoi University of Science and Technology, Hanoi 11615, Vietnam*
tuan.nguyenanh@hust.edu.vn - 0009-0001-5057-5289
[3] *School of Mechanical Engineering, Hanoi University of Science and Technology, Hanoi 11615, Vietnam*
linh.nhatuong@hust.edu.vn - 0009-0006-6975-5075
[4] *Faculty of Aerospace Engineering, Le Quy Don Technical University, Hanoi 11917, Vietnam*
chu.h-quan.fas@lqdtu.edu.vn - 0000-0002-9312-0508
[5] *School of Mechanical Engineering, Hanoi University of Science and Technology, Hanoi 11615, Vietnam*
truong.dinhcong@hust.edu.vn - 0000-0001-5357-1534

Abstract

Drones have a major drawback which prevents them from being used extensively - the excessive noise they produce. This article presents an optimization process of aerodynamic noise reduction for a novel design called the Toroidal Propeller, which consists of two blades looping joined in a manner where the end of one blade arches back into the other, has been designed by the Aerospace Propulsion Systems (APSs) research team at School of Mechanical Engineering, Hanoi University of Science and Technology. In addition, four toroidal propellers with different curved shapes (pitch) and Number of Blades (NOB) are considered. The goal of this research is to evaluate the effects of modifying the geometry design of the Toroidal Propeller on the intensity of blade tip vortex and aerodynamic flow characteristics passing through the blade. The ultimate goal is to decrease blade tip vortex and turbulence produced by the blade, which can help estimate the sound pressure level and minimize it without causing significant performance losses. Based on the outcome results, the models of the four geometry studies are compared in terms of Acoustic Power Level (APL), Surface Acoustic Power Level (SAPL), Thrust, Torque, and Power. In general, the propeller model with NOB of 3 provides the most optimal efficiency in terms of both Thrust and APL. At the output cross-section, the APL dropped from nearly 139 dB to 121 dB, while thrust increased from almost 6.2N to 8.7N compared to the first version of the Toroidal Propeller model.

Keywords

Toroidal Propeller
Blade Number
Thrust
Acoustic Power Level
Surface Acoustic Power Level

Time Scale of Article

Received 21 December 2023
Revised until 27 March 2024
Accepted 1 April 2024
Online date 21 June 2024

1. Introduction

Unmanned aerial vehicles (UAVs) have become increasingly useful in both military and civil applications over the past few years. Among the various vehicle power configurations, rotary-wing vehicles with vertical take-off and landing abilities remain popular, while propellers are the most commonly used. The propeller is a key component of a rotorcraft, providing the necessary

*: Corresponding Author Cong-truong Dinh, truong.dinhcong@hust.edu.vn
DOI: 10.23890/IJAST.vm05is01.0102

propulsion to enable aircraft movement (Dantsker, O.D., 2022). Drones are small, remote-controlled aircraft used for services like package delivery, aerial photography, and more. They're cost-effective, eco-friendly, and can navigate tight spaces where humans can't go. In 2017, the psychoacoustic experiments were conducted by NASA Langley Research Center, the findings indicate that humans are more responsive to the noise generated by small multirotor drones than to noise from other forms of traffic (Krishnamurthy, S., 2021). This finding suggests that the use of quieter propellers could potentially accelerate the public's acceptance and commercial adoption of drones. Since drones are often heard before they are seen, it is important to reduce their sound footprint to make them less detectable. The engine and propeller of the UAVs contribute the most to the noise and reducing the noise of propellers is a challenging task as the designs that produce less noise can have reduced efficiency. Designing quiet propellers is an area of active research. Some studies have explored ways to decrease propeller noise (Gur and Rosen, 2009; Wu et al., 2019; Chirico et al., 2018; Wisniewski et al., 2015; Wisniewski et al., 2015; Demoret and Wisniewski, 2019; Wisniewski and Van Treuren, 2022; Axel Schulz, 2023).

Gur and Rosen (2009) focused on utilizing a silent propeller on a mini-UAV using electrical power. The study conducted by the researchers provided valuable insights into the factors affecting the performance and noise generated by the propeller. By analyzing blade shape, cone angle, diameter, speed, and NOB, they discovered that increasing NOB significantly makes the propeller quieter.

Wu et al. (2019) conducted a study on propeller noise and it was found that the loudest noise is produced at the blade tip. They employed numerical techniques to explore how propeller geometry and rotational speed can help the development of design a quieter propeller. The study revealed that the noise generated by a propeller is made up of a low-frequency sound that remains constant and high-frequency sounds that occur at specific points throughout the operation of the propeller. With increasing revolutions per minute, the high-frequency sounds become more prominent. To reduce the noise, the researchers altered the blade geometry along the spanwise direction while the blade width was expanded in a radial direction. According to a study by Chirico et al. (2018), the application of computational fluid dynamics (CFD) can be instrumental in the estimation of APL and noise spectra for different blade shapes and hub geometries. According to the research findings, designing a blade that operates at slow speed rotation and features inboard migration of spanwise loading is deemed to be extremely quiet and isn't causing notable disadvantages.

The efficacy of various combinations of radius, pitch, and NOB on aerodynamic efficiency and APL have been studied by Wisniewski et al. (2015) through experimental investigations. They identified the ideal pitch in which the APL is minimized. The results also revealed that the noise generated was heavily dependent on the propeller's rotational speed. The research also by Wisniewski and colleagues (2015) conducted a study to investigate how propeller performance and noise are affected by aerofoil shape and tip configuration. The study included four airfoils, with the GM15 airfoil emerging as the top performer for two-bladed propellers. The study also found that propellers with Oval tips outperformed those with round, tapered, or flat tips. Based on these findings, a hybrid propeller was developed to achieve optimal performance by combining the GM15 airfoil with an Oval tip. According to a study by Demoret and Wisniewski (2019), the principal cause of propeller noise is blade-tip vortices. To mitigate this issue, they suggested that the blade-tip rotational speed or vortex strength be decreased. Recently, research conducted by Wisniewski and Van Treuren (2022) explored new designs of propellers that have less thrust-load at the blade-tip. This can be attributed to the reduction in the vortex strength of the blade-tip, which resulted in a decrease in the level of sound pressure and the necessary power.

Axel Schulz (2023) has studied the impact of modifying the trailing edge of a drone propeller manufactured by APC Propellers. The results from the simulations show that a modification can reduce the tonal noise caused by the vortex feedback mechanism between leading edge (LE) and trailing edge (TE) as well as the overall sound level in the broadband component of the noise. However, a modification where the material is removed results in a reduction of propeller lift force. The place of the modification seems to play a big role in the overall sound characteristic of the propeller. The best-performing propeller had a sinusoidal cutaway along the entire TE.

The objective of this project is to analyze the impact of modifying the blade shape and wing-tip configurations to decrease the intensity of wing-tip vortices, minimize turbulence in the flow across the blade and, as a result, reduce the noise generated by the propeller. This article is also mainly focused on examining computational methods for predicting propeller performance and acoustic power levels. During the simulations, the propeller's rotational speed is tested at varying minimum to maximum speeds. The data collected from these simulations are used to compare the thrust and torque produced. The propellers are set to rotate at a consistent and unchanging rate of speed in the second simulation, and the corresponding APL and SAPL values are estimated from the collected data.

The recent research conducted by MIT University

Cambridge on the toroidal propeller is certainly an interesting development for the drone industry. The researchers claim that these propellers produce less high pitch noise compared to traditional propellers, without any loss in efficiency (MIT Lincoln Laboratory, 2022; Sebastian, T. and Strem, C., 2020). If proven successful, the use of toroidal propellers could revolutionize the drone industry. For decades, researchers and companies have been studying and developing the concept of Ring Wings, which involves rotating an airfoil in a toroidal shape. This idea eventually led to the development of various propellers used today. This concept was found to reduce noise and increase efficiency, and many researchers and marine companies continued to build on it. This design was patented in the 1980s without much discussion, but recent MIT experiments have renewed interest in its propeller design, opening up new possibilities for its utilization.

The MIT toroidal propeller design features a pair of interlocking blades. Specifically, the two blades cleverly intertwine in a manner whereby the tip of one curve back into the other, reducing drag from swirling air tunnels (vortices) at their tips and improves the overall stiffness of the propeller, which helps to reduce the noise. The propeller's toroidal shape helps minimize blade-tip vortex by constraining the flow and controlling spillover of the edges. The number of blades and pitch also affect noise and vibration. Due to the blade's curved shape and the non-linear relationship between blade angle and performance, establishing the pitch in toroidal propellers is a complex process. The key features of this Toroidal propeller have been outlined by MIT which include: lowers the signals in the frequency range that humans are most sensitive to; without the need for additional components, it reduces noise and avoids adding weight or consuming power; reduces the chances of the rotating propeller will coming into contact with objects or surfaces in the drone's trajectory, minimizing the risk of cutting, catching, or clipping; Reliably manufacture this using additive techniques to produce thrust similar to a multirotor drone propeller, which enables the customization of the propeller for different models and types of multirotor. Tests conducted on commercial quadcopters using toroidal propellers have shown in Fig.1 that they can produce thrust levels comparable to conventional propellers at similar power levels. These propellers produce reduced noise levels, allowing drones to operate without harming human hearing at half the distance.

The article is structured in the following way: firstly, it reviews the methods used for aero-acoustic modeling. Secondly, it describes the test cases, followed by an explanation of the computational grids, the flow solver, and the computational setup. Thirdly, it presents the results and discusses them. Lastly, the article provides concluding remarks.

2. Aerodynamic Characteristics of Propellers

The traditional design of propellers typically comprises radiating blades and rotating hub. The blades are angled at a specific pitch to create a helical shape and rotate around the hub. The propeller causes forward motion by using its blades to push against air, powered by the engine or motor (Gerr, D., 1989). Nevertheless, the amount of the thrust produced by a propeller is not always constant and depends on factors such as the propeller's rotational and incoming flow velocities. Hence, tests conducted on propellers often involve examining their performance under a variety of operating conditions (Vargas Loureiro, E. et al., 2021). To optimize rotorcraft performance and energy efficiency, consider propeller variations and aerodynamic parameters. The propeller's performance is evaluated based on normalized coefficients such as efficiency (η), power coefficient (CP), and the thrust coefficient (CT), which can be calculated using equations (1) from Ref. (Seddon, J. and Newman, S., 2011):

$$C_T = \frac{T}{\rho n^2 D^4}, C_P = \frac{P}{\rho n^3 D^5}, \eta = \frac{TV}{P} \quad (1)$$

where P and T represent power (W) and the thrust (N), respectively. D, n, ρ, *and* V represent propeller diameter (m), rotational velocity (rev/s), air density (kg/m^3), and the forward speed of a vehicle propelled by a propeller (m/s), respectively. As velocity (V) approaches zero, propeller efficiency (η) also approaches zero, and propeller thrust becomes the static thrust (T).

3. Aero-Acoustic Modeling Methods

The propeller noise is comprised of two main components: vortex (broadband) and rotational (tones) noise. Broadband noise, commonly known as vortex noise, is generated due to the presence of blade-tip and LE vortices, free-stream turbulence, and separated flows.

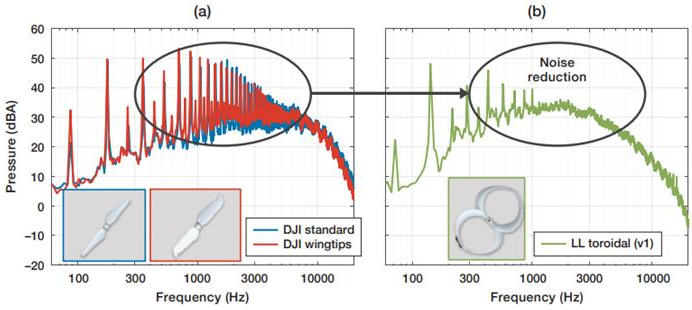

Fig. 1. The toroidal propeller (b) used on DJI's quadrotors in comparison to the conventional propellers (a) shows a noteworthy decrease in noise produced by the toroidal propeller.

Rotating blades induce a velocity gradient from the hub to the tip, resulting in a broad range of shedding frequencies associated with vortex shedding. The strength of shedding vortices is directly proportional to the vortex noise, and the noise is mainly caused by the tip frequency, as it is related to the velocity of the section to the sixth power.

All sounds that are related to the harmonics of the blade passage frequency are referred to as rotational noise. As the harmonic order increases, the sound pressure level decreases. Any irregularities in the blade geometry and/or the blade spacing in the azimuthal direction can result in additional sub-harmonics in the noise spectrum (Chirico et al., 2018). Chirico et al. (2018), state that subsonic wing-tip rotation produces two types of noise: monopole due to blade thickness and dipole due to aerodynamic load variations on the blade. When blade-tip Mach numbers range from approximately 0.6 to 0.7, the loading noise predominates. However, as Mach numbers increase, the thickness noise becomes more prominent. The propeller thrust and torque create rotational noise, which increases with larger diameter or fewer blade numbers. The source of the noise diminishes as the distance from it increases in a manner that varies inversely with the square of the distance (Roskam, J. and Lan, C., 1997).

Methods for estimating propeller rotational and vortex noise were introduced by Made and Kurtz in their study (Marte, J.E. and Kurtz, D.W., 1970). When it comes to conventional propellers with moderate forward velocities and tip speeds, the estimation of rotational noise can be achieved by:

$$p_{rms} = \frac{169.3 \cdot m \cdot B \cdot R \cdot M_t}{S \cdot A}\left[\frac{0.76 \cdot P_h}{M_t^2 - T \cdot \cos\theta}\right] \cdot J_{mb}(x) \qquad (2)$$

where:

p_{rms} = rms APL in dynes/cm^2

S = distance from propeller hub to observer, ft

Ph = absorbed power, horsepower

X = The Bessel function's argument, 0.8MtmB sinθ

Θ = angle from forward propeller axis to observer

B = NOB

M = harmonic's orders

R = propeller radius, ft

A = propeller disc area, ft2

Mt = tip Mach number

T = thrust, lb

This formula shows that the amount of noise rises as the absorbed power and diameter increase, the number of blades decreases, particularly when the tip speed is increased. The APL of the noise's vortex produced by traditional propellers can be approximated by this formula:

$$SPL = 10 \cdot log \frac{k \cdot A_b \cdot (V_{0.7})^6}{10^{-16}} \qquad (3)$$

where:

k =the proportionality constant;

$V_{0.7}$ = velocity at 0.7 radius

Ab = the area of blade, ft^2

The equation demonstrates that the noise caused by the vortex is heavily dependent on the speed of the blade. Increasing the blade velocity by two times results in an 18 dB increase in SPL. It's important to note that decreasing the blade velocity will affect the propeller's performance. An alternative solution is to decrease the vortex strength represented by C_L, the lift coefficient, in the equation below.

$$SPL = 10 \cdot log \frac{6.1 \cdot 10^{-27} \cdot A_b \cdot (V_{0.7})^6}{10^{-16}} + 20 \cdot log \frac{C_L}{0.4} \qquad (4)$$

One way to decrease propeller vortex noise is by lessening the intensity of the tip vortex. This can be achieved by decreasing lift production near the tips of the propeller.

4. Description of Numerical Methods

CFD models are utilized to replicate 3D flows that are time-dependent, incompressible, and viscous by applying the Navier-Stokes equations of momentum and mass conservation through discrete techniques (Stokkermans et al., 2019; Klimchenko and Baeder, 2020; Stuermer, 2008).

In this study, commercially available software called ANSYS-FLUENT 2019 R1 is used to conduct RANS-based simulations.

(a) (b)

Fig. 2. 3D Toroidal Propeller models (a) Bi-loop Toroidal Propeller version 1-2-3 (b) Tri-loop Toroidal Propeller

In the beginning, the model geometry of the Bi-loop Toroidal Propeller is created in Fusion 360 by using the MIT Toroidal Propeller as a citation, the geometric framework of the Tri-loop Toroidal Propeller also created, are shown in Fig. 2, which is then imported to ANSYS. This part provides further details about how to develop the CFD model. It covers aspects such as defining the computational region, conditions at its boundaries, creating the mesh, and assessing its quality, as well as configuring the solver parameters.

4.1 Boundary Conditions and Computational Domain

Fig.3 displays a diagram outlining the numerical region and conditions at its boundaries. In order to implement the multiple reference frame (MRF) model, the division of the computational domain results in two distinct zones: an internal rotating fluid zone (Rotation-Domain) and an external stationary fluid zone (Fluid-Domain). The cylindrical shape of a stationary fluid zone is employed to mimic a significant portion of the surrounding air to create a realistic simulation. This setup is in line with several previous research (Stokkermans et al., 2020; Kim, D. et al., 2021; Li, Y. et al., 2023). It is possible to select a domain that is sufficiently extensive to avoid affecting the results. The stationary fluid zone has a length of 22D and a diameter of 11D. It represents the area where the fluid remains still. The flow field near the propeller is depicted by a cylindrical rotating fluid zone that has a length of 0.4D and a diameter of 1.1D. The geometric center of the rotating region is positioned at 25mm from the inlet side and 20mm from the outlet side. The propeller model is situated within the rotating fluid zone, which moves with the same rotor rotational speed. There are two interfaces present at the interface where the stationary and rotating fluid zones meet. The interface in the rotating fluid zone is referred to as Interface 1, while the other is called Interface 2 (Liu, X. et al., 2022; Gómez-Iradi, S., 2009).

About the boundary conditions, the inlet face of the region of fluid that remains stationary is specified as a pressure inlet. However, no information has been provided on the turbulence intensity and viscosity ratio of the test case.

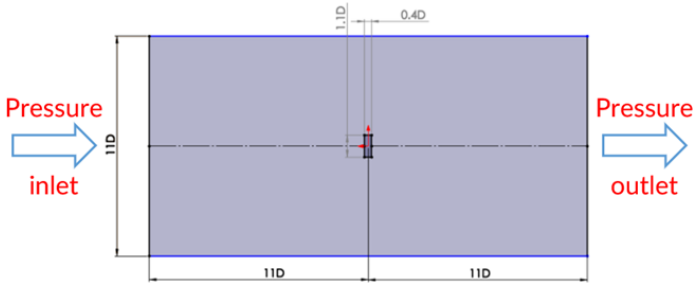

Fig. 3. Computational domain

According to the FLUENT user manual (2019), a turbulence intensity of 5% and a viscosity ratio of 10 have been selected. This selection has been made because the case is an open flow.

The working fluid has a constant density of 1.225 kg/m^3 and viscosity of 1.7894e-05 kg/m.s. The pressure outlet with a static pressure of 0 Pa is defined as the outlet boundary condition. The pressure difference is set to zero as the outlet flows into a continuous free-stream. The four remaining faces are defined as free-slip walls, while the no-slip wall, that surrounds the rotating fluid zone is set as the rotor surface. To prevent any flow through the wall and create a boundary layer, the propeller is subjected to a wall boundary condition, which is set to a no-slip wall. Since the roughness is unknown, the constant is set to 0.5. The objective of these configurations is to simulate a conventional operation environment. The stationary and rotating regions' geometric boundaries are simulated based on several prior CFD analyses (Vargas Loureiro, E. et al., 2021; Garofano-Soldado, A., 2022; Céspedes M., J.F. and Lopez M., O.D., 2019). The sides of the domain have a symmetry boundary condition since the flow is uniform in this area. Since the symmetry boundary condition is far away from the propeller, it should remain unaffected by it and maintain its free-stream properties.

4.2 Mesh Generation and Evaluation

Since the computational domain is partitioned into two zones: the Fluid-Domain and the Rotation-Domain, two meshing methods are applied to two different zones. The Fluid-Domain mesh is generated by using ICEM CFD with blocking technique, a high-quality mesh is created through this method, with the individual mesh elements generated in the form of hexahedral elements. The area of the stationary fluid zone where the rotating fluid zone is situated has a refined mesh near both the distance along the axis and the distance radially from the center. The Fluid-Domain mesh has approximately 1.3 million nodes and elements. Fig. 4a shows the meshing process of the external stationary fluid zone.

The ANSYS meshing tool is used to generate the meshes for the Rotation-Domain - an internal rotating fluid zone. Using this tool is advantageous since it allows for complex geometries to be meshed (Goh, S.C. and Schlüter, J.U., 2016). The Rotation-Domain is segmented into unstructured meshes containing tetrahedral-shaped elements, as shown in Fig. 4 ((b)-(e)). The rotating fluid zone has meshed that become more refined as they get closer to the rotor surface. To capture small flow structures in close proximity to solid walls, the inflation option is employed. The boundary layer is discretized into prism elements, with a growth rate of 1.2 and a maximum of 12 layers, based on similar previous research (Céspedes M., J.F. and Lopez M., O.D., 2019).

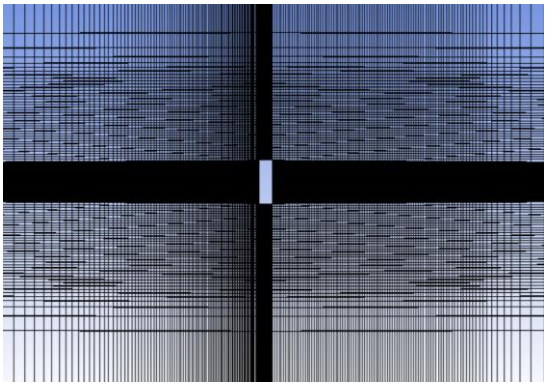

(a)

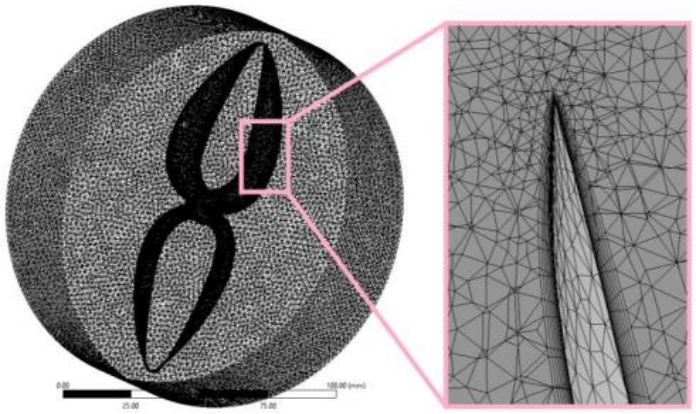

(b)

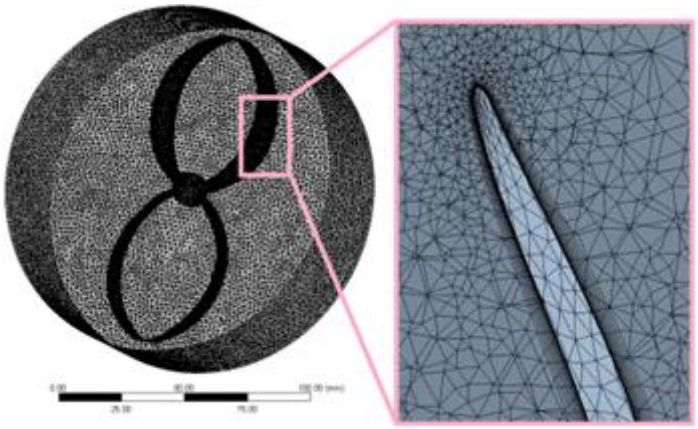

(c)

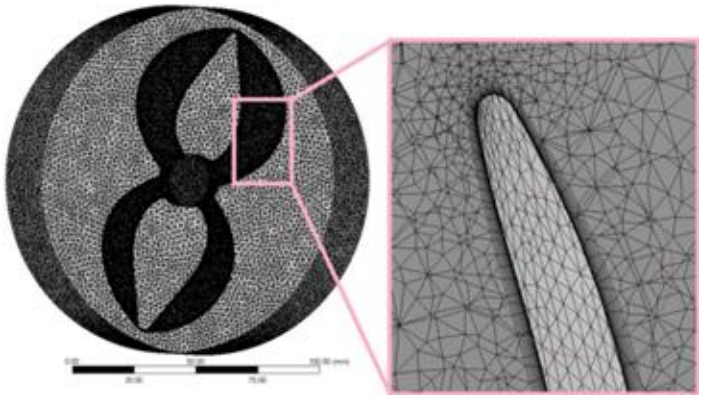

(d)

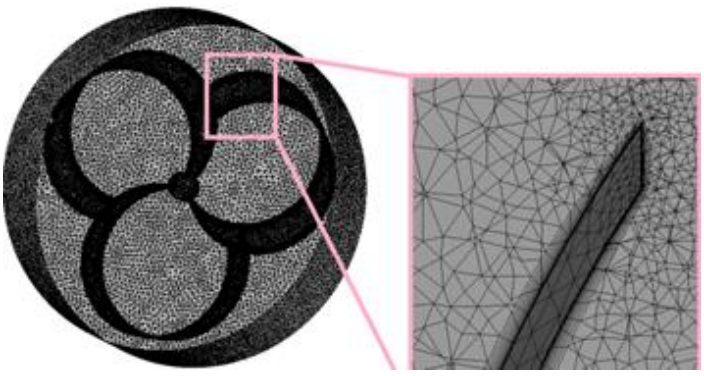

(e)

Fig. 4. (a) Middle Z cut plane of The Fluid-Domain mesh is generated by using ICEM CFD; The internal rotating fluid zone mesh and boundary layers section view of the (b) Bi-loop Toroidal Propeller V1 (c) Bi-loop Toroidal Propeller V2 (d) Bi-loop Toroidal Propeller V3 (e) Tri-loop Toroidal Propeller

For a rotational velocity of 20,000 RPM and a chord length equal to 3/4 of the radius position of the propeller, the initial layer thickness is established at 0.005 mm, which corresponds to an average $y^+ = 3.5$. This ensures that the first grid cell falls within a reasonable range of $1 < y^+ < 5$ (Veríssimo, R., 2016; Ewing, P., 2015). Body meshes are also used in the stationary fluid zone to capture most of the simulation's details, along with surface meshes.

To ensure dependable and precise outcomes while optimizing computational resources, a mesh-independence study is conducted to assess the static performance of the propeller. The study evaluated four sets of mesh refinement for four models. The third and fourth Mesh have approximately 4.1 and 5.0 million elements, respectively, on the finer grid side as shown in Fig. 5 for Bi-loop Toroidal V1; 4.6 and 5.7 million elements for V2; 4.1 and 5.3 million elements for V3; 5.1 and 6.4 million elements for Tri-loop Toroidal Propeller. After comparing the results, we have concluded that Mesh 3 is the optimal choice for further calculations. The reason for this choice is that the Thrust values obtained from Mesh 3 are very close to those obtained from Mesh 4, with differences ranging from 0.27% to 1.65%. By opting for Mesh 3 instead of the fourth Mesh, we significantly reduce computational resources while maintaining the accuracy of the results.

4.3 Solver Settings

The ANSYS-FLUENT is used to perform numerical simulations, employing a shear stress transport (SST) k-ω turbulence model that includes the best features of k-ε and k-ω models. It provides the k-ε model's free-flow liberation away from the wall, and the k-ω model's accurate expression near the wall boundary layer (Pérez G., A.M., 2017).

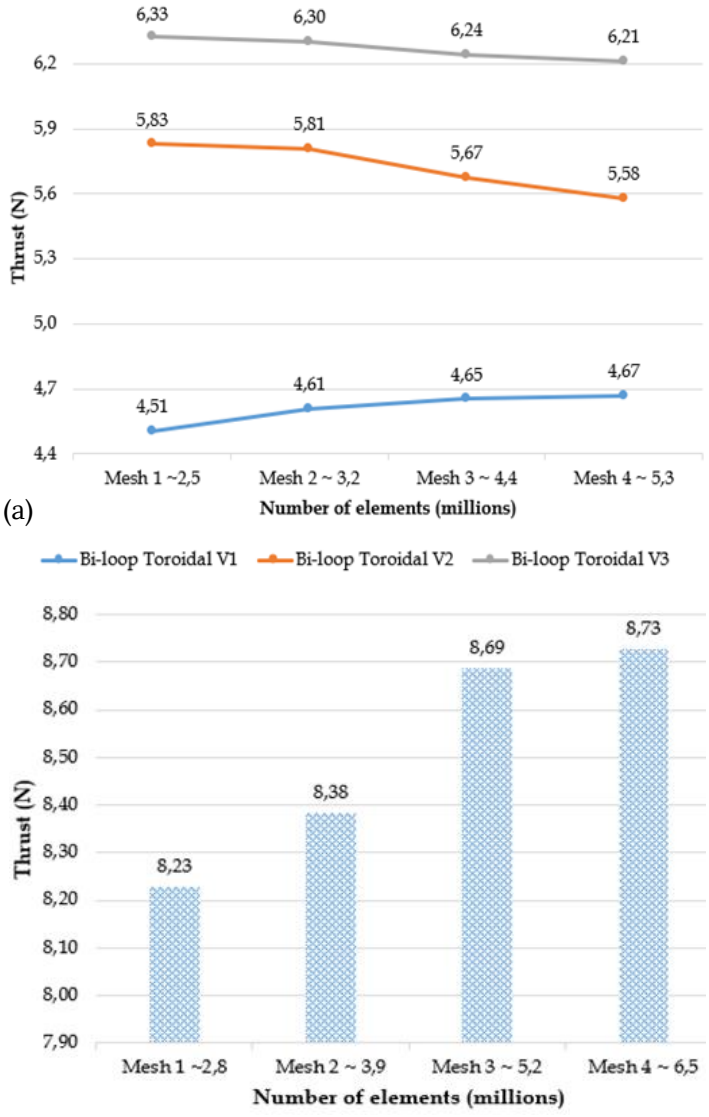

Fig. 5. The comparison between thrust and the number of elements for different types of mesh in the mesh independence evaluation (a) Bi-loop Toroidal Propeller V1-2-3 (b) Tri-loop Toroidal Propeller

Based on initial tests with one foil, the Coupled scheme appears to be a suitable option when dealing with a poor mesh that requires the preservation of coupling between velocity and pressure. The sliding mesh interfaces can cause the mesh to become uncoupled, even though the mesh itself is not problematic. To ensure better accuracy compared to the first order, Second Order Upwind is chosen for the pressure and momentum discretization. According to the FLUENT user manual (2019), second order accuracy is recommended when the flow is not aligned with the mesh. In the case of Toroidal Propeller, the mesh is always rotating, thus it is generally misaligned. The First Order Upwind scheme is selected to discretize the turbulent behaviors in RANS simulations, as shown in Table 1. As these behaviors quickly dissipate, they will not travel through many misaligned cells. In the theory section, it is shown how the local behavior of turbulent properties is contained by applying significant damping to their production.

When setting up the acoustic model, a Broadband Noise Source (BNS) Model is used. In Computational Aeroacoustics (CAA), there are various methods to study the acoustical properties of a system. One such method involves applying a BNS model to a steady-state Reynolds-Averaged Navier-Stokes (RANS) Computational Fluid Dynamics (CFD) to learn about the BNS (Wagner, C. et al., 2007). Insight into the source of broadband noise in BNS models can be gained through the use of statistical turbulence quantities obtained from RANS results, semi-empirical correlations, and Lighthill's acoustic analogy. These source terms can help locate and compare noise sources, indicating that BNS models are effective in identifying the primary regions generating noise in a flow domain. Additionally, they provide a way to compare different design variations, allowing for the screening of noisier options and identification of primary noise sources (Wagner, C. et al., 2007; Stanko, T.S. et al., 2008). BNS model parameters are shown in Table 2.

Simulation conducted on a computer with a CPU of Intel(R) Core(TM) i7-9700 processor featuring 8 cores and 8 processors and took a total of 256 hours for 32 cases. Each case took about 8 hours to complete, including 12 mesh independence evaluation cases and 20 optimization simulation cases.

5. Results and Discussions

5.1 Propeller Performance at Different RPM

Predictions of the propeller's performance in simulations that vary in RPM are shown in the initial findings. Specifically, four models of the Toroidal Propeller were simulated with an RPM-sweep motion, whereby the RPM varies from 10,000 to 20,000. During each timestep, Fluent extracts thrust, velocity, and torque data for each of these models. These parameters, combined with theoretical calculations, yield rotational velocity (ω), power (P), and Power Coefficient (Cp).

The blade geometry changes in the Bi-loop Toroidal Propeller have increased the propeller thrust, with the highest thrust generated by the V3 model at 10,000 rpm. As the rotation speed increases, the difference in thrust between the three Bi-loop models becomes more pronounced, ranging from 1 N to 1.5 N at 20,000 rpm. This is due to the increase in rotor chord length, resulting in a larger aerodynamic area in contact with the air and increasing the camber of the propeller. The Tri-loop Toroidal Propeller generates more thrust than the Bi-loop Toroidal Propeller due to more number of blades, with a significant difference in thrust of about 2.5 N to 4 N.

Table 1. Solver Settings

Parameters	Solution Methods	Model
Solver	Pressure-Base, Steady, Velocity Formulation - Absolute	
Viscous Model	k – ω SST	k: Second Order Upwind ω: First Order Upwind
Pressure velocity – coupling	Coupled	
Momentum		Second Order Upwind
Pressure		Second Order
Turbulent Kinetic Energy		First Order Upwind
Specific Dissipation Rate		First Order Upwind
Gradient		Least squares cell based

Fig. 6 shows that the Bi-loop Toroidal Propeller wing has a wider maximum width in its later version, resulting in an invisible increase in torque.

Table 2.BNS Model Parameters

Far-Field Density (kg/m^3)	1.225
Far-Field Sound Speed (m/s)	340
Reference Acoustic Power (W)	1e-12
Number of Realizations	200
Number of Fourier Modes	50

The Tri-loop Toroidal Propeller wing performs best at 15,000 - 18,000 rpm and a large difference in torque is observed at 20,000 rpm. Also in Fig. 6, we see a gradual increase in torque and power due to the change in wing geometry in the later version. This change also reduces the power coefficient as the rotation speed increases. Additionally, the Tri-loop Toroidal Propeller shows an optimal power coefficient between 15,000 rpm and 18,000 rpm due to the power coefficient formula (1) where Cp is directly proportional to P and inversely proportional to n3 rotation speed.

5.2. Aerodynamic Characteristic Of The Toroidal Propeller

Fig. 7 shows the pressure distribution on the surface of four Toroidal Propeller models that the difference in surface pressure between the body and the edge of the blade creates lift on the wing. A larger pressure difference results in a greater lift force. The three Bi-loop Toroidal models all show that the pressure near the wing tip is larger than the wing hub.

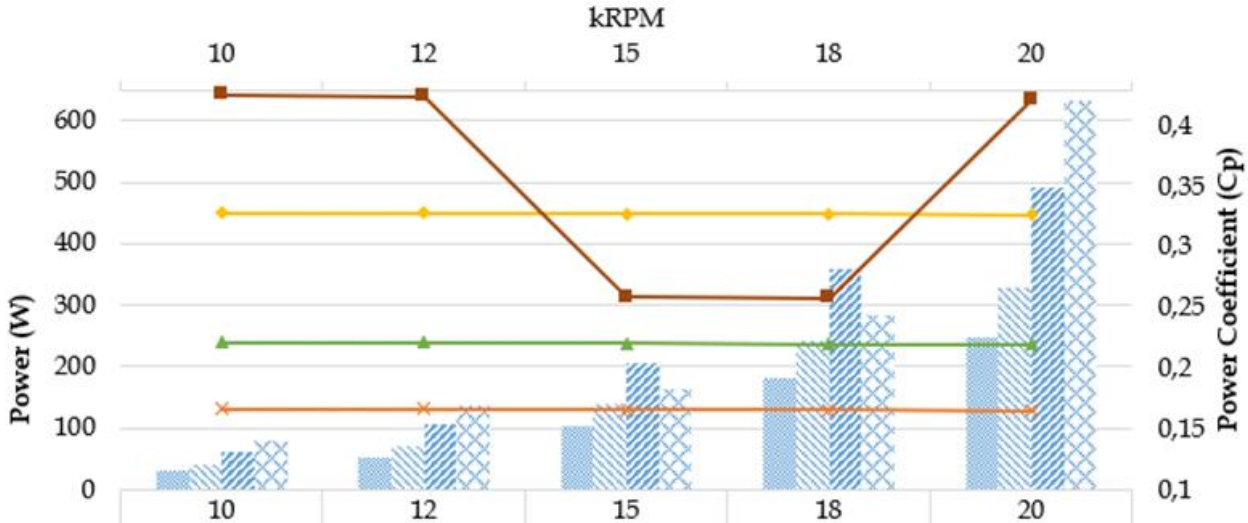

	10	12	15	18	20
Bi-loop V1	31,25	53,94	105,24	181,72	248,29
Bi-loop V2	41,58	71,73	139,7	240,94	330,15
Bi-loop V3	61,62	106,31	207,34	358,02	490,97
Tri-loop	79,82	137,54	164	282,68	632,2
Bi-loop V1	0,16679	0,16661	0,16643	0,1663	0,16564
Bi-loop V2	0,22193	0,22155	0,22091	0,22049	0,22025
Bi-loop V3	0,32885	0,32834	0,32787	0,32764	0,32754
Tri-loop	0,426	0,42479	0,25934	0,25868	0,42176

(a)

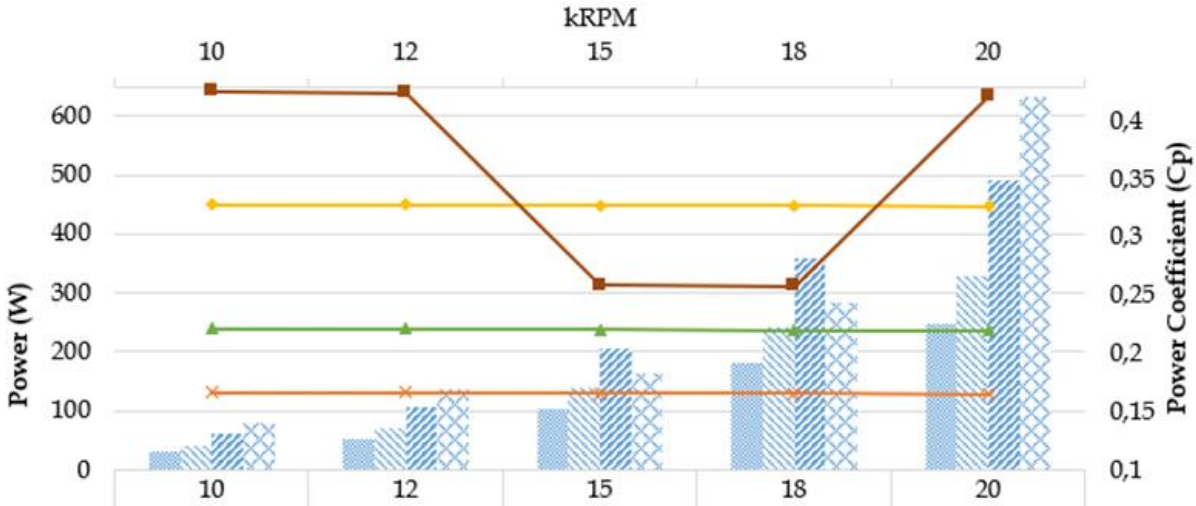

	10	12	15	18	20
Bi-loop V1	31,25	53,94	105,24	181,72	248,29
Bi-loop V2	41,58	71,73	139,7	240,94	330,15
Bi-loop V3	61,62	106,31	207,34	358,02	490,97
Tri-loop	79,82	137,54	164	282,68	632,2
Bi-loop V1	0,16679	0,16661	0,16643	0,1663	0,16564
Bi-loop V2	0,22193	0,22155	0,22091	0,22049	0,22025
Bi-loop V3	0,32885	0,32834	0,32787	0,32764	0,32754
Tri-loop	0,426	0,42479	0,25934	0,25868	0,42176

(b)

Fig. 6. (a) Thrust (column) versus Torque (line), (b) Power (column) versus Power Coefficient Cp (line) of four Toroidal Propeller models which the RPM changes from 10,000 to 20,000.

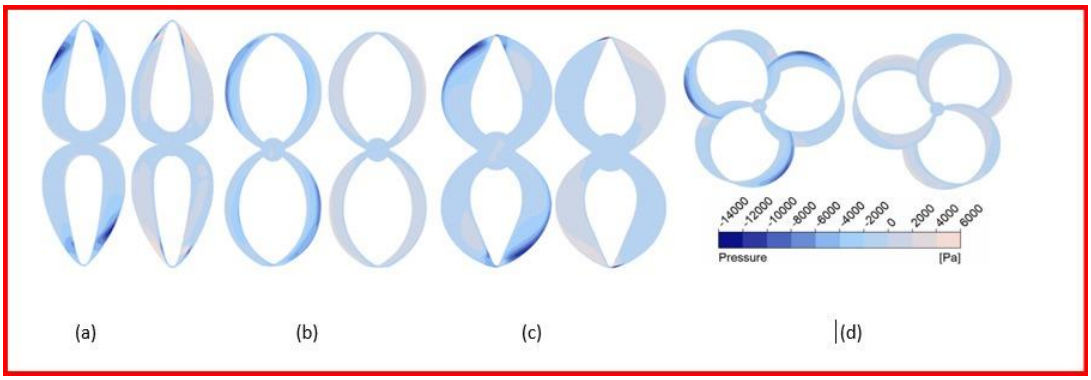

Fig. 7. Distributed application on upper surfaces (Right) and lower surfaces (Left) of (a) Bi-loop Toroidal V1 (b) Bi-loop Toroidal V2 (c) Bi-loop Toroidal V3 (d) Tri-loop Toroidal.

Bi-loop Toroidal Propeller V1 shows that the differential pressure distribution is mainly concentrated near the wing tip, whereas Bi-loop Toroidal Propeller V2 and V3 have a more evenly distributed pressure differential over the entire span wing. This partly explains why Bi-loop Toroidal Propeller V2 and V3 give better results in terms of thrust. As for the Tri-loop Toroidal Propeller, due to the uniform wing cross-sections, the pressure concentrated at the tip is not as obvious as the Bi-loop Toroidal Propeller, but the pressure is spread quite evenly over the entire wing surface.

As shown in Fig. 8, the Toroidal Propeller V1 illustrates the presence of a vortex in the flow outside the blade rotation area, at the hub, and at the wing-tip. This phenomenon occurs due to the high intensity of the vortex at the tip of the blade, which influences the outlet stream. Bi-Loop Toroidal Propeller V2 only generates vortex at the wing-tip, but the intensity is insufficient to impact the outflow, unlike V1. Bi-Loop Toroidal Propeller V3, like V2, only generates a vortex at the wing-tip, which is also insufficient to impact outflow too. Through Fig. 8 the flow lines passing through the cross-sections of the four models, we can see that the Bi-loop Toroidal Propeller V1 had vortex losses in the output stream, however V2 and later versions have corrected this. Comparing between V2 and V3, we can see that the flow path coming out of the propeller of Bi-loop V3 is wider

and larger than that of V2, this explains the thrust generated by the V3 blade is much larger than the two versions. previous model. The streamline passing through the Tri-loop Toroidal Propeller is not symmetrical about the x-axis, unlike the previous three Bi-loop Toroidal models. This is because the Tri-loop model has three blades, resulting in an asymmetrical streamline passing through the cross-section of the propeller. The wing-tip vortices of the three Bi-loop Toroidal models have visibly decreased with each improvement. The first model, Bi-loop Toroidal V1, had severe wing-tip vortices that caused damage to the rotor's outer rotation area. This is due, in part, to the thicker loop shape of the wing-tip section. However, V2 and V3 have overcome this problem by having a thinner loop shape that allows for better aerodynamic flow. The Tri-loop Toroidal model has also significantly reduced vortex intensity due to its geometric design since the Tri-loop Toroidal does not really have wing tips, the structural sections of the wings are made even and looped. together, so that the vortex appears at the leading edge and spreads evenly over the surface of the wing.

The wing-tip vortices of the three Bi-loop Toroidal models have visibly decreased with each improvement. The first model, Bi-loop Toroidal V1, had severe wing-tip vortices that caused damage to the rotor's outer rotation area. This is due, in part, to the thicker loop shape of the wing-tip section. However, V2 and V3 have overcome this problem by having a thinner loop shape that allows for better aerodynamic flow. The Tri-loop Toroidal model has also significantly reduced vortex intensity due to its geometric design since the Tri-loop Toroidal does not really have wing tips, the structural sections of the wings are made even and looped. together, so that the vortex appears at the leading edge and spreads evenly over the surface of the wing.

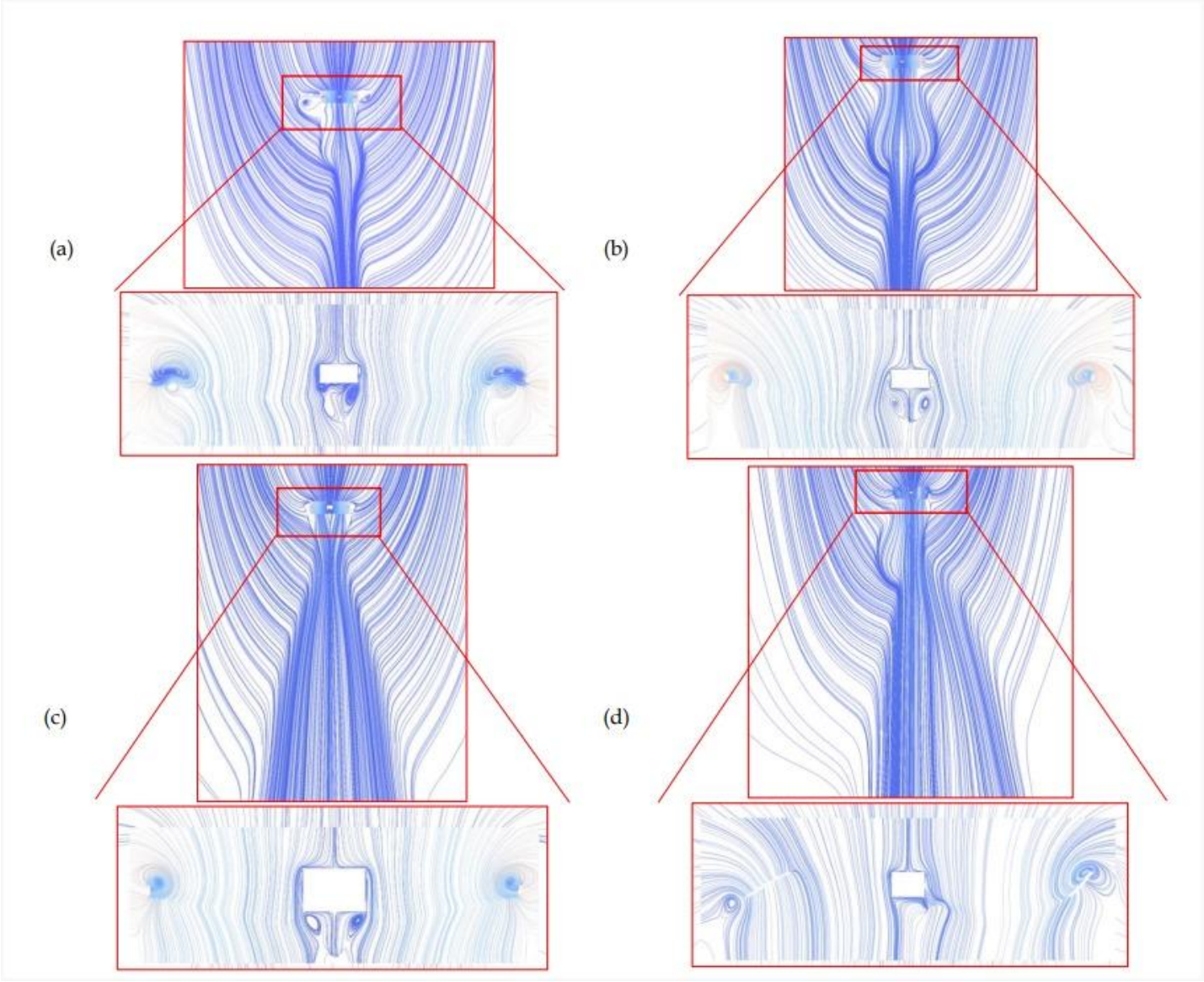

Fig. 8. Section of Streamline through (a) Bi-loop Toroidal Propeller V1 (b) Bi-loop Toroidal Propeller V2 (c) Bi-loop Toroidal Propeller V3 (d) Tri-loop Toroidal Propeller

5.3 Acoustic Characteristic of the Toroidal Propeller

5.3.1 Qualitative results of Surface Acoustic Power Level (dB) and Acoustic Power Level (dB)

According to previous theoretical predictions, Fig. 9 shows that the noise generated by the propeller around the hub region is relatively small and gradually increases towards the wing-tip, reaching its maximum there. However, the peak surface acoustic power level shows signs of gradually increasing from Bi-loop V1 to V3 models. This can be simply explained by the fact that the acoustic power level on the surface of the blade is greatly influenced by the blade geometry.

As the torque increases, the blade experiences greater friction with the air flow, which leads to the gradual increase in the acoustic power level on the surface of the blade. Fig. 10 illustrates the Acoustic Power Level (APL) power distribution directly related to the propeller output flow. For the Bi-loop Toroidal V1 model, the APL distribution is uneven and concentrated around the wing-tip due to the significant vortices created by the propeller, which cause flow disturbance. However, with the improvements made in the Bi-loop Toroidal V2 model, the APL at the wing-tip has significantly decreased.

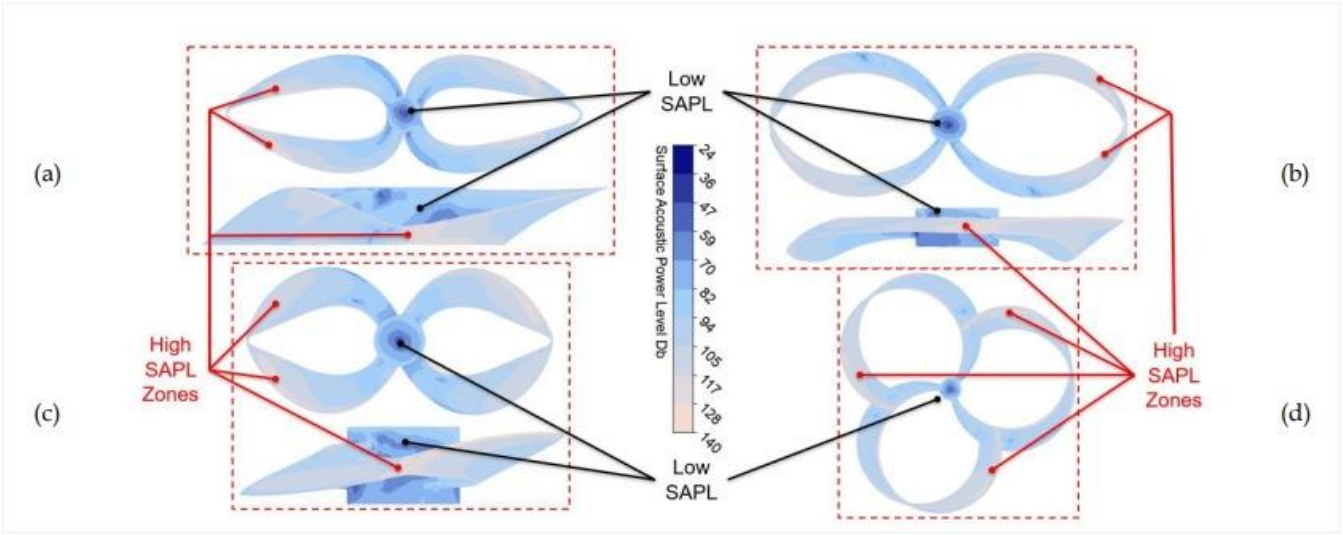

Fig. 9. Surface Acoustic Power Level (dB) (Upper surface) of (a) Bi-loop Toroidal V1 (b) Bi-loop Toroidal V2 (c) Bi-loop Toroidal V3 (d) Tri-loop Toroidal

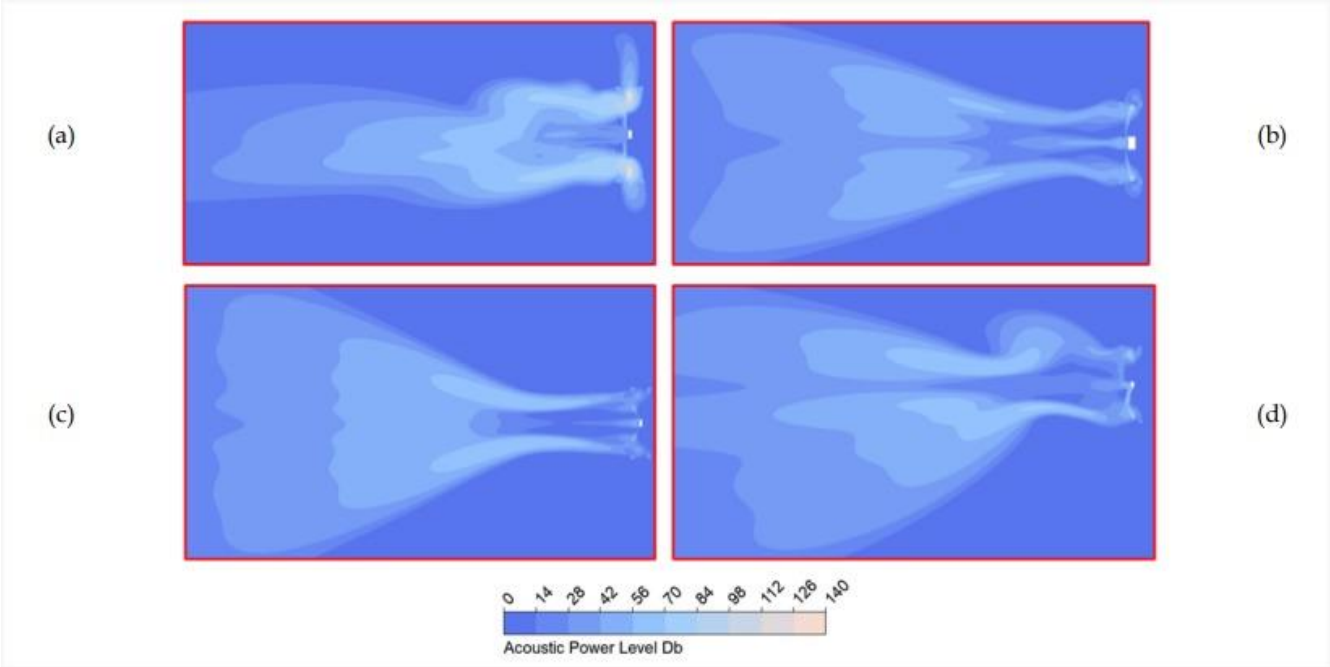

Fig. 10. Acoustic Power Level (dB) on outflow of (a) Bi-loop Toroidal V1 (b) Bi-loop Toroidal V2 (c) Bi-loop Toroidal V3 (d) Tri-loop Toroidal

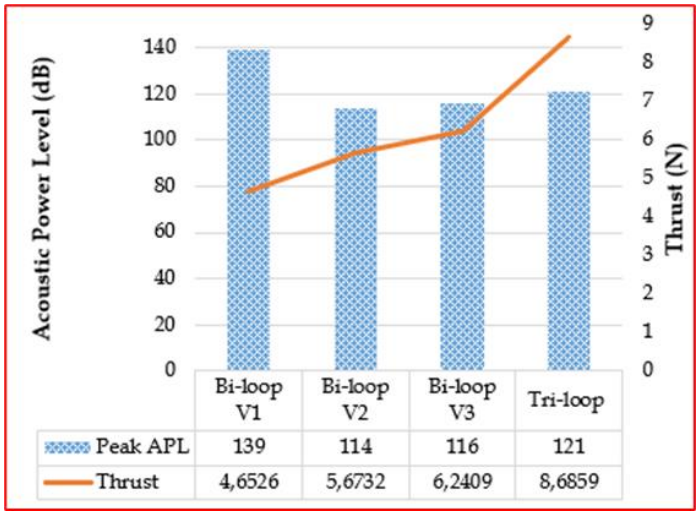

Fig. 11. Peak Acoustic Power Level (dB) versus Thrust (N)

5.3.2 Quantitative Results of Acoustic Power Level (Db)

In Fig. 11, the APL peak has decreased from 139 dB to 114 dB, indicating an 18% reduction in aerodynamic noise compared to the previous model. Similarly, the Bi-loop Toroidal V3 model has also shown improved noise performance, although there is a slight increase of 116 dB compared to 114 dB of V2 (an increase of 1.7%). In return, it offers more optimal propeller thrust performance, which has increased by 9.13%. As for the Tri-loop Toroidal model, although it generates a slightly larger APL peak than the two Bi-loop Toroidal models V3 and V2 (up 4.13% compared to V3 and up 5.79% compared to V2), its thrust created is the most optimal among all four models. This is due to the increased number of blades, resulting in better thrust performance.

6. Conclusions

In this study, four different designs of Toroidal propellers are considered. These designs included a Bi-loop and a Tri-loop Toroidal propellers with different geometric shapes. Two distinct numerical configurations are utilized to evaluate the propeller aerodynamic and acoustic properties. The analysis of performance metrics is based on rotational speed sweeps, while APL data are obtained by using the BNS model, with the propellers spinning at constant RPMs. The results are compared between the four models, and it is shown that the Tri-loop Toroidal propeller provided the most optimal efficiency in terms of both thrust and APL. Among the Bi-loop models, Bi-loop Toroidal V3 produced the most optimal results compared to the two previous Bi-loop Toroidal mockups. This study also confirmed that varying the Toroidal geometries through four versions with different cross-sectional shapes and wing-tips, helped reduce the tip vortices. This stabilized the air flow through the propeller and optimized the thrust and APL generated. Moreover, the numbers in this paper are purely simulation results of Toroidal propeller due to experimental data. Future work will involve experimental studies on the Toroidal propeller model to compare simulation results, optimize the design, and practice different numerical acoustic approaches like the Ffowcs Williams-Hawkings for transient flow solution.

Acknowledgment

This research is funded by the Ministry of Education and Training (MoET) under Project No. B2023-BKA-11, and the cooperation research between HUST, LQDTU and Viettel Aerospace Institute (VTX).

CRediT Author Statement

Vu Xuan-Duc: Software, Validation, Investigation, Writing- Original draft preparation. **Nguyen Anh-Tuan**: Reviewing and Editing. **Nha Tuong-Linh**: Reviewing and Editing. **Chu Hoang-Quan**: Conceptualization, Methodology, Visualization. **Dinh Cong-Truong**: Data curation, Supervision.

Nomenclature

Cp	: Power coefficient
CT	: Thrust coefficient
D	: Propeller diameter (m)
n	: Rotational velocity (rev.s-1)
P	: Power (W)
T	: Thrust (N)
V	: Forward speed (m.s-1)
η	: Efficiency
ρ	: Air density (kg.m-3)

Abbreviations

APL	: Acoustic Power Level
CFD	: Computational Fluid Dynamic
NOB	: Number of Blade
RANS	: Reynolds Average Navier-Stokes
SAPL	: Surface Acoustic Power Level

References

ANSYS. Inc, 2019. ANSYS Fluent User's Manual. Release 2019 R2.

Céspedes M., J.F., Lopez M., O.D., 2019. Simulation and validation of the aerodynamic performance of a quadcopter in hover condition using overset mesh, in: AIAA Aviation 2019 Forum. American Institute of Aeronautics and Astronautics Inc, AIAA.

Chirico, G., Barakos, G.N., Bown, N., 2018. Numerical aeroacoustic analysis of propeller designs. Aeronautical Journal 122, 283–315.

Dantsker, O.D., 2022. Performance Testing of APC Electric Fixed-Blade UAV Propellers, in: AIAA AVIATION 2022 Forum. American Institute of Aeronautics and Astronautics Inc, AIAA.

Demoret, A.C., Wisniewski, C.F., 2019. The impact of a notched leading edge on performance and noise signature of unmanned aerial vehicle propellers, in: AIAA Scitech 2019 Forum. American Institute of Aeronautics and Astronautics Inc, AIAA.

Ewing, P., 2015. Best practices for aerospace aerodynamics, in: STAR East Asia Conference, Singapore.

Garofano-Soldado, A., Sanchez-Cuevas, P.J., ... Ollero, A., 2022. Numerical-experimental evaluation and modelling of aerodynamic ground effect for small-scale tilted propellers at low Reynolds numbers. Aerospace Science and Technology.

Gerr, D., 1989. Propeller Handbook, in: International Marine Publishing.

Goh, S.C., Schlüter, J.U., 2016. Numerical simulation of a Savonius turbine above an infinite-width forward facing step. Wind Engineering 40, 134–147.

Gómez-Iradi, S., Steijl, R., Barakos, G.N., 2009. Development and validation of a cfd technique for the aerodynamic analysis of HAWT. Journal of Solar Energy Engineering, Transactions of the ASME 131, 0310091–03100913

Gur, O., Rosen, A., 2009. Design of a quiet propeller for an electric mini unmanned air vehicle. Journal of Propulsion and Power 25, 717–728.

Kim, D., Lee, Y., ... Park, D., 2021. Aerodynamic analysis and static stability analysis of Manned/unmanned distributed propulsion aircrafts using actuator methods. Journal of Wind Engineering and Industrial Aerodynamics 214.

Klimchenko, V., Baeder, J., 2020. CFD/CSD study of interactional aerodynamics of a coaxial compound helicopter in high-speed forward flight, in: AIAA Scitech 2020 Forum. American Institute of Aeronautics and Astronautics Inc, AIAA.

Krishnamurthy, S., 2021. Remote Psychoacoustic Test for Urban Air Mobility Vehicle Noise Human Response, in: Langley Research Center Hampton, Virginia, United States.

Li, Y., Li, X., ... Zhong, S., 2023. Experimental and numerical investigations on rotor noise in axial descending flight. Physical Review Fluids 8.

Liu, X., Zhao, D., Oo, N.L., 2022. Numerical prediction of the power coefficient improvements of three laterally aligned Savonius wind turbines above a forward-facing step. Journal of Wind Engineering and Industrial Aerodynamics 228.

Marte, J.E., Kurtz, D.W., 1970. A Review of Aerodynamic Noise from Propellers, Rotors, and Lift Fans, JPL Technical Report 32-1462.

MIT Lincoln Laboratory, 2022. Toroidal Propeller.

Misiorowski, M., Gandhi, F., Oberai, A.A., 2019. Computational study on rotor interactional effects for a quadcopter in edgewise flight. AIAA Journal 57, 5309–5319.

Pérez G., A.M., López, O.D., Escobar, J.A., 2017. Computational study of the wake of a quadcopter propeller in hover, in: 23rd AIAA Computational Fluid Dynamics Conference, 2017. American Institute of Aeronautics and Astronautics Inc, AIAA.

Roskam, J., Lan, C., 1997. Airplane Aerodynamics and Performance, in: Airplane Design and Analysis, Design, Analysis and Research Corporation.

Schulz, A., 2023. Development of a Low Noise Drone Propeller Using CFD Simulations. Lund University.

Sebastian, T., Strem, C., 2020. Toroidal Propeller - US Patent (MIT).

Seddon, J., Newman, S., 2011. Basic Helicopter Aerodynamics, Basic Helicopter Aerodynamics. Wiley.

Stanko, T.S., Ingham, D.B., ... Pourkashanian, M., 2008. Computational fluid dynamic prediction of noise from a cold turbulent propane jet, in: Proceedings of the ASME Turbo Expo. pp. 645–652.

Stokkermans, T.C., Van Arnhem, N., ... Veldhuis, L.L.A., 2019. Validation and comparison of RANS propeller modeling methods for tip-mounted applications. AIAA Journal 57, 566–580

Stokkermans, T., Veldhuis, L., ... Eglin, P., 2020. Breakdown of aerodynamic interactions for the lateral rotors on a compound helicopter. Aerospace Science and Technology 101.

Stuermer, A., 2008. Unsteady CFD simulations of contra-rotating propeller propulsion systems, in: 44th AIAA/ASME/SAE/ASEE Joint Propulsion Conference and Exhibit.

Vargas Loureiro, E., Oliveira, N.L., ... de Castro Lemonge,

A.C., 2021. Evaluation of low fidelity and CFD methods for the aerodynamic performance of a small propeller. Aerospace Science and Technology 108.

Veríssimo, R., 2016. Best Practice Guidelines in External Aerodynamics CFD: Applied to Unmanned Aerial Vehicles at Cruise Conditions, in: Doctoral dissertation, Academia da Forc¸a Aérea.

Wagner, C., Hüttl, T., Sagaut, P., 2007. Large-eddy simulation for acoustics, Large-Eddy Simulation for Acoustics. Cambridge University Press.

Wisniewski, C.F., Byerley, A.R., ... Liller, W.R., 2015. The influence of airfoil shape, tip geometry, reynolds number and chord length on small propeller performance and noise, in: 33rd AIAA Applied Aerodynamics Conference. American Institute of Aeronautics and Astronautics Inc, AIAA

Wisniewski, C.F., Byerley, A.R., ... Wisniewski, N., 2015. Experimental evaluation of open propeller aerodynamic performance and aero-acoustic behavior, in: 33rd AIAA Applied Aerodynamics Conference. American Institute of Aeronautics and Astronautics Inc, AIAA.

Wisniewski, C.F., Treuren K.V., 2022. Novel UAS propeller design part I: using an unloaded tip to reduce power requirements and lower generated sound levels for propellers designed for minimum induced drag, in: Proceedings of ASME Turbo Expo 2022 Turbomachinery Technical Conference and Exposition, pp. GT2022-81579.

Wu, Y., Ai, Y.T., ... Chen, Y., 2019. A Novel Aerodynamic Noise Reduction Method Based on Improving Spanwise Blade Shape for Electric Propeller Aircraft. International Journal of Aerospace Engineering 2019.

International Journal of Aviation Science and Technology

Research Article

Navigating the Work Passion and Safety Behavior Examining the Role of Safety Locus of Control in the Aviation Sector

İnan Eryılmaz[1], Tugay Öney[2*], Yeşim Tüm Kılıç[3], Tuğba Erhan[4]

[1] *Suleyman Demirel University, School Civil Aviation, Department of Aviation Management, Isparta, Türkiye*
inaneryilmaz@sdu.edu.tr - 0000-0001-8307-2402

[2] *Nevsehir Hacı Bektas Veli University, Institute of Social Sciences, Department of Business, Nevsehir, Türkiye*
tugay128@hotmail.com - 0000-0003-2883-5889

[3] *Nevsehir Hacı Bektas Veli University, Institute of Social Sciences, Department of Business, Nevsehir, Türkiye*
yesim.9444@gmail.com - 0000-0001-9897-8119

[4] *Suleyman Demirel University, Faculty of Economics and Administrative Sciences, Department of Business, Isparta, Türkiye*
tugbaerhan@sdu.edu.tr - 0000-0002-5697-490X

Abstract

"Safety" is a very essential factor in human-technology interaction in the aviation industry. There are limited number of studies on determining the strong emotions and motivations that improve the safety behavior perceptions of employees under intense workload and stress in the aviation industry, that cares about the importance to compliance with developing information, communication and security technologies. The aim of the research, which focuses on filling this gap in findings, is to reveal the effect of work passion levels of aviation industry employees on their perception of safety behavior and to determine whether safety locus of control plays a mediating role in this relationship. The research sample consists of employees working in different departments in the Turkish civil aviation industry (n = 541). After confirmatory factor analysis was performed to test the model and hypotheses of the research, Medmod macro was used to test multiple regression analysis and indirect effects. Research findings demonstrate that engaging in harmonious passion is a positive predictor of safety behavior. On the other hand, it was found that obsessive passion did not affect safety behavior. Additionally, it was observed that internal locus of control had a full mediating role in the relationship between harmonious passion, obsessive passion, and safety behavior. On the other contrary, it was determined that external locus of control did not play a mediating role in the relationship between harmonious passion, obsessive passion and safety behavior. Inferences were made from the research findings, research limitations were highlighted, and suggestions for the sector and future research were presented.

Keywords

Work Passion
Safety Locus of Control
Safety Behavior
Aviation Sector

Time Scale of Article

Received 13 November 2023
Revised until 22 March 2024
Accepted 17 April 2024
Online date 21 June 2024

1. Introduction

Work passion, which is an intense form of psychological emotions and motivation, is a primary motivational force that leads people to spend time achieving high competence and perfecting their skills in a particular activity (Vallerand, 2008) and (Ahn, Back, and Lee, 2019). On the other hand, work passion is considered a

*: Corresponding Author Tugay Öney, tugay128@hotmail.com
DOI: 10.23890/IJAST.vm05is01.0103

motivational structure from an organizational perspective that includes both emotional and cognitive components (Kong and Ho, 2018). Vallerand et al. (2003) examine the concept of work passion as harmonious and obsessive in two dimensions. While harmonious passion is characterized by self-directed motivation, obsessive passion is defined by controlled motivation, an individual continues the job depending on unexpected situations, pressures, or consequences (Smith et al., 2023). Contemporary organizations have regular attempts and efforts to increase employees' commitment and work passion; however, it may be challenging to take action and examine the effects of work passion on employees' behavior due to the motivational structure contained in the phenomenon of passion that is important in terms of allowing new interpretations and judgments about various situations. Dokuman and Akıncı (2001: 94) state that safety and human factors, specifically in the aviation sector, can be in coordination and gain meaningful power when integrated to reduce flight-related hazards and risks and keep them at an optimum level. In addition, work passion, which emotionally impacts behavior, is an essential determinant of employees' attitudes, perceptions, and social norms, such as organizational citizenship and proactive safety behaviors. Based on these policies, in cultures where uncertainty avoidance (Gladwin, 1981), which indicates a lack of tolerance for uncertainty and ambiguity, is high, organizational employees are tense, while in cultures where uncertainty avoidance is low, organizational employees are more comfortable. Therefore, it can be said that the existence of hierarchical rules in the aviation sector facilitates safety behavior by avoiding uncertainty.

Safety behavior encompasses supporting safety protocols for newly participated employees, assisting others to do their jobs safely, and offering safety-related advice. However, safety behaviors reflect more voluntary individual behaviors by managers and employees acknowledged in job descriptions or formal reward systems. Therefore, they are often seen as unique, unusual, and challenging practices (Grant et al., 2009). Safety behavior is discussed in two dimensions: compliance and participation, consistent with the latest theoretical safety performance models (Griffin and Neal, 2000; Hofmann, Morgeson, and Gerras, 2003). Neal and Griffin (2006) describe safety compliance as the activities carried out by members of an organization to ensure workplace safety, while safety participation is defined as the actions that organizational members frequently take to develop a safe environment.

Although implementing safety practices and processes is crucial in the aviation sector, employees' perceptions of these processes are equally critical (Eryılmaz et al., 2019). Since the safety phenomenon in the aviation system is a dynamic feature, safety-related risks must be constantly reduced. Keeping the safety risks under control is crucial as aviation has an open and active system that can balance production and protection (ICAO, 2013). All employees working in different units of the aviation industry have essential responsibilities in keeping safety risks under optimal control level. However, employees' perceptions of safety may differ depending on many reasons. Locus of control is how individuals perceive their behaviors, situations they experience, and consequences of other life events that can be controlled with personal effort. It is related to expectations regarding future events (Jones and Wuebker, 1993) and (Özgener and Ulu, 2018). Individuals' perception of safety may have negative effects. When the statistical summary of aircraft accidents in global operations is examined, the fact that 39% of the fatal accidents that occurred between 1999 and 2008 were reported to be due to loss of control during flight (Boeing Airplane Company, 2008) reveals the need to improve the perceptions of aviation sector employees regarding the locus of control.

It is evaluated that it will contribute to the literature on compliance with safety behavior within the scope of safety-related organizational citizenship behavior against many dangerous and risky situations that employees with work passion encounter in organizations (Fugas et al., 2011). In this study, the following questions were addressed: How and in what direction do the dimensions of work passion impact safety behavior in the Turkish civil aviation sector? Does it make any difference/change in work passion dimensions on safety behavior with the safety locus of control? Hence, this research targets to investigate work passion among aviation sector employees, which is crucial for ensuring flight safety, revealing their perceptions of safety behavior. Although the relationships between passion dimensions and many organizational and individual level behaviors are extensively discussed in the literature, studies examining the relationship between work passion dimensions and safety behavior in the aviation industry are quite limited. However, the fact that the role of the safety locus of control variable, which may be effective in the relationship between these two variables, has not been examined constitutes the originality of current study.

1.1. Work Passion

Passion is a robust predisposition tendency toward an activity or work the person likes, values, and feels identified with spending time and energy (Houlfort et al., 2015). It regulates emotional reactions to accomplish tasks that sustain or foster constructive emotions (Pollack et al., 2020). Furthermore, passion is an intense emotional state that strengthens the mind and motivates the individual to create new ideas/goals, gives a sense of purposefulness, contributes to the commitment to the

activity, and makes a lasting and significant impact on the behavior (Pathak and Srivastava, 2020). Work passion exists within the framework of a particular activity, and it becomes a part of a person's identity, transforming motivational power that includes a constant love for a work activity and making the training valuable and meaningful (Smith et al., 2023).

The foundations of the phenomenon of work passion are based on the SDT by Deci and Ryan (1985). Competence, autonomy, and relatedness are psychological needs (Hodgins and Knee, 2002, p. 87; Ho et al., 2018, p. 114–115). Deprivation of these three basic needs harms motivation and well-being (Ryan and Deci, 2020). Precisely, the satisfaction of these three psychological needs and the behaviors that constitute the input of tendencies and development toward an activity can be in the form of intrinsic or extrinsic motivation (Deci and Ryan, 1985). The autonomy-control continuum is a central dimension that distinguishes motivation types within SDT. Behaviors described as controlled in SDT are behaviors in which the individual feels under external or internal pressure or forced to act. Intrinsically motivated behaviors, on the other hand, are performed out of interest, and the primary "reward" is the spontaneous feelings of impact and pleasure accompanying the behaviors. Intrinsic motivation differs from extrinsic motivation, which involves behaviors aimed at achieving a distinct external outcome, such as receiving an extrinsic reward or social approval, avoiding punishment, or performing a valued outcome (Ryan and Deci, 2017).

In the Dualistic Model of Passion by Vallerand et al. (2003), harmonious and obsessive passion differ significantly in their relationships with cognitive, emotional, and motivational results (Curran et al., 2015, p. 632). Individuals with harmonious passion freely and willingly consider their work as personally meaningful, regardless of circumstances, and can participate in their professional activities in an open, flexible, and conscious way that allows for positive experiences (Houlfort et al., 2015), (Ali et al., 2020) and (Astakhova et al., 2022). Obsessive passion is characterized by individuals internalizing controlled and compelling work activities, creating a relational or internal pressure to engage in these work activities. Employees exposed to such internalization or pressure feel that they "cannot stop themselves from engaging in passionate activity" because the excitement resulting from participation in the activity becomes uncontrollable. This situation increases the possibility of employees experiencing conflicts with other aspects of life, causing them to feel frustrated when they do not participate in their professional activities and which makes it impossible to revitalize and recharge one's cognitive, emotional, and behavioral repertoire (Vallerand et al., 2003), (Houlfort et al., 2015), (Ali et al., 2020) and (Tu et al., 2023). In other words, obsessive passion produces negative consequences and reduces positive emotional experiences (Gülbahar and Özkan, 2023).

1.2. Safety Behavior

Safety is one of the top priorities of the aviation sector. The reason for this is that accidents are inevitable as a result of any compromise made in safety. Human resources experts and researchers believe 70% to 80% of aviation accidents can be attributed to a human factor within the causal chain (Shappell and Wiegmann, 1996). Silitonga et al. (2022) found that in the Indonesian civil aviation institution, the primary cause of aircraft accidents was 75% due to the human element. This determination highlights the human factor, the reasons for accidents and the failure to comply with several procedural aspects, which are the primary operating systems of the aviation sector. Therefore, in reducing accidents in the aviation sector, it becomes necessary to attach importance to regulatory policies and behaviors regarding safety issues to direct the human factor effectively. On the other hand, policies, resources, and process practices related to safety behavior require particular effort and time. If this effort and time cannot be provided, employees may experience presenteeism in the workplace as they feel unsafe at work (Öney et al., 2022). Therefore, investigating the safety factor that impacts employee behavior is even more critical regarding sustainability and continuity in the workplace.

Neal and Griffin (1997) developed the concept of safety behavior in a two-dimensional model that distinguishes between task and contextual performance. Safety compliance is "adhering to safety procedures and safely performing work." Safety participation involves "assisting co-workers, promoting the safety program in the workplace, showing initiative, and making efforts to improve safety in the workplace," which helps develop supportive environment participation (Neal, Griffin and Hart, 2000).

Organizational dehumanization (Caesens and Brison, 2023), organizational security (Liu et al., 2020), organizational support (Liu, Yang, and Mei, 2021), and organizational citizenship behavior (Maryam et al., 2021) are among the topics that are studied in the organizational behavior literature associated with the concept of safety behavior. In the studies conducted on the aviation sector sample, safety behavior is related to organizational trust and organizational commitment (Liu, Yang, and Mei, 2021), organizational safety climate (Maneechaeye and Potipiroon, 2022), and self-efficacy (Chen and Chen, 2014). It is assumed that aviation sector employees with harmonious passion will proactively engage in safety-related actions, therefore it is evaluated that individuals with obsessive passion are expected to be less inclined to participate in these actions due to

their insistent attitude towards perfectionism in the assigned tasks. Ali et al. (2020), in their study examining the relationship between spiritual leadership and employees' safety performance and the role of harmonious safety passion in this relationship 305 supervisors and employees, found that harmonious safety passion mediates the positive relationships between spiritual leadership and employees' safety compliance and participation. Considering the results of the study conducted by Chen (2021: 6), which examined the effect of work passion on safety behavior in a sample of Taiwanese aircraft maintenance technicians working in five national airline companies, it has been determined that obsessive passion affects safety compliance and safety participation behaviors significantly and negatively, whereas harmonious passion affects both types of safety behaviors significantly and positively. The study conducted by Wu et al. (2023) on Chinese airline pilots revealed a positive and significant relationship between harmonious safety passion and safe behavior. Based on the relevant literature, the following hypotheses have been put forward:

Hypothesis 1: Harmonious passion positively predicts safety behavior.

Hypothesis 2: Obsessive passion negatively predicts safety behavior.

1.3. Safety Locus of Control

Aviation safety and security have been the center of attention and the most crucial concern perceived by the aviation industry. Safety is "the condition in which the probability of giving harm to people or property damage that is reduced to an ongoing identification and the level of risk management and how it is maintained at the same level or below that level" (ICAO, 2013).

The concept of locus of control was structured within the Social Learning Theory, first discussed in Julian B. Rotter's (1954) work titled "Social Learning and Clinical Psychology," and it was used to determine the center of responsibility in behavioral control (Gül and Beyşenova, 2018). Locus of control is people's belief about what controls the events they experience. It is related to attributing the rewards people obtain or success and failure to a result of the person's attitudes and behaviors or factors such as luck and fate beyond their control (Özgener and Ulu, 2018). Rotter (1966) developed the generalized expectancy measure, often called LOC reveals the perceived personal control structure (Hunter and Stewart, 2012,). Rotter (1966) discussed the locus of control in two sub-dimensions: internal locus of control and external locus of control. Individuals who are internally focused on control are more creative, attributing the events that happen to their own mental abilities, effort, and resilience (Küçükkaragöz, 2020). External part of control often feel mercy toward circumstances through their lives because they attribute both causes and solutions (Heinström, 2010). At the same time, individuals with an "Intrinsic" safety locus of control orientation (e.g., high safety consciousness) expect an unforeseen association between individual movements and any accidents or damages to be potentially experienced (Jones and Wuebker, 1993).

Locus of control is an essential determinant of safety-related issues. An internal orientation is often considered safer attitudes (Chittaro, 2014). Wichman and Ball (1983), looking at the results of their study of 200 general aviation pilots, showed that aviators have a significantly higher internal locus of control than the general US population and will exhibit strong self-serving biases concerning their skill level and safety. Hunter (2002) employed the safety locus of control scale to address the internality-externality structure among pilots. As a result of the research, pilots with higher internal orientation experienced less dangerous aviation events than pilots with external orientation. Similarly, Hunter and Stewart (2012) in their study examining the relationship between locus of control and accident involvement among aviation employees in the US Army, observed that aviators with a higher internal locus of control experienced fewer accidents than those with a lower locus of control. In light of these findings, it is seen that the concept of safety directly and indirectly impacts accidents and incidents in the aviation sector.

However, You et al. (2013), in their study on 193 commercial airline pilots at China Southern Airlines, found that internal locus of control directly affects safe operation behaviors. Zhu et al. (2022), in their study on a sample of 597 mine workers, found that the safety locus of control affects adaptation and safety. Their findings revealed that it did not have a moderation effect. The following hypotheses are established according to the relevant literature:

Hypothesis 3: Internal locus of control mediates between harmonious passion and safety behavior.

Hypothesis 4: External locus of control mediates between harmonious passion and safety behavior.

Hypothesis 5: Internal locus of control mediates between obsessive passion and safety behavior

Hypothesis 6: External locus of control mediates between obsessive passion and safety behavior.

2. Method

The study includes a population of employees in the Turkish Civil Aviation sector. However, due to the lack of opportunity to reach all employees in the aviation sector in Türkiye and the time and budget constraints encountered during the data collection phase, it was evaluated as appropriate to use the sample selection

method in the research. 541 survey forms were returned from 657 surveys distributed to aviation industry employees. The response rate of the surveys was 82%. Considering similar studies, this rate seems sufficient to represent the sample (Chen, 2021), (Zhu et al., 2022).

The reason why aviation industry employees were chosen as a sample is that there is a need to examine the factors affecting the perceptions of safety behavior, which plays a key role in flight operations in the aviation industry, where human relations, information technologies, and innovative applications interact with each other. This is due to the importance of preserving a qualified workforce and effectively managing employee behavior in the aviation sector. The researchers conducted the data collection activity between 22 June and 12 October 2023 after receiving the approval of the Süleyman Demirel University Social and Human Sciences Ethics Committee dated 21.06.2023 and numbered 139/9. In the survey form prepared within the scope of the research, participants were asked questions including demographic variables considered to encompass gender, age, marital status, education level, work experience, and occupational position, as well as research scales. This research aims to examine the effect of work passion levels of aviation sector employees on their perceptions of safety behavior and investigate the mediating effect of safety locus of control.

2.1. Measurement Tools

In this research, in which the survey technique was adopted, the data were obtained through a questionnaire containing the work passion scale, safety locus of control scale, safety behavior scale and demographic characteristics of the participants. The data obtained from the participants were analyzed using IBM SPSS 25 and Jamovi 2.3.28 statistical programs. The detailed information about the scales used in this study are given as follows:

***Work Passion Scale*:** "Work Passion Scale" developed by Vallerand et al. (2003) was used to determine the work passion levels of employees in the aviation sector. The work passion scale is a 5-point Likert and consists of 14 items (1 = Strongly Disagree; 5 = Strongly Agree). The work passion scale has two dimensions: harmonious passion (7 items) and obsessive passion (7 items). In addition, the validity and reliability of the Turkish version of the work passion scale was tested by Kelecek and Aşçı (2013). As a result of CFA, the two-factor structure of the scale was confirmed without removing any items. The goodness of fit values for factor analysis are $\chi 2/df=4.586$, RMSEA=0.081, CFI= 0.93, TLI= 0.91. Cronbach Alpha of the harmonious passion subscale was 0.87, and it was 0.82 for obsessive passion.

***Safety Behavior Scale*:** The "Safety Behavior Scale" developed by Neal et al. (2000) revealed the safety behavior perceptions of employees in the aviation sector. This scale is a 5-point Likert type and consists of 6 items (1 = Strongly Disagree; 5 = Strongly Agree). The safety behavior scale has two subscales: Safety compliance (3 items) and safety participation (3 items). The goodness of fit values for the two-factor structure of the safety behavior scale are $\chi 2/df=2.716$, RMSEA=0.056, CFI= 0.99, TLI= 0.98. In this study, the reliability coefficient of the safety compliance scale was 0.84, and the reliability coefficient of the safety participation scale was 0.80. Cronbach Alpha (internal consistency) coefficient for the entire scale was determined to be 0.86.

***Safety Locus of Control Scale*:** "Aviation Safety Locus of Control Scale" was developed by Hunter (2002) to measure aviation sector employees' safety locus of control tendencies. The 5-point Likert scale consists of 20 items (1 = Strongly Disagree; 5 = Strongly Agree). The goodness of fit values for the factor analysis, in which the two-dimensional structure of the scale was confirmed in the same way, was found to be $\chi 2/df=4.045$, RMSEA=0.079, CFI= 0.94, AGFI= 0.90. The reliability coefficients of the subdimensions of the scale were determined as internal locus of control 0.85 and external locus of control 0.82.

2.2. Research Model and Data Analysis

In line with the literature, the basic assumption of the study is that harmonious and obsessive passion, which are dimensions of work passion, will impact safety compliance and participation, which are dimensions of safety behavior. It is thought that the safety locus of control sub-dimensions will mediate between work passion and safety behavior (Fig. 1).

The data of this research was obtained from employees working in public and private organizations in the Turkish civil aviation sector. In this study, missing data was first imputed. Following this, since the number of surveys was over 200, Skewness and Kurtosis values were checked to test the normal distribution assumption of the data. According to the research findings, skewness values are in the range of -.909/.932, and kurtosis values

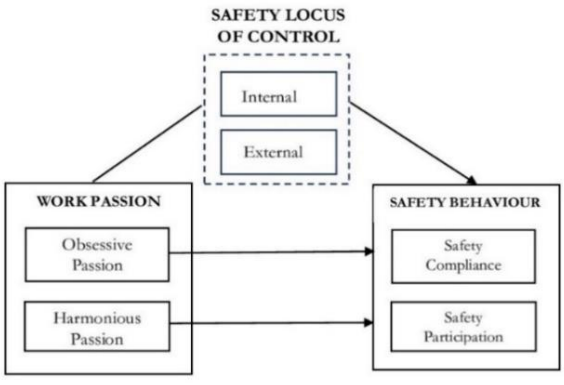

Fig. 1. Research Model

are in the range of .035/1.813. Since the skewness values are below ±3 and the kurtosis values are below ±7, it can be stated that the data set is normally distributed (Kline, 2011), (Tabachnick and Fidell, 2013).

Confirmatory factor analysis (CFA) and multiple linear regression analysis were used to test these models and hypotheses, and the Medmod macro in the Jamovi program was used to reveal the effects of the mediator variable.

3. Results and Discussion

The data of the demographic characteristics of the sample included in the study (n=541) demonstrating gender, age, marital status, education level, work experience, and position are as follows.

106 (19.6%) of the aviation sector employees were female, and 435 (80.4%) were male. When the participants' marital status is analyzed, it is seen that 59.9% are married, 39.2% are single, and 0.9% do not specify their marital status. When the education level of the participants is analyzed, it is seen that 72.2% of them have undergraduate and postgraduate education. When the age class distribution of the employees in the aviation sector is analyzed, it is observed that 68.2% of the respondents are between the ages of 26-41. The average work experience of the respondents is approximately 9 years. It is observed that almost half of the respondents have work experience between 1-5 years. Finally, when the participants' positions in the study are examined, it is seen that 62.2% of them consist of pilots, cabin attendants, aircraft maintenance technicians, flight operations officers, ARFF officers, and air traffic controllers, who have a direct relationship and influence on flights.

When the correlation analysis results in Table 2 are examined, it was observed that there were significant relationships between harmonious passion (r=,500; p<0.01) and obsessive passion (r=,344; p<0.01).

In addition, it has been revealed that there is a statistically positive and significant relationship between harmonious passion, one of the work passion dimensions, and safety compliance (r=,465; p<0.01) and safety participation (r=,439; p<0.01), which are the safety behavior dimensions. Similarly, a positive and significant relationship was found between obsessive passion, one of the work passion dimensions, and safety compliance (r=,231; p<0.01) and safety participation (r=,378; p<0.01), which are the safety behavior dimensions. Finally, it was determined that there was a positive and significant relationship between internal locus of control and safety behavior (r=,242; p<0.01).

As seen in Table 3, the model in which work passion dimensions (harmonious passion, obsessive passion) included is statistically significant (R^2 =0.252; $F_{(2-538)}$=91.800; p<.001). This model explains 25.2% of the total variance in safety behavior. In the model, it was observed that harmonious passion had a statistically positive and significant effect on safety behavior (β = .314 p<.001), while obsessive passion had a positive but non-significant effect (β = .052 p>.05), thus, H_1 hypothesis was supported, while H_2 hypothesis was rejected.

Table 1. Findings Related to the Demographic Characteristics of the Participants Once

Demographic Characteristics	f	(%)	Demographic Characteristics	f	(%)
Gender			**Work Experience**		
Female	106	19.6	1 to 5 years	241	44.6
Male	435	80.4	6 to 10 years	107	19.8
Marital Status			11 to 15 years	83	15.3
Married	324	59.9	16 years and over	110	20.3
Single	212	39.2	**Your Position at Workplace**		
Do not want to specify	5	0.9	Apron Traffic Officer	25	4.6
Education Level			Flight Operations Officer	34	6.3
High School	14	2.6	Administrative Affairs Clerk	10	1.8
Vocational School	136	25.2	Aircraft Maintenance Technicians	77	14.3
Faculty	328	60.6	Air Traffic Controller	53	9.8
Master's Degree/Doctoral Degree	63	11.6	Passenger (Guest) Services Officer	51	9.4
Age			ARFF Officer	53	9.8
25 years and below	53	9.8	Dispatcher	29	5.4
26-33 years old	221	40.7	Pilot	61	11.3
34-41 years old	149	27.5	Load Master	15	2.8
42-49 years old	98	18.1	Cargo Officer	18	3.3
50 years and over	22	3.9	Security Officer	11	2.0
			Cabin Attendant	58	10.7
			Other	46	8.5

Table 2. Descriptive Statistics and Intercorrelations Among Study Variables

Variables	Mean(x̄)	Sd.	1	2	3	4	5	6	7
1. HP	4.01	.665	(0.87)						
2. OP	2.85	.765	.574**	(0.82)					
3. ILOC	3.88	.514	.158**	.148**	(0.85)				
4. ELOC	2.61	.608	.087*	.108*	-.095*	(0.82)			
5. SC	4.60	.473	.465**	.231**	.183**	-.023	(0.84)		
6. SP	4.26	.556	.439**	.378**	.248**	-.014	.627**	(0.80)	
7. SB	4.43	.464	.500**	.344**	.242**	-.020	.242**	.885**	(0.86)

HP: Harmonious Passion, OP: Obsessive Passion, SC: Safety Compliance, SP: Safety Participation, SB: Safety Behavior
ILOC: Internal Locus of Control, ELOC: External Locus of Control
*p<0.05, **p<0.01, Values in parentheses are Cronbach Alpha coefficients.

In the study, indirect effects were analyzed with the Medmod macro in the Jamovi statistical analysis program. This research used the Jamovi statistical analysis program Medmod plug-in to conduct a mediator effect analysis. For the regression (mediator effect analysis) analysis performed with the indirect effect approach based on this bootstrap technique, bootstrap coefficients were calculated with 1,000 resampling options at a 95% confidence interval (Hayes, 2009). Table 4 presents the results of the research's total, direct, and indirect effects as the independent variable's harmonious passion, the dependent variable's safety behavior, and the internal locus of control of the mediating effect.

When the mediating effect of internal locus of control between harmonious passion and safety behavior is examined in Table 4, it was determined that the 95% confidence interval Bootstrap estimates for the indirect effect were between 0.00788 and 0.0315. When there is no zero (0) in the 95% confidence interval, it is accepted that the indirect effect differs significantly from zero (0) at the p<0.05 significance level. Therefore, it is understood that the internal locus of control mediates between harmonious passion and safe behavior, and the H_3 hypothesis is supported (β = 0.0185; 95% CI [0.00788 to 0.0315). However, it is also seen that there is a mediating effect of 5.29%. Table 5 presents the results of the independent variable's total, direct, and indirect effects on harmonious passion, the dependent variable on safety behavior, and the external locus of control of the mediating effect.

When the mediating effect of external locus of control between harmonious passion and safety behavior is examined in Table 5, it was determined that the 95% confidence interval Bootstrap estimates for the indirect effect were between -0.00519 and 0.0205. When the 95% confidence interval is zero (0), the indirect effect is considered non-significant at the p>0.05 significance level.

Table 3. Regression Analysis Results

Dependent Variable	Independent Variables	Beta	t	p	F	Model (p)	R2	Adjusted R2
Model					91.800	.000**	.255	.252
Safety behaviour	Constant	3.020	28.488	.000**				
	Harmonious Passion	.314	9.910	.000**				
	Obsessive Passion	.052	1.881	.060				

*p<0.05, **p<0.001 locus of control of the mediating effect.

Table 4. Indirect Effects of Internal Locus of Control on the Relationship between Harmonious Passion and Safety Behavior

		Mediation Effect of ILOC		
Dependent Variable: Safety Behaviour		**Indirect**	**Direct**	**Total**
95% Confidence Interval	Lower	0.00788	0.27000	0.28818
	Upper	0.0315	0.3964	0.4147
	Z	2.98	10.31	10.92
	p	0.003	< .001	< .001
	(β)	0.0185	0.3304	0.3488
	% Mediation	5.29	94.71	100.00

*p<0.05; ILOC: Internal Locus of Control

Table 5. Indirect Effects of External Locus of Control on the Relationship between Harmonious Passion and Safety Behavior

Mediation Effect of ELOC				
Dependent Variable: Safety Behaviour		**Indirect**	**Direct**	**Total**
95% Confidence Interval	Lower	-0.00519	0.26839	0.27648
	Upper	0.0205	0.4615	0.4641
	Z	0.873	7.644	7.840
	p	0.383	< .001	< .001
	(β)	0.00559	0.36207	0.36766
	% Mediation	1.52	98.48	100.00

*p<0.05; ELOC: External Locus of Control.

Table 6. Indirect Effects of Internal Locus of Control on the Relationship between Obsessive Passion and Safety Behavior

Mediation Effect of ILOC				
Dependent Variable: Safety Behavior		**Indirect**	**Direct**	**Total**
95% Confidence Interval	Lower	0.00677	0.13409	0.15091
	Upper	0.0310	0.2465	0.2635
	Z	2.80	6.40	7.11
	p	0.005	< .001	< .001
	(β)	0.0176	0.1913	0.2089
	% Mediation	8.42	91.58	100.00

*p<0.05; ILOC: Internal Locus of Control

Table 7. Indirect Effects of External Locus of Control on the Relationship between Obsessive Passion and Safety Behavior

Mediation Effect of ELOC				
Dependent Variable: Safety Behavior		**Indirect**	**Direct**	**Total**
95% Confidence Interval	Lower	-0.00105	0.14571	0.15273
	Upper	0.0169	0.3091	0.3155
	Z	1.15	5.31	5.53
	p	0.251	< .001	< .001
	(β)	0.00550	0.22789	0.23339
	% Mediation	2.35	97.65	100.00

*p<0.05; ELOC: External Locus of Control.

Therefore, it is understood that external locus of control does not mediate between harmonious passion and safety behavior, and the H_4 hypothesis is not supported (β = 0.00559; 95% CI [-0.00519 to 0.0205).

Table 6 shows the mediating effect of internal locus of control between obsessive passion and safety behavior. It was determined that the 95% confidence interval Bootstrap estimates for the indirect effect were between 0.00677 and 0.0310. When there is no zero (0) in the 95% confidence interval, it is accepted that the indirect effect differs significantly from zero (0) at the p<0.05 significance level. Therefore, it is seen that the internal locus of control mediates between obsessive passion and safe behavior, and the H_5 hypothesis is supported (β = 0.0176; 95% CI [0.00677 to 0.0310). However, it is also seen that there is a mediating effect of 8.42%.

Table 7 presents the results of the total, direct, and indirect effects of the independent variable as obsessive passion, the dependent variable as safety behavior, and the mediating effect as external locus of control are presented.

The mediating is presented in Table 7. It was determined that the 95% confidence interval Bootstrap estimates for the indirect effect were between -0.00105 and 0.0169. When the 95% confidence interval is zero (0), the indirect effect is considered to have a non-significant effect at the p>0.05 significance level. Therefore, it is found that the external locus of control does not mediate between obsessive passion and safety behavior, and the H_6 hypothesis is not supported (β = 0.00550; 95% CI [-0.00105 to 0.0169).

4. Conclusion

In the aviation industry, since the human factor provides an important input in the entire process, from the design phase to the completion of operations and even post-flight checks, it is very important to anticipate and manage potential human errors and their impact levels

(Demirtaş and Kaya, 2023). When the hull loss accidents that occurred worldwide from 2012 to 2021 are examined, the flight crew is responsible for 26% (Boeing Airplane Company, 2021). When the flight safety agency's aircraft accidents that occurred between 2017 and 2022 are examined, a total of 15 accidents are reported. It has been reported that 6 of them are caused by loss of control (Flight Safety Foundation, 2022), and it is reported that the human factor causes errors and violations. Again, Heinrich (1959) revealed that 88% of workplace accidents were caused by unsafe behavior. For this reason, it is essential to examine all kinds of emotions, attitudes, and impulses that lead to unsafe behavior that may endanger flight safety for aviation sector employees in terms of ensuring aviation safety. In this, the research endeavors to uncover how the passion for work among aviation sector workers influences their perception of safety behavior. Additionally, the study explores whether the locus of control regarding safety plays a mediating role in this impact.

The study's findings indicate that harmonious passion, a facet of work passion, positively and significantly influences safety behavior. Similar findings have been found in the literature (Ali et al., 2020; Chen, 2021; Wu et al., 2023). In fact, Chen (2021) states that aircraft maintenance technicians with a harmonious passion for work will be willing to engage in both safety compliance and participation behavior, and when they perceive a harmonious balance between their work and other activities in life, their work will integrate well with their lives. On the other hand, obsessive passion, one of the dimensions of work passion, was found to have a positive but insignificant effect on safety behavior. However, there are studies in the literature that obsessive passion has negative effects on many types of behavior other than safety behavior (Carbonneau and Vallerand, 2013), (Junot, et al., 2017), (Luu, 2019) and (Wan et al., 2022). Therefore, these findings differ from the literature.

The findings revealed that the internal locus of control, one of the dimensions of safety control focus, plays a full mediating role in both the relationship between harmonious passion and safety behavior and the relationship between obsessive passion and safety behavior. Similar study findings have been found in the literature (Zigarmi, et al., 2018), (Turksoy and Tutuncu, 2021). Obsessive work passion is more complex in terms of its inherent combination of positive and negative characteristics than harmonious work passion. Vallerand et al. (2003) state that people with obsessive passion allow internal conditions to take control, even though they love their jobs. This shows that obsessive work passion has a complex relationship with job performance (Kong and Ho, 2018). On the other hand, it was determined that the external locus of control, one of the dimensions of safety control focus, did not play a mediating role in both the relationship between harmonious passion and safety behavior and the relationship between obsessive passion and safety behavior.

This study also has some suggestions that will provide contributions to the literature and organizations.

In this study, it was found that harmonious passion increases or improves safety behavior. Therefore, aviation sector businesses should seek to increase harmonious passion. The first one of these pursuits is to provide organizational support for employees in aviation sector businesses to be more passionate, innovative, creative and productive (Karimi and Alipour, 2011). Secondly, Chen (2022) argues that designing a work-family harmony model for aviation industry employees and ensuring that rewards are compatible with the needs of the family can reduce stress and increase work passion, because increasing harmonious passion in the aviation industry involves developing deep and sustainable passion within the work while maintaining a healthy balance in the lives of employees. Therefore, airline companies can help increase the well-being of their employees by determining an organizational culture that supports work-life balance, practices and policies in this direction, and designing flexible work programs that will help promote work-life balance. Such management practices are expected to positively affect employees' work passion and ultimately increase safety motivation.

Another finding of this study is that harmonious passion together with internal locus of control will increase safety behavior. So, first of all, aviation organizations should adopt practices that will encourage internal locus of control. In this context, the aim is to develop policies specifically for the selection of employees with emotional intelligence, empathy, decision-making and behavioral development skills during recruitment processes. Secondly, in the aviation industry, where safety is important, mechanisms of reward, promotion, and acceptance and value within the group that will contribute to employees' orientation towards safety behavior should be implemented. Thirdly, considering the limited attention capacity and the intense, stressful workload in the aviation industry, it is inevitable to think within certain patterns after a while. For this reason, aviation sector businesses should organize conscious awareness-based cognitive therapy and stress reduction programs at regular intervals so that their employees can both get out of this ruminative thinking restriction and develop the internal locus of control motivation that can have positive effects on their perception of safety behavior (Atalay, 2022). Fourthly, since shift work schedules are widely implemented in the aviation industry, it is also suggested by Chen (2021) that more attention should be paid to task design and schedules to

reduce the potential for employees to become obsessed with their work. Forest et al. (2011) suggested that a management style that supports autonomy can both encourage harmonious passion and prevent obsessive passion for work. Finally, it is evaluated that the accurate and complete transfer of knowledge and experience by managers in trainings that can raise awareness on employees' feelings, attitudes and behaviors in the workplace will have a positive impact on both employees' work passion and safety behavior.

The current research has some limitations. The research sample, the choice of snowball sampling method, the online application of the survey, and its cross-sectional nature are some of the limitations. As in all studies using the survey method, in the current study, social desirability anxiety and common method bias may occur to a certain extent, and misleadingly statistically significant relationships may be observed (Crowne and Marlowe, 1964). Thus, conducting studies with a larger sample size and including organizational variables in the model will provide more profound results for future studies on safety in aviation.

CRediT Author Statement

İnan Eryılmaz: Conceptualization, Methodology, Formal Analysis, Visualization, Investigation, Supervision, Writing – original draft, Writing-Reviewing and Editing, Project Administration. **Tugay Öney**: Conceptualization, Methodology, Formal Analysis, Visualization, Investigation, Supervision, Writing – original draft, Writing-Reviewing and Editing. **Yeşim Tüm Kılıç**: Conceptualization, Methodology, Formal Analysis, Visualization, Investigation, Supervision, Writing – original draft, Writing-Reviewing and Editing. **Tuğba Erhan**: Conceptualization, Methodology, Formal Analysis, Visualization, Investigation, Supervision, Writing – original draft, Project Administration.

Nomenclature

ARFF : Aircraft Rescue and Fire Fighting

CFA : Confirmatory Factor Analysis

ELOC : External Locus of Control

HP : Harmonious Passion

ILOC : Internal Locus of Control

OP : Obsessive Passion

SDT : Self-Determination Theory

SC : Safety Compliance

SP : Safety Participation

SB : Safety Behavior

References

Ali, M. et al. (2020) 'A positive human health perspective on how spiritual leadership weaves its influence on employee safety performance: The role of harmonious safety passion', Safety Science, 131, p. 104923.

Ahn, J., Back, K.J., and Lee, C.K. (2019) 'A new dualistic approach to brand attitude: The role of passion among integrated resort customers', International Journal of Hospitality Management, 78, pp. 261-267.

Astakhova, M. et al. (2022) 'Passion for work passion research: Taming breadth and promoting depth', Journal of Organizational Behavior, 43(9), pp. 1463–1474.

Atalay, Z. (2022) Bilinçli Farkındalık: Farkındalıkla Anda Kalabilme Sanatı. İstanbul: İnkılap Yayınevi.

Boeing Airplane Company (2008) Airplanes: Statistical summary of commercial jet airplane accidents worldwide operations | 1959 – 2008. Available at: Erişim tarihi: 01.09.2023.

Boeing Airplane Company (2021) Airplanes: Statistical summary of commercial jet airplane accidents worldwide operations | 1959 – 2021. Available at: Erişim tarihi: 01.09.2023.

Caesens, G. and Brison, N. (2023) 'The relationship between organizational dehumanization and safety behaviors', Safety Science, 158.

Carbonneau, N. and Vallerand, R. (2013) 'On the role of harmonious and obsessive romantic passion in conflict behavior', Motivation and Emotion, 37(4), pp. 743–757.

Chen, C. and Chen, S. (2014) 'Measuring the effects of safety management system practices, morality leadership and self-efficacy on pilots' safety behaviors: Safety motivation as a mediator', Safety Science, 62, pp. 376–385.

Chen, S. C. (2022) 'Off-stage heroes: The antecedents and consequences of job passion among civil aviation maintenance crew', The International Journal of Aerospace Psychology, 32(2-3), pp. 95-113.

Chen, S.-C. (2021) 'A dualistic model of air technician safety behavior: Application of the reformulation of attitude theory', Research in Transportation Business & Management, 41, pp. 1–8.

Chittaro, L. (2014) 'Changing user's safety locus of control through persuasive play: An application to aviation safety', in A. Spagnolli, L. Chittaro, and L. Gamberini (eds) Persuasive Technology: 9th International Conference. Padua, Italy: Springer International

Publishing (Lecture Notes in Computer Science), pp. 31–42.

Crowne, D. and Marlowe, D. (1964) The Approval Motive: Studies in Evaluative Dependence. New York: Wiley.

Curran, T. et al. (2015) 'The psychology of passion: A meta-analytical review of a decade of research on intrapersonal outcomes', Motivation and Emotion, 39(5), pp. 631–655.

Deci, E. and Ryan, R. (1985) Intrinsic Motivation and Self-Determination in Human Behavior | SpringerLink. New York: Plenum Press.

Demirtaş, Ö. and Kaya, B. (2023) 'Havacılık Kazalarında İnsan Faktörü', in Ö. Demirtaş (ed.) Havacılık Yönetimi ve Çağdaş Yaklaşımlar. Ankara: Nobel Akademik Yayıncılık., pp. 1–21.

Dokuman, İ., and Akıncı, G. (2001) 'Uçuşa elverişlilik sertifikasyonunda emniyet ile insan faktörlerine yeni bir bakış', IX. Ulusal Uçak, Havacılık ve Uzay Mühendisliği Kurultayı Bildiriler Kitabı, Eskişehir: MMO Yayınları.

Erceylan, N., Eryılmaz, İ. & Atilla, G. (2022) 'İş Sonrası Toparlanmanın Yaşam Tatmini Üzerindeki Etkisi: İşe Tutulmanın Aracı Rolü', Süleyman Demirel Üniversitesi Vizyoner Dergisi , 13(30), pp. 236-250.

Eryılmaz, İ., Dirik, D. and Odabaşoğlu, Ş. (2019) 'Güvenlik iklimi algısı ve iş performansı ilişkisinde genel öz yeterliliğin düzenleyici rolü: Helikopter teknisyenleri üzerine bir araştırma', Manas Sosyal Araştırmalar Dergisi, 8(2), pp. 1854–1870.

Flight Safety Foundation (2022) Airliner accidents 2017-2022. Available at: https://aviation-safety.net/database/2022-analysis Erişim tarihi: 01.09.2023 (Accessed: 1 September 2023).

Forest, J., Mageau, G. A., Sarrazin, C., & Morin, E. M. (2011) 'Work is my passion: The different affective, behavioural, and cognitive consequences of harmonious and obsessive passion toward work', Canadian Journal of Administrative Sciences, 28(1), pp. 27-40.

Fugas, C. S., Meliá, J. L. and Silva, S. A. (2011) 'The "is" and the "ought": How do perceived social norms influence safety behaviors at work?', Journal of Occupational Health Psychology, 16(1), pp. 67-79.

Gladwin, T. N. (1981) 'Culture's consequences: International differences in work-related values', The Academy of Management Review, 6(4), pp. 681-683.

Grant, A.M., Parker, S. and Collins, C. (2009) 'Getting credit for proactive behavior: Supervisor reactions depend on what you value and how you feel', Personnel Psychology, 62(1), pp. 31–55.

Griffin, M. and Neal, A. (2000) 'Perceptions of safety at work: A framework for linking safety climate to safety performance, knowledge, and motivation.', Journal of Occupational Health Psychology, 5(3), pp. 347–358.

Gül, H. and Beyşenova, A. (2018) 'Kontrol odağı ve girişimcilik eğilimi ilişkisi: KTMÜ öğrencileri üzerine bir araştırma', MANAS Sosyal Araştırmalar Dergisi, 7(2), pp. 213–234.

Gülbahar, Y. and Özkan, O. (2023) 'The antecedents and outcomes of obsessive passion in the workplace', Current Psychology, 42, pp. 21263–21277.

Hayes, A. (2009) 'Beyond Baron and Kenny: Statistical Mediation Analysis in the New Millennium', Communication Monographs, 76(4), pp. 408–420.

Heinrich, H. (1959) Industrial accident prevention: A scientific approach. 4th Edition. New York: McGraw-Hill Book Company.

Heinström, J. (2010) From Fear to Flow: Personality and Information Interaction. Oxford: Chandos Publishing.

Ho, V. et al. (2018) 'Promoting harmonious work passion among unmotivated employees: A two-nation investigation of the compensatory function of cooperative psychological climate', Journal of Vocational Behavior, 106, pp. 112–125.

Hodgins, H. and Knee, C.R. (2002) 'The Integrating Self and Conscious Experience', in E. Deci and R.M. Ryan (eds) Handbook of Self-Determination Research. University of Rochester Press, pp. 87–100.

Hofmann, D.A., Morgeson, F.P. and Gerras, S.J. (2003) 'Climate as a moderator of the relationship between leader-member exchange and content specific citizenship: Safety climate as an exemplar', Journal of Applied Psychology, 88(1), pp. 170–178.

Houlfort, N. et al. (2015) 'The role of passion for work and need satisfaction in psychological adjustment to retirement', Journal of Vocational Behavior, 88, pp. 84–94.

Hunter, D. (2002) 'Development of an aviation safety locus of control scale', Aviation Space and Environmental Medicine, 73(12), pp. 1184–1188.

Hunter, D. and Stewart, J. (2012) 'Safety locus of control and accident involvement among army aviators', The International Journal of Aviation Psychology, 22(2), pp. 144–163.

ICAO (2013) Safety management manual (SMM). 3.ed. Montreal: ICAO.

Jones, J.W., & Wuebker, L.J. (1993) 'Safety locus of control and employees' accidents', Journal of Business and

Psychology, 7(4), pp. 449–457.

Junot, A., Paquet, Y. and Martin-Krumm, C. (2017) 'Passion for outdoor activities and environmental behaviors: A look at emotions related to passionate activities', Journal of Environmental Psychology, 53, pp. 177–184.

Karimi, R. and Alipour, F. (2011) 'Reduce Job stress in Organizations: Role of Locus of Control', 2(18), pp. 232–236.

Kelecek, S. and Aşçı, F. (2013) '"Tutkunluk ölçeği"nin üniversite sporcuları için geçerlilik ve güvenilirlik çalışması', Turkiye Klinikleri Journal of Sport Science, 5(2), pp. 80–85.

Kline, R.B. (2011) Principles and Practice Of Structural Equation Modeling. 3rd Edition (Guilford Pres., New York).

Kong, D. and Ho, V. (2018) 'The performance implication of obsessive work passion: unpacking the moderating and mediating mechanisms from a conservation of resources perspective', European Journal of Work and Organizational Psychology, 27(2), pp. 269–279.

Küçükkaragöz, H. (2020) 'Davranışların kaynağı olarak kontrol odağı', in Y. Kındap Tepe (ed.) Disiplinlerarası Perspektif: Davranış Araştırmaları. Ankara: İksad Yayınevi, pp. 59–88.

Liu, S. et al. (2020) 'Multiple mediating effects in the relationship between employees' trust in organizational safety and safety participation behavior', Safety Science, 125.

Liu, S., Yang, X. and Mei, Q. (2021) 'The effect of perceived organizational support for safety and organizational commitment on employee safety behavior: a meta-analysis', International Journal of Occupational Safety and Ergonomics, 27(4), pp. 1154–1165.

Luu, T.T. (2019) 'Can diversity climate shape service innovative behavior in Vietnamese and Brazilian tour companies? The role of work passion', Tourism Management, 72, pp. 326–339.

Maneechaeye, P. and Potipiroon, W. (2022) 'The impact of fleet-level and organization-level safety climates on safety behavior among Thai civilian pilots: The role of safety motivation', Safety Science, 147, pp. 1–9.

Maryam, S. et al. (2021) 'Effects of safety climate and employee engagement towards organisational citizenship behaviour of sewage workers', Asian Journal of Business and Accounting, 14(1), pp. 253–275.

Neal, A. and Griffin, M. (1997) 'Perceptions of safety at work: Developing a model to link organizational safety climate and individual behavior.', in. 12th Annual Conference of the Society for Industrial and Organizational Psychology.

Neal, A., Griffin, M. A. (2006) 'A study of the lagged relationships among safety climate, safety motivation, safety behavior, and accidents at the individual and group levels', Journal of Applied psychology, 91(4), pp. 946–953.

Neal, A., Griffin, M. A. and Hart, P. M. (2000) 'The impact of organizational climate on safety climate and individual behavior', Safety Science, 34(1-3), pp. 99-109.

Öney, T., Eryilmaz, İ. and Şimşek, H. (2022) 'Does fear of COVID-19 effect presenteeism? A research in the context of perception of job ınsecurity', Journal of Organizational Behavior Review, 4(2), pp. 242–265.

Özgener, Ş., & Ulu, S. (2018). Yükleme (Atfetme). İçinde H. Tutar (Ed.), Davranış Bilimleri: Kavramlar ve Kuramlar (ss. 235-262). Ankara: Seçkin Yayıncılık.

Pathak, D. and Srivastava, S. (2020) 'Journey from passion to satisfaction: Roles of belongingness and psychological empowerment: A study on social workers', International Journal of Sociology and Social Policy, 40(3/4), pp. 321–341.

Pollack, J. et al. (2020) 'Passion at work: A meta-analysis of individual work outcomes', Journal of Organizational Behavior, 41(4), pp. 311–331.

Rotter, J. (1966) 'Generalized expectancies for internal versus external control of reinforcement', Psychological Monographs: General and Applied, 80(1), pp. 1–28.

Ryan, R. and Deci, E. (2017) Self-determination theory: Basic psychological needs in motivation, development, and wellness. New York, NY, US: The Guilford Press (Self-determination theory: Basic psychological needs in motivation, development, and wellness).

Ryan, R. and Deci, E. (2020) 'Intrinsic and extrinsic motivation from a self-determination theory perspective: Definitions, theory, practices, and future directions', Contemporary Educational Psychology, 61, p. 101860.

Shappell, S. and Wiegmann, D. (1996) 'U.S. naval aviation mishaps, 1977-92: Differences between single- and dual-piloted aircraft', Aviation, Space, and Environmental Medicine, 67(1), pp. 65–69.

Silitonga, T. et al. (2022) 'Civil aviation safety evaluation based on the principle of international civic aviation organization (ICAO)', International journal of health sciences, pp. 10188–10210.

Smith, R. et al. (2023) 'A content validation of work

passion: Was the passion ever there?', Journal of Business and Psychology, 38(1), pp. 191–213.

Tabachnick, B.G. and Fidell, L.S. (2013) Using Multivariate Statistics. (Sixth ed.). Pearson, Boston.

Tu, Y. et al. (2023) 'Obsessive passion, opportunity recognition, and entrepreneurial performance: The dual moderating effect of the fear of failure', Frontiers in Psychology, 13, pp. 1–14.

Turksoy, S. and Tutuncu, O. (2021) 'An analysis of the relationship between work engagement, work locus of control, passion, and parasitism in coastal hotels', European Journal of Tourism Research, 29, pp. 1-19.

Vallerand, R. et al. (2003) 'Les passions de l'âme: On obsessive and harmonious passion.', Journal of Personality and Social Psychology, 85(4), pp. 756–767.

Vallerand, R. J. (2008) 'On the psychology of passion: In search of what makes people's lives most worth living', Canadian Psychology, 49(1), pp. 1-13.

Wan, M. et al. (2022) 'Does work passion influence prosocial behaviors at work and home? Examining the underlying work–family mechanisms', Journal of Organizational Behavior, 43(9), pp. 1516–1534.

Wichman, H. and Ball, J. (1983) 'Locus of control, self-serving biases, and attitudes towards safety in general aviation pilots', Aviation, Space, and Environmental Medicine, 54(6), pp. 507–510.

Wu, Y. et al. (2023) 'The influence of safety-specific transformational leadership on safety behavior among Chinese airline pilots: The role of harmonious safety passion and organizational identification –', Safety Science, 166, pp. 1–36.

You, X., Ji, M. and Han, H. (2013) 'The effects of risk perception and flight experience on airline pilots' locus of control with regard to safety operation behaviors', Accident Analysis and Prevention, 57, pp. 131–139.

Zhu, Y. et al. (2022) 'High-performance work systems and safety performance in the mining sector: Exploring the mediating influence of workforce agility and moderating effect of safety locus of control', Current Psychology [Preprint].

Zigarmi, D., Galloway, F.J. and Roberts, T. (2018) 'Work locus of control, motivational regulation, employee work passion, and work intentions: An empirical investigation of an appraisal model', Journal of Happiness Studies, 19(1), pp. 231–256.

International Journal of Aviation Science and Technology

Research Article

The Innovation in Air Plasma Spray for Hardfacing

Duong Vu*

Duy Tan University, School of Engineering Technology, Vietnam, Danang
vuduong@duytan.edu.vn - 0000-0002-4795-2522

Abstract

Thermal spray coating plays a significant role in industry. The wear-resistant deposition helps to provide a longer life cycle for the components. There is an ongoing effort to develop coatings that improve the coefficient of friction. Compared with other deposition techniques, plasma spray coating can be recommended for a wide range of substrate materials to produce a stable, wear-resistant material. The plasma-sprayed deposition not only improves tribological performance but also embeds the desired mechanical and physical properties. In plasma spray technology, the inert gas used is mostly plasma jet. To create the wear-resistant coatings, the engineers apply self-flux or cermet powder, both of which are expensive materials. Some positive results of deposition using the amorphous powder encouraged the engineers and researchers. But in a few of the investigations on the air plasma spray Fe-based powder, the plasma generation gas is ordinary air. This innovation served to save on production costs. The aim of this work is the study of Fe-based spraying, applying the modification of a plasma torch. Both of the innovations help to enhance the hardfacing effect for wear resistance.

Keywords

Wear Resistance
Deposition
Microstructure
Production Cost
Kinetics of Stream

Time Scale of Article

Received 20 November 2023
Revised until 28 May 2024
Accepted 28 May 2024
Online date 21 June 2024

1. Literature Review

Thermal spraying found wide applications in the struggle against the introduction of the service life of the component operating in a heavy environment. There is a huge demand for this area due to its efficiency, not only in aerospace but also in other branches of industry. The total global coating revenue was raised to USD 9.69 billion in 2021, and it is expected to reach USD 19.02 billion by 2030. (Straits Research Report to 2030) Aerospace coatings with very specific performance can be considered a special solution for eliminating the risk of the degradation of the components due to severe operation in aircraft. It is noted that there is a high demand to design new materials in this industry since the whole cycle of service in the aerospace industry requires a specific standard specification. The operation of the aerospace components required the special depositions assigned to avoid any air instability, thermal fluctuation, or unstable pressures. The protective layers also provide the aircraft with the ability to resist the harmful chemical effects of the environment. The newly developed coating materials show the advantages outlined, helping the aerospace industry save on production costs. The APEC countries are strongly involved in global boom competition, creating new chances and challenges for aerospace coating growth. The main drive for the expansion of the Asia-Pacific region market is derived from the rising aerospace and aviation industries in these countries. The strong stream of passenger circulation and international business contributed to an enhanced huge project of aerospace development in all related aspects. The boom in aircraft production and the new routes are leading to an expansion of the aerospace coatings market. According

*: Corresponding Author Duong Vu, vuduong@duytan.edu.vn
DOI: 10.23890/IJAST.vm05is01.0104

to recent forecasts, the growing capacity and contract between companies in the APEC community created good opportunities for the development and manufacturing of new coatings in the aerospace industry. According to The Insight Partners, the aerospace coating industry will increase from US$ 1.81 billion in 2019 to US$ 2.92 billion by 2027. (Partners, 2023). It is useful to introduce some applications of the thermal spraying process used by big companies such as Boeing and Airbus. Thermal spray coatings of hard chrome are environmentally safe. The newly developed High Velocity Oxygen- Fuel (HVOF)-sprayed coatings are far superior in wear resistance and corrosion resistance compared with the traditional spraying processes. In companies like Boeing and Airbus, metallic carbide coatings like WC-CoCr using HVOF technology are applied to improve the sliding wear resistance of hydraulic actuators and landing gear components. In the jet engine, severe operation conditions like fluctuating temperatures, high levels of oxidation, and strong erosive corrosion caused an intensive degradation problem, leading to the design of specific coating compositions with advanced spraying systems. Thermal spray technologies and processes, like (HVOF) and air plasma spray (APS), are applied to deposit on these components the state-of-the-art layer, increasing their service life. The components in the aircraft engine and landing section became more efficient in terms of higher speed and less fuel consumption due to reliable and advanced spray processes. It is recommended that the entire specific quality standard, including the guidelines and testing procedure, be binding to not only engine manufacturers but also authorized maintenance and repair contractors. Depending on the operating environment, each component of an aircraft engine exhibits specifications that reduce their service life. The Atmospheric Plasma Spraying (APS) process is well known in the industry to reduce the harmful impact of environmental operations. It is useful to nominate these applications, such as the specific deposition that improves the tribology and enhances the corrosive resistance in the engine block. The wear resistance of components plays an important role in saving costs during service life in industry.

The reliability of components is determined by the technical criteria setting the schedule for their maintenance. Based on these arguments, it is necessary to increase the wear resistance as the milestone factor in the running of any dynamic combination. (Joshi and Nylen, 2019; Sadeghi et al., 2019).

The thermal barrier coatings (TBCs) deposited by special ceramic materials exhibit significant low thermal conductivity even under high heat flow. The high demand for increased efficiency of machine components operating in heavy conditions in the aerospace and automotive industries using TBC coatings constitutes a specific worldwide effort. (Mondal et al., 2021).

The newly developed APS processes are spreading to the coating market. Cermet, consisting of a ceramic core with the main ingredient carbide, is reinforced by a metallic binder. There is a successful combination between hardness and strength, varying not only the composition but also the structure, providing a well-known wear-resistant material. The other advantage of cermet is that it also recognizes a super characteristic against an erosive environment. (Hussainova and Antonov, 2007). The new type of group-cermet Ti (C, N)-based exhibits state-of-the art performance with heightened high wear resistance and high erosive resistance, especially at high temperatures. They have better fracture toughness against cemented carbide since the solid-solusion phase is costituted (De la Obra et al., 2016).

However, as rules, they also have demerits, such as poor oxidation resistance at high temperatures and inherent brittleness. A core ceramic ingredient commonly constitutes up to 80% of a remain, which is a metal-binding matrix (Jose et al., 2022). Amorphous materials are the most advanced group of wear-resistant materials with outstanding properties. The principle of formation amorphis is the disordered structure of an alloy by rapid solidification; is it worth investigating this process during the deposition coating? (Wang et al., 2016) presented the analysis on the corrosion resistance of the Fe-Cr-Mo-C-B alloy material for High Velocity Air Fuel (HVAF) coating, and the results confirmed the prospective deposition from Fe-based amorphous materials. The recent papers focused on the arc efficiency, the density of the plasma stream, the acceleration of particles, and the productivity of spraying. For the direct-current plasma torch, the arc length is self - adjusting. It is noted the reduction in voltage since the fluctuation of the plasma stream caused the shunting effect. The other side effect is the fluctuation in the plasma power flow, resulting in a negative quality of the surface layer. Some publications focused on the influence of the density of current around the anode and its count on the service life of the torch. On the other side, there are very few publications investigating the possibility of ordinary air as a substitution for the notable inert gas, in spite of its cost savings. The bilateral impact of ordinary air in spraying Fe-based alloys varies depending on the specific tribology condition. The significant result recommends the use of ordinary air in thermal spraying Fe-based alloys due to the new count of plasma torch with the limited range of input parameters (Kuzmin et al., 2021; Kuzmin et al., 2017). The tribology and friction conditions are the subject of many publications relating to the spraying materials since the difference in hardness of

the deposition and substrate determines the mutual relationship. Friction and wear are in close relation and could be considered the reducing factor of power in mechanical systems. Based on the above-mentioned analysis, the target of this paper is to develop an innovative plasma torch using ordinary air as plasma generation to deposit the Fe-based material to improve the hardness of the coating. The quality of the surface layer deposited is evaluated, referring to the hardfacing formation. The input factors and characteristics of the feedstock are analyzed by quantitative relations.

2. Methodology

In the experiment on spraying materials, the system SG-100 TAFA-Praxair was involved. The chemical composition of four Fe-based powders (Vu and Thu., 2021) was analyzed using the device SM-6510LV. The results of the analysis are presented in Table 1.

It is necessary to define the impact of the oxygen from the open atmosphere on the composition of the deposition, including the oxygen percentage contained in the feedstock material and coatings. The analyzer G8 Galileo (Germany), working upon the principle of definite melt extraction, was used for this purpose. The kinetic energy of the particle stream plays a significant role in providing a strong adhesion bond between the coating and the substrate. Adhesion can be considered an important criterion for the performance of the deposited layer. That is why the high-speed camera Shimadzu HPV-2 was involved during the experiment. Besides the kinetic energy, the heating of the particle during short-time flight to the substrate makes it more plastic, leading to good deformation and the creation of strong cohesion in the coating. It is better to measure the enthalpy of the plasma stream instead of a separate particle since only the particle stream is the main total thermal factor. The method of enthalpy definition in the system was presented in (Zhang et al., 2012). As mentioned above, the cycle life of the aerospace component depends on its wear resistance since it is in severe conditions. The suitable standard for the evaluation is the ASTM G133 standard. The efficiency of the plasma stream depends on the concentration of heating and accelerated particles in the feedstock, especially under the influence of the atmospheric environment. On the other hand, the method of introduction of the powder onto the plasma torch also impacts the productivity of the deposition. These requirements are solved by the newly developed design of the plasma torch, which consists of a number of intermediate sections that are thermally and electrically isolated. Further innovation is the installation of a special swirler in a cascaded plasma torch, creating a spiral vortex flow.

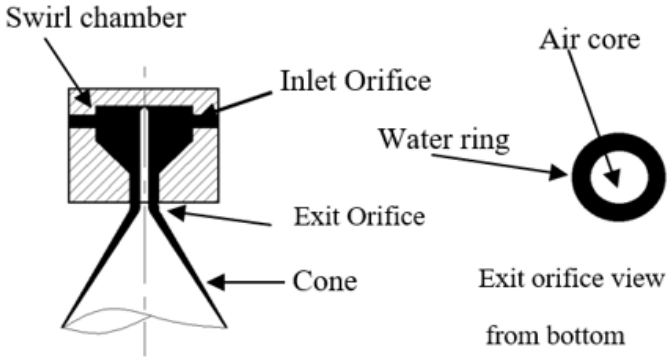

Fig.1. Swirler

The flow under the pessure of the gas stream and the dynamics process will press the arc stream along with the arc column, including the outer space. All these improvements enhance the stability of the plasma stream and the productivity of the deposition cycle. (Fig. 1).

The swirler installed on the plasma torch creates vortex circulation into the chamber, improving the mixture between the feedstock particles and plasma stream. By pressing the plasma stream, it will be isolated partially from the walls of the plasma chamber and encourage the voltage of the plasma jet to be elevated.

3. Experiment & Result

Case study 1:

The aim of the experiment is to enhance the thermal efficiency to increase the specific enthalpy of the plasma stream, including the feedstock material. It can be achieved by varying the injection angle in the swirler simultaneously with the spraying conditions, namely the flow rate of gas, arc voltage, and arc current.

- Current I = 135 A, voltage U = 220 V, and flow rate of air G = 1.2 g/s.
- Current I = 180 A, voltage U = 220 V, and flow rate of air G = 1.35 g/s.

In these spraying experiments, the spraying distance was kept constant at L = 120 mm. The increased enthalpy in the plasma stream also facilitates the oxidation of the Fe-based powder. The level of oxidation can be evaluated by comparing the oxygen content in the feedstock and the coating layer. The results of the experiment are presented in Table 2.

It is found a slightly the oxidation in the deposited layer. The oxidation of the feedstock happened due to the plasma stream generated by ordinary air, and the whole plasma jet with the Fe-based particle was conducted in an open-air environment. The oxygen in the environment reacted with the material of the particle, consequently increasing the oxygen content in the

sprayed layer. The elevated hardfacing in this case helped to increase the wear resistance, illustrating a positive effect on oxidation.

Case study 2:

In this experiment, the loss of alloy elements by the variation of the input parameters will impact the hardness of the deposited layer. The range of setting parameters is as follows:

- Current I = 130 A, voltage U = 203 V, flow rate of air G = 2.35 g/s.
- Current I = 170 A, voltage U =220 V, flow rate of air G = 2.35 g/s.

In both modes of spraying, the spraying distance was keep constant at L = 130 mm.

It is interesting that in version 2, when the particle velocity increased, the flight time of the particle in a rich oxygen environment reduced, but it is also noted that the elevated oxidation level in the plasma jet, since the power of the plasma jet caused the high temperature, resulted in the strong activation of the alloy composition. The bilateral effect of the acceleration of the feedstock particle was found, taking into account the influence of the plasma jet power.

The result of the analysis of the chemical composition and hardness definitions presented in Table 3.

In all experiments, the loss of elements happened since the spraying process was implemented in the open atmosphere using ordinary air as the plasma generation. However, the increased power of the plasma jet (version 2) is the additional reason for the greater loss of elements. It is easy to observe the slight loss of some elements, such as Cr, Mo, and Ni, which can originate from an error in the chemical analysis. Thus, the violation is considered acceptable. For the powders H4 and H10, the increased nitrogen content (N2) is noted. It is assumed that the chemical interaction between the melted metallic particles and the environment leads to the definite involvement of nitrogen from the surrounding atmosphere.

The target of this experiment is to evaluate the wear resistance and bonding strength of the coating layer under the variable current of the plasma jet and its flow rate in the air. The feedstock in this case study was nominated for material X5 since its hardness reached the highest in comparison with all remaining alloys in the previous experiment. That is why it is useful to access the habit of this alloy material under the changing main conditions of the spraying process, such as the power of the plasma jets via the current of plasma and the flow rate of the air.

From of all four materials, powder X5 exhibits the highest hardness.

Case study 3:

In this case study, the wear resistance of the deposited layers will change under the varying flow rate of the air without changing the plasma current. All the parameters of these experiments are shown in Table 4.

Data in Table 4 shows a tendency that the elevating current of plasma (plasma power) has accelerated particles, which results in an increasing wear resistance of deposition from materials X5.

Table 1. Chemical composition of powders.

Code	C	Cr	B	Mo	Ni	Mn	Si	Nb	V	W
H4	0.11	32.9	0.10	3.30	5.0	1.05	0.70	-	-	-
B5	0.06	35.3	0.40	3.50	10.5	1.05	0.91	-	-	-
H10	0.41	12.5	-	0.70	-	0.54	0.66	0.73	0.35	6.10
X5	0.73	5.0	0.25	4.20	-	1.25	0.84	0.54	1.20	-

Table 2. Evaluation of the oxidation level.

Code	Case	Content of the oxygen, %	
		Feedstock materials	Deposited layer
H4	1	0.20	1.75
	2	0.21	1.16
B5	1	0.29	1.35
	2	0.31	0.08
H10	1	0.19	1.25
	2	0.20	0.92
	1	0.13	1.60
	2	0.15	1.55

Table 3. Result of the experiment in case study 2.

No	Mark	Lot	Chemical composition of alloy / level of loss in relative %											Hardness
			C	Cr	B	Mo	Ni	Mn	Si	N	Nb	V	W	HRC
1	H4	1	0.1	29.6	0.09	3.36	4.37	0.69	-	0.4	-	-	-	44
		2	9.1	10.1	10.0	(1.82)	12.6	34.3	-	33.4	-	-	-	
2	H4	1	0.1	29.6	0.08	3.35	4.5	0.55	0.35	0.5	-	-	-	46-52
		2	9.1	10.1	20.0	(1.52)	10.0	47.6	50.0	66.7	-	-	-	
3	H10	1	0.09	34.1	0.88	3.4	10.5	0.27	0.67	0.5	-	-	-	41-45
		2	(50)	3.4	16.2	2.9	20	46	26.4	0.0	-	-	-	
4	H10	1	0.09	35.1	0.27	3.49	10.5	0.92	0.67	0.5	-	-	-	41-43
		2	(61.7)	0.45	46.0	0.3	0.0	12.4	26.4	(0.2)	-	-	-	
5	B5	1	0.38	11.1	-	0.66	-	0.5	-	-	0.56	0.27	5.9	34 -42
		2	6.1	11.2	-	5.7	-	7.4	-	-	23.3	22.9	3.3	
6	B5	1	0.37	10.5	-	0.7	-	0.4	-	-	0.48	0.27	5.9	46-52
		2	9.8	16.0	-	0.0	-	25.9	-	-	34.3	22.9	3.3	
7	X5	1	0.52	5.25	0.15	4.0	-	1.2	-	-	0.56	1.06	-	50-54
		2	28.8	(5.0)	40.0	4.8	-	4.0	-	-	(3.7)	11.7	-	
8	X5	1	0.41	5.2	0.1	4.0	-	1.0	-	-	0.55	1.1	-	45-52
		2	43.8	(4.0)	60.0	4.8	-	20.0	-	-	(1.9)	8.4	-	

The low velocity encouraged deep melting of the particles, which subsequently strengthened the cohesion bond between particles in the coating, significantly improving the wear. But unfortunately, if the flow rate of gas continuously increases, it will have a negative influence on the cohesive bond, reducing its wear resistance because of the uncomplete heating state.

The continued acceleration of particles over the definite threshold positively improves the cohesion and adhesion bonds, resulting in increased wear resistance. This is evidence of the velocity factor (kinetic energy) over the thermal (heating) channel. In other words, it is suggested that the general tendency of wear resistance is changing significantly along with the flow rate of the air. This relationship almost coincides with the changing adhesion bond, excluding the case of the very low flow rates of the air. The reason for this case is probably the fact that the low velocity affects not only the good coherence bond but also the poor adhesion bond. The fifth mode in Table 4 simultaneously presented a high value for the wear resistance and the adhesion bond. It is recommended to continue the investigation in more detail in the future.

4. Conclusion

The newly developed plasma torch construction, using cascaded intersections between anode and cathode with the injection annular swirler, is a valuable contribution to a significant improvement in the wear resistance of the coating. Plasma spraying of the Fe-based powder using an advanced torch helps to increase the productivity of the deposition process. The final aim is enhanced hardness, which helps increase the service time of the components operating in a hostile environment, such as in aerospace and aircraft systems. The result of the preliminary study using newly developed amorphous Fe-based powders for atmospheric plasma spray opened up prospective ways of saving production costs and attracted the managers, constructors, and contractors who made suitable recommendations in industry.

In the future study, it is expected to conduct a complete experiment with multiple target functions of the spray process. It is expected to open up a new advanced performance of the plasma coatings since the hardfacing plays a significant role in improving production costs for the aerospace industry. The intensive mode of spraying (number 5 in Tab.4) is the most successful.

Table. 4 Wear resistance and adhesion bond of coatings X5 upon the flow rate of the air.

Number	Current I, A	Flow rate G, g/s	Wear resistance in relative units	Adhesion bond, MPa	Assessment
1	160	0.55	22	23	Fail
2	160	1.13	54	40	Good
3	160	1.76	39	35	Fair
4	185	0.75	30	46	Fair
5	185	1.42	68	56	Very good
6	185	1.76	40	54	Good

Nomenclature

APEC : Asia-Pacific Economic Cooperation

TBC : Thermal barrier coating

HVOF : High Velocity Oxygen- Fuel

APS : Air plasma spray

HVAF : High Velocity Air Fuel

ASTM : American Society for Testing Materials

CRediT Author Statement

Vu Duong: Conceptualization, Methodology, Validation, Formal Analysis, Investigation, Data Curation, Writing – Original Draft, Review & Editing, Supervision.

References

De La Obra, A.G. et al. (2017) 'A new family of cermets: Chemically complex but microstructurally simple,' International Journal of Refractory & Hard Metals, 63, pp. 17–25. https://doi.org/10.1016/j.ijrmhm.2016.04.011.

Hussainova, I. and Antonov, M. (2007) 'Assessment of cermets performance in erosive media,' International Journal of Materials & Product Technology/International Journal of Material & Product Technology, 28(3/4), p. 361. https://doi.org/10.1504/ijmpt.2007.013085.

Jose, S.A., John, M. and Menezes, P.L. (2022) 'CeRMet Systems: synthesis, properties, and applications,' Ceramics, 5(2), pp. 210–236. https://doi.org/10.3390/ceramics5020018.

Joshi, S.V. and Nylén, P. (2019) 'Advanced coatings by thermal spray processes,' Technologies, 7(4), p. 79. https://doi.org/10.3390/technologies7040079.

Kuzmin, V. et al. (2017b) 'Equipment and technologies of air-plasma spraying of functional coatings,' MATEC Web of Conferences, 129, p. 01052. https://doi.org/10.1051/matecconf/201712901052.

Kuzmin, V. et al. (2021) 'Supersonic air-plasma spraying of carbide ceramic coatings,' Materials Today: Proceedings, 38, pp. 1974–1979. https://doi.org/10.1016/j.matpr.2020.09.150.

Mondal, K. et al. (2021) 'Thermal Barrier Coatings Overview: Design, Manufacturing, and Applications in High-Temperature Industries,' Industrial & Engineering Chemistry Research, 60(17), pp. 6061–6077. https://doi.org/10.1021/acs.iecr.1c00788.

Partners, I. (2023) 'Aerospace coating market revenue projected to cross $2.92 billion by 2027 | The Insight Partners,' GlobeNewswire News Room, 27 September. https://www.globenewswire.com/news-release/2023/09/27/2750349/0/en/Aerospace-Coating-Market-Revenue-Projected-to-Cross-2-92-Billion-by-2027-The-Insight-Partners.html.

(Straits Research Report to 2030) Reports, straitsresearch.com. Available at: https://straitsresearch.com/report/ceramic-coating-market.

Sadeghi, E., Markocsan, N. and Joshi, S. (2019) 'Advances in Corrosion-Resistant thermal spray coatings for renewable energy power plants. Part I: Effect of Composition and Microstructure,' Journal of Thermal Spray Technology, 28(8), pp. 1749–1788. https://doi.org/10.1007/s11666-019-00938-1.

Vu, D. and Le Thu, Q., 2021. The bilateral influence of main parameters in plasma spray using the air as primary gas on tribology of Fe-based amorphous coatings. In Proceedings of the second International Conference on Advanced Mechanical Engineering, Automation, and Sustainable Development (AMAS).

Wang, G. et al. (2016) 'Spraying of Fe-based amorphous coating with high corrosion resistance by HVAF,' Journal of Manufacturing Processes, 22, pp. 34–38. https://doi.org/10.1016/j.jmapro.2016.01.009.

Zhang, N. et al. (2012) 'Measurement of specific enthalpy under very low pressure plasma spray condition,' Journal of Thermal Spray Technology, 21(3–4), pp. 489–495. https://doi.org/10.1007/s11666-012-9738-1.

International Journal of Aviation Science and Technology

Research Article

Urban Air Mobility (UAM) Network. Case Study: Baku Metropolitan Area

Tapdig Imanov*

Cyprus Science University, Aviation Vocational School, Kyrenia, Cyprus,
timanov@yahoo.com - 0000-0002-5667-5678

Abstract

The development and implementation of the Urban Air Mobility transportation system, using electric vertical takeoff and landing (e-VTOL) aircrafts are the most promising solutions to mitigate growing congestion in big cities. The multiple studies and assumed forecasts indicate a transformation of urban and regional transportation infrastructure while applying the air mobility concept. This study analyzes the feasibility of UAM operations focused on the selection of service segmentation with relevant use cases, which allows for define suitable air vehicle configurations for optimization of possible air network development for Baku city and suburban areas. The result of the study introduces air vehicle features, including flight range, payload ratio, as well as several aspects of weather condition for safe operations, and outlines approaches to defining suitable regulatory framework requirements for public departments. The findings provide a practical perspective for urban planners and involved single companies, which may be useful guidelines at the initial stages of UAM services and obtaining significant information about e-VTOL aircraft and their design configurations to overcome arising barriers in the implementation processes.

Keywords

Operations
Urban Air Mobility
Electric Aircrafts
Use-Case
Network

Time Scale of Article

Received 5 February 2024
Revised until 26 May 2024
Accepted 30 May 2024
Online date 21 June 2024

1. Introduction

The global aviation industry continues to evolve, increasing safe operation, applying highly automated systems (Jazzar et al., 2022) and technological changes, transferring urban ground transportation into airspace operations over large cities by implementing unmanned aerial vehicles (UAV). Unmanned flights had fascinated society's imagination for thousands of years (Balakrishnan et al., 2018), from the time of the 8th century mentioned in the "One Thousand and One Nights" flying carpet (Magic Carpet), collection of Middle Eastern tales (Schwartz, 2023). Confirmation of existing borders between seas and incredible different structures of the finger ends of each personality, now the concept of magic flying cars becomes an unavoidable reality, although nobody would believe that a hundred years ago.

Application of enhanced design concepts, development of sustainable battery technologies, and combination of distributed and electric propulsion systems, have led to the creation of various configurations of electrical vertical take-off and landing (VTOL) vehicles for urban passenger air transportation at low altitudes (Shamiyeh et al., 2018). Implementation of the UAM concept assumes an expanded market to ensure the growth of a multi-modal air transportation system with flexible and high-speed features carrying individuals around urban environments over short to medium distances. The advantage of the new transport mode is that it allows safely and efficiently faster movements through the air reducing trip times and enabling direct node-based

*: Corresponding Author Tapdig Imanov, timanov@yahoo.com
DOI: 10.23890/IJAST.vm05is01.0105

routing (Antcliff et al., 2016; Straubinger et al., 2021).

In the last two decades, Azerbaijan has made large investments-billions of dollars in road infrastructure across the country - setting up new highways and renewing long distance roads. Within the biggest metropolitan area, particularly in Baku and suburban areas, there have been laid new roads, alternative crossways, bridges, and several parking zones, however traffic congestion is still a major problem. Especially the dramatic road jams in town with very slow traffic, delaying the movements over an hour in peak periods. Although the investigations by Duranton and Turner (2011) and later on Hymel (2019) suggested that building roads is not a solution to reduce urban traffic congestions. Comprehensive solutions to alleviate traffic congestion in large cities are becoming necessary for the implementation of new transportation modes that provide high-speed mobility. In this context, the Urban Air Mobility concept is the best approach to entry to service, envisioning low-volume passenger vehicles, and e-VTOL aircraft able to complete aerial missions at low altitudes (Melton et al., 2014).

The purpose of this study is to investigate the use of eVTOL aircraft in the airspace of the Baku metropolitan area, considering passenger segmentations use cases, network planning, vertiport and navigation infrastructure requirements, weather conditions and suitable aircraft selection. The theoretical setting and other presented equations formulated in this paper have practical and theoretical implications for local researchers to consider for future empirical investigations, as well as for stakeholders and decision makers to overcome the challenges, relying on the technical specification of important components of e-VTOL aircraft. In addition, the study is filling a gap in the literature dedicated to UAM operations, particularly the the point of view of Azerbaijan, which is the first represented research topic.

Therefore, Section 2 is Literature Review, Section 3 is representing a detailed e-VTOL Aircraft Design Architecture and Configuration, Section 4 implies Theoretical Setting, Section 5 consists of a Description of the Study area and weather characteristics, Section 6 demonstrates a Result and Discussion, and finally the Section 7 is a Conclusion.

2. Literature Review

Initially, Moore (2010) suggested a growth on-demand mobility (ODM) model in UAM operations, using electric propulsion aircraft. Later on, Patterson et al. (2012), studied its potential benefits and application problems. For the optimization, development, and rapid spread of highly automated systems, Alharasees et al. (2022) highlighted the air vehicle operator's role and responsibility, offering to change working conditions and apply new management methods.

Contribute to the realization of UAM operations in European airspace, EASA (2022) has reviewed more than 150 different e-VTOL aircraft configurations that are currently in the development stages and has issued a document named Special Condition SC-VTOL-01 to enable a fair certification specification, either for traditional aircraft or helicopters.

In addition, the collaborative document, Version 2.0 Concept of Operations (ConOps), was recently issued by FAA (2023) based on feedback from Version 1.0 Con Ops, considered by the National Aeronautics and Space Administration (NASA, 2020) and industry stakeholders. This current document describes key points of overall Advanced Air Mobility (AAM) concept aimed at upgrading an urban air transportation system and infrastructure, covering operation stages, operator function, vertiport consideration, traffic management, airspace corridor evaluation, as well as weather and obstacles within the UAM environments (FAA, 2023).

Besides scientific studies, NASA performed numerous seminars setting up road mapping for ODM aimed at identifying potential problems and appropriate solutions arising in the maturity process. The result of these workshops identified significant interest in the use of e-VTOL for inter and intra city missions and between the regions from future perspectives (NIA, 2017; Uber, 2016). Gradually growing community interest and associated with future benefits realization of UAM mobility using e-VTOL aircrafts applying in various business segments require an effective program to develop a subset of the operational infrastructures. Researchers in the UAM operation fields consider aggregate coverage of involved infrastructure through the utilization of regulatory frameworks and national civil aviation regulations.

The study by Mazur et al. (2022) introduced detailed analysis to determine the main goals of international regulatory agencies (ICAO, FAA, and EASA) and applicability of existing regulations for future operations relating to e-VTOL aircraft carrying passengers and freight over populated large cities. The authors identified that UAM operational subsystems required standard design and applications to ensure safety and efficiency under international requirements. In this context, Kale et al. (2023) argue that airspace management and air traffic control are big challenges with a high volume of air traffic in the future, prompting the funding of NextGen, SESAR, and other international large-scale programs.

The study by Alharasees et al. (2023) demonstrated the importance of communication systems ensuring effective feedback between ground station operators (vertiports, helipads, and vertihubs), ATC, and pilots, as

well as high level Information Technology (IT) applications to serve, navigation and surveillance. Furthermore, environment protection (noise, pollution, emission) consequently, reduces its negative effects and other objectives closely linked to airplane operations, as recommended in the studies performed by Ekici et al. (2013), Karakoc et al., (2016) and Yazar et al., (2018). Urban Air Mobility actually consists of service segmentation with various business model operation functions within urban environments as part of public air transport depending on population demands. A detailed introduction of the rest of the infrastructure including, the air vehicle operator, airspace traffic management, ground facilities (vertiports, communication), and maintenance concerns is briefly considered as the study subject of this paper.

3. e-VTOL Aircraft Design Concept, Performance, and Configurations

The air vehicles proposed for UAM operation equipped with an electric propulsion system (rotor, propeller), fed by enhanced battery technologies, rely on high density battery packs with a protection system and an electronic speed controller system, while producing a low emission, most probably equal to zero. Most design firms work on concepts with separated propulsion and a multirotor tilting system, concentrating to reducing noise levels up to 55 decibels (dB), (Butterworth-Hayes and Stevenson, 2019; Di Vito et al., 2023) less than a helicopter.

The basic design of e-VTOL aircraft has several configurations which include wingless, fixed- wing and tilt-wing concepts providing lift and cruise, vectored thrust, and hybrid thrust functions. Wingless e-VTOL air vehicles consist of a different number of multirotor propulsions, powering the thrust for hover and forward flight simultaneously. Powered lift aircraft with fixed-wings are able to fly significantly at high altitudes with efficient speed in cruise, carrying out extended ranges which exceed the capabilities over wingless types.

The most 150 leading Original Equipment Manufacturers are in the process of design developments on the 27 different types of fixed wing with tilt-rotor and vectored thrust configurations (Hirschberg, 2019; Darvishpoor et al., 2020) in strong competition. However, fixed- wing mounted tilt-rotor configuration causes a drag during take-off and landings.

Tilt-wing design with tilt-rotor is capable for long range, and very efficient during hovering take-off and landing. On the other hand, tilt-wing configuration creates high stress and vibrations, because the tilt actuators are placed in the fuselage section and along the wing roots Kraenzler et al., 2019; Akash et al., 2021).

Multi-rotor e-VTOL aircraft are equipped with three or more motors with appropriate propellers that generate thrust during take-off and forward flight by sustaining aerodynamic stability. The lift and cruise configured air vehicles use one set of motors for hovering, and other sets provide thrust during cruise. In the different prototypes e-VTOL vehicles also introduced the use of electric ducted fans (Bacchini and Cestino, 2019) and reliable Distributed Electric Propulsion (DEP) systems (Fard et al., 2022). Different design architectures and battery specifications of future e-VTOL air vehicle is represented in Figure 1.

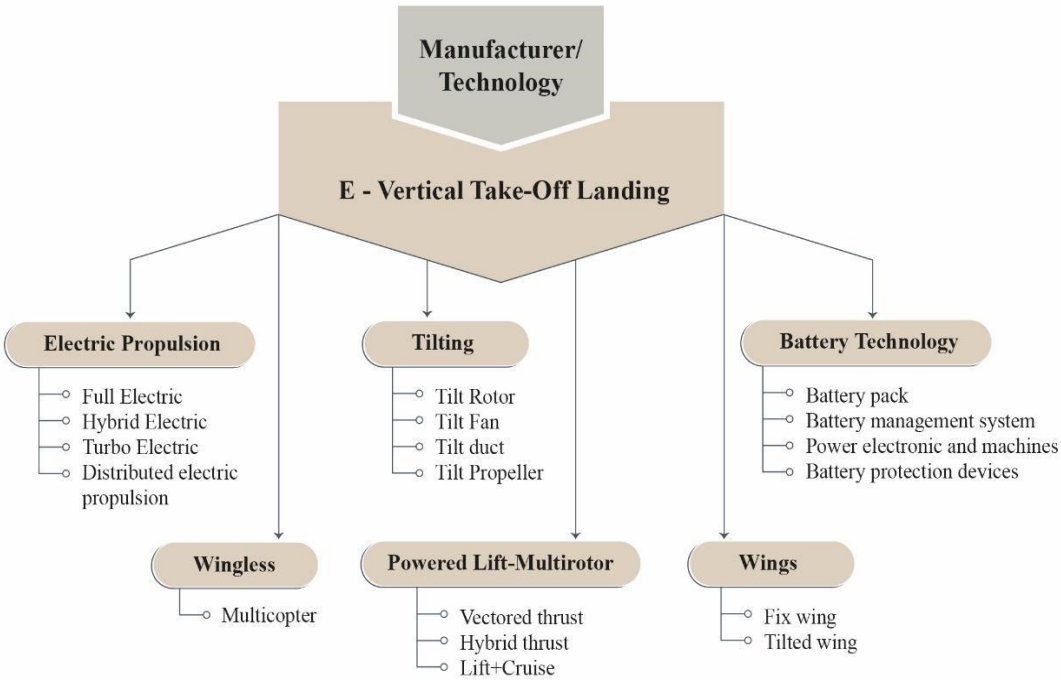

Fig. 1. The e-VTOL design type and parameters of future e-VTOL air vehicles

Table 1. Commercial performance of e-VTOL aircrafts (Source: VFS, 2023)

Manufacturer	e - VTOL	PAX	Range km	Speed km/h	ALT Meter	Empty Weight, kg	Payload kg	MTOW kg
Airbus	City Airbus	1+3	80	120	3100	1950	250	2200
Archer	Midnight	1+4	80	240	610	1050	450	1500
Beta Tech	ALIA-250	4	463	270	2438	2540	635	3175
E-Hang Intel. Tech	EHang216	2	35	130	3000	360	260	620
Jaunt Air Mobility	Jaunt Journey	1+4	129	282	1829	1633	453	2722
Joby Aviation	S4	5	290	322	3350	1950	453	2404
Lilium	Lilium jet	7	300	300	3048	1800	700	2500
Vertical Airspace	VA-X4	4	161	241	3000	2750	450	3200
Volocopter	VoloCity	2	65	110	1981	700	200	900
Wisk aero	Cora	2	100	180	900	1088	180	1268

Features and technical data of e-VTOL aircraft differed by variety of operation performances in terms of take-off weight, payload capacity, passenger seats, cruise speed, and flight distance. Those main operational parameters of UAM aircraft are important for future UAM operators to define the objective of established companies to predict their area of activity. A summary of willing aircraft mission capabilities found in the open sources is shown in Table 1. The majority of proposed features can be considered when purchasing UAM air vehicles suitable for the geographic location of the given country

The above-mentioned shortlist is considered to be high-level propulsion technologies for today's design concept of UAM vehicles introduced by the top ten Original Equipment Manufacturers. Among them there are different e-VTOLs with different design philosophy as a wingless multi-copter, hybrid, lift + cruise, tilt-rotor, tilt rotor + wing, and thrust vector concepts (Vieira et al., 2019). CityAirbus, EHang, and Volocopter have a range less than 100 km which is suitable for short distances within metropolitan areas; Joby S4, Alia-250, and Lilium Jet have a long-distance capability of over 300 km, while ensuring connectivity between regional cities, the remaining aircraft aiming to operate between city centers and suburbs/rural areas. The airspace coverage area consists of a maximum cruise altitude of up to 3350 meters, which makes it very important to follow noise requirements at every range of height levels.

Requirements applicable for air vehicles to ensure UAM network operation are manifold and depend on particular regions. In order to evaluate their mission effectiveness, profitability, and economic feasibility, a vital role plays in determining the specific required power of motors and propellers as well as the energy efficiency of batteries to meet the operational objectives of UAM operations at selected routes. Table 2 stipulates the current design configuration of ten e-VTOL aircraft manufacturers with a number of rotors, motors, and propellers specifications for optimization of future operation of the offered vehicles types. However, the given parameters may differ from real characteristics taking into account several factors. The presented characteristics are important relative to cruise, landing maneuvering, and hover/vertical flight efficiency, which would shift the initial design accounts and lead to completely different optimal features.

Table 2. Design configuration of future e-VTOL air vehicles (Source: VFS, 2023)

Manufacturer	e - VTOL	Design Configuration
Airbus	City Airbus	Multicopter, 8 pitch rotors and 8 ducted propellers
Archer	Midnight	Vectored Thrust 12 Elec. Propellers, 6 Tilt and 6 Fixed Propellers
Beta Tech	ALIA-250	5 Electric Motors, 5 Propellers, 4 Fixed and 1 pusher Propeller
EHang Intel.Tech	EHang216	Multicopter, 16 lift thrust rotors and 16 propellers
Jaunt Air Mobility	Jaunt journey	Electric Rotorcraft 4 Propellers, 1 Rotorblade, 5 Electric Motors, Tilted Rotor
Joby Aviation	S4	Vectored Thrust 6 tilt propellers and electric motor
Lilium	Lilium jet	Vectored Thrust 36 ducted Fans 36 electric motors, Tilted controllable flaps
Vertical Airspace	VA-X4	Multicopter 8 propellers and electric motors, Tilted Rotor
Volocopter	VoloCity	Multicopter, 18 pitched propeller, 18 rotors
Wisk aero	Cora Gen 5	Multicopter, 12 propellers and1 Forward flight pusher propeller

4. Theoretical Setting

Theoretical setting considers the importance of reliability of key components, mainly powertrains and battery technology. Electric motor/propeller parameters are important, because of their direct relations to the power (required) requirement (called specific power) during vertical flights, called hovering phases ((take-off (TO) and landing)). During hover (TO/landing) the e-VTOL aircraft use all motors, flying in multi-rotor mode, until switching to cruise mode.

Efficiency and high performance vertical and cruise powers, classified as power required, of electric propulsion systems for e-VTOL aircraft, largely determine their capacity in terms of payload and range of operation (Palaia et al., 2021a; Ugwueze et al., 2023).

The initial energy source of e-VTOL aircraft has been highlighted as a determinant of payloads that rely on battery specific energy density depending on battery weight, which consists of packs, energy management, and thermal protection systems.

The variation of the battery weight depends on the specific energy density controlled by its rates, and the payload range is calculated considering the battery weight for the fully loaded aircraft using the total energy availability. Moreover, the availability of total energy is computed by adding the energy required for each mission phase, which the flight range is extended with a decreasing number of passengers (Akash et al., 2021).

The introduced equations (1-10) describe electric propulsion modeled according to the actuator disk theory, which is similarly applicable for wingless and powered lift configurations. The battery system power models presented in this study are used to classification battery specifications in operational and demand terms for each mission phase of e-VTOL vehicles.

The model describes the assumption that air flow across the rotor disk is constant and weight (W) is equal to the thrust (T) produced by rotor disk, therefore ideal specific power (SP) during hover stage is consequently, equal to product of rotor thrust and induced velocity (T_{v_i}), *which* ($SP_{hover,i} = T_{v_i}$), where;

$$T_{v_i} = \frac{T^{3/2}}{\sqrt{2\rho A}} \tag{1}$$

For accurate estimation of hovering power and to account losses because of the profile drag acting on the rotor blades introduced a figure of merit (FM), which represents the actual specific power (SP) required for hover ($SP_{hover} = SP_{hover,i} \,/\, FM$) is expressed as following (Eq 2)

$$SP_{hover} = \frac{T^{3/2}}{FM\,\sqrt{2\rho A}} \tag{2}$$

The specific power for the climb and descend determinants as ratio between specific power during climb and descent (P_{climb} and $P_{descend}$) to the power during hovering (P_{hover}) that use the e-VTOL aircrafts $\left(\frac{P_{climb}}{P_{hover}} \; and \; \frac{P_{descend}}{P_{hover}}\right)$ whereas, climb and descend velocity is equal to vertical velocity ($V_{climb} = V_{descend} = V_v$).

In the case if the ratios (V_v/v_{hover}) more than or equal to zero, the vehicle is moving to upward direction, and vice versa, if the value is less than or equal to zero, the vehicle is in the downward position. Consequently, the specific power (SP) for climb and descend is expressed as follows, according to (Eq 3 and 4);

$$SP_{climb} = \frac{V_v}{2v_{hover}} + \sqrt{\left(\frac{V_v}{2v_{hover}}\right)^2 + 1} \tag{3}$$

and

$$SP_{descend} = \frac{V_v}{2v_{hover}} + \sqrt{\left(\frac{V_v}{2v_{hover}}\right)^2 - 1} \tag{4}$$

Equations (2, 3 and 4) represent the specific power that complete the power models required for vertical flights (Mattingly et al., 2002; Newman, 2007; Johnson, 2012; Gudmundsson, 2013; Palaia et al., 2021b; Ugwueze et al., 2023). However, depending on technological improvement, in the future it can be replaced with new design configurations applying modern concepts and theories.

NOTE: Power required is used as actual power required and expressed as specific power (SP) requirements.

However, at cruise altitude, the flight dynamics differ between the powered lift and wingless types. The powered lift type is considered a fixed-winged aircraft, and the corresponding fixed-wing power models are applied, with adaptations for a battery energy source. The SP to cruise for the powered lift (PL) aircraft types ($SP_{PL\ cruise}$)

is expressed referring to (Eq 5).

$$SP_{PL\ cruise} = \frac{1}{\eta_{prop}} D\, V_{cruise} \tag{5}$$

The specific power required at cruise flight level is lower than the in vertical modes (hover, TO and landing) accordingly, a variable pitch propeller has been assumed in order to avoid a reduction in propeller efficiency (η_{prop}).

Meanwhile, the wingless e-VTOL type is modeled as rotorcraft in forward flight and the SP to sustain the wingless (WL) air vehicle types during forward flight and the SP to sustain the wingless (WL) air vehicle types during forward flight ($SP_{WL\ cruise}$), the applicable (Eq 6) is given as;

$$SP_{WL\ cruise} = T\,(V_{cruise}\ sin\ sin\ \alpha + v_i) \tag{6}$$

The function of total drag (D) and its thrust (T)

determinants the angle of attack (α) in variation during flight depending on taking the cruise velocity (V_{cruise}).

Specific energy demand during vertical flights which covers hover, climb and landing phases absolutely obtained from the (Eq 7) as follow;

$$BSP_{hover} = \frac{1}{\omega_{bat}} \frac{g}{\eta_h} \sqrt{\frac{\sigma}{2\rho_{air}}} \quad (7)$$

Analysis of the power requirements and demand of e-VTOLs batteries reveal high discharge rate during vertical flights, however during cruise flight the battery consumes less energy slowing down the discharge trend. The energy estimation is adjusted to account for two aspects of flight, which include the cruise flight and trip duration (Yang et al., 2021). The battery requirements for specific power during a cruise are as follows (Eq 8);

$$BSP_{cruise} = \frac{1}{\omega_{bat}} \frac{g}{\eta_c} \frac{V_{cr}}{\frac{L}{D}} \quad (8)$$

The energy requirement for cruise flights is based on load factor, depending of the trip length, which calculating according to Breguet range formula (Eq 9), (Patterson et al., 2012; Kasliwal et al., 2019),

$$R_{trip} = SE_{trip} \frac{L}{D} \frac{\eta_c}{g} \omega_{bat} \quad (9)$$

Energy storage capacity is measuring its operational suitability, which average usable battery efficiency typical for lithium-ion batteries varies between 80% and 90% (Yu et al., 2020; Zhao et al., 2021), while specific energy density is between 170 Wh/kg and 350 Wh/kg (Adu-Gyamfi and Good, 2022). The number of charging cycles of lithium-ion batteries impacts their life cycle and longevity, as well as charging level over time. The charging times of batteries are accounts according to (Eq 10),

$$t_{char} = \frac{SE_{trip}}{SP_{char}} = \frac{R_{trip}}{SP_{char}} \frac{g}{\eta_c \omega_{bat} \frac{L}{D}} \quad (10)$$

The minimum state of charge is 20%, and setting the minimum capacity protects the battery from damage, improves the overall battery life, and reduces maintenance costs. Full-electric e-VTOL aircraft operating for UAM missions, may also utilize the extra battery reserve to be able to use if an exceptional emergency occurs at a low battery level (Ugwueze et al, 2023). The given main technical data statements for electric motors/propellers and battery characteristics have the same purposes for the safety operation of e-VTOL aircraft as well as a visual introduction for readers and future stakeholders. The aim is to accept the importance of systems upon operation and to consider future fleet management and maintenance actions to ensure prescriptive safety in the proposed region.

5. Description of the Study Area

Baku is selected as a large and most traffic congested city during the daily working hours, which proposes to analyze the feasibility to applying UAM mission models to solve the intra-city transportation challenges. However, suburban road connections with city centers also desire improvement to mitigate congestion by using the UAM concept. In order to satisfy the explored mission requirements, it is necessary to define accurate population distribution, flight destinations, air routes, landing areas for vertiport locations, and weather conditions that are not specifically ordinary for air transportation at low altitude, particularly in Baku megapolices. For this study, the first priority junctions are air-routes between the city center and nearby districts that have a tighter relationship relating to business and cultural matters. Because of excessive traffic congestion between these geographic areas, it has become necessary to create air connection routes in order to mitigate the challenges on the roads entering city centers from four directions. Due to the allocation of most administrative authorities, health care service centers, universities, and entertainment facilities in downtown surroundings congestion remains a huge problem for the urban population and its guests.

The considered network design area is the city center and surrounding suburban places, which have 12 administrative regions, and 59 townships (Presidential Library, 2019). These township cover 2140 sq.km of land surface, with total populations consisting of 2.464.162 at the end of 2023, and average density 1092 people per 1 sq.km (WPR, 2024).

According to Baku General Plan, developed until 2040, the city center will be classified into applied three types;

1. The main center-which includes the central districts of Baku city (Nasimi, Sabail, Yasamal, Narimanov, Khatai) ensures a hub of administrative and business services, as well as cultural events and touristic purposes.

2. Municipality centers-located nearby from downtown (Hovsan, Sabuncu, Lokbatan, Zigh, Khirdalan*Binagadi) as a suburbanly populated area providing access to city centers from several efficiently managed public ground transportations.

3. The regional urban centers-located far away at the edge of the metropolitan area, were assigned the strategically important entry gate directions to Baku center from the North (Sumgait*), West (Alat) and East (Mardakan). These three regional centers hold significant land capabilities, enabling the expansion of useful territory and population growth advantages in the region.

Note*: Khirdalan and Sumgait are out of the Administrative Boundaries of Baku City.

The Baku General Plan proposes a polycentric development model based on the existing context, which aims to ensure equal levels and opportunities of appropriate services for each city resident. Thus, the proposed multiple urban centers system is a guide for common spatial development, which in turn will improve the quality of life of the population (Arxcom, 2024).

5.1 Weather Characteristics of the Study Area

Baku metropolitan area has its own specific environment, especially geographical location surrounding Caspian Sea and vulnerable weather conditions accompanied by intensive north winds and gusts. Boundary conditions for flight operation existed a long time upon entry into commercial aviation, which limited even the life cycle of the airframe because of high humidity. Air vehicles suitable for this study most certainly will combine various technical and commercial characteristics, taking into account the unstable weather conditions typical of Baku city and suburban areas.

(A). Density altitude (DA) is the pressure altitude above mean sea level (MSL) corrected for non-standard temperature, in which the air has a certain value of density. DA is a unit describing the performance metric of the aircraft; thus, air density is an important weather factor impacting aerodynamic and engine power output features accordingly, the calculation of density altitude allows to define the accurate elevation for landing and take-off for aircraft.

Density Altitude calculations are beginning to find out the value of air density, first considering ideal gas low ((Rd = J / (kg X deg K) = 287.05 for dry air)), using the standard ISA sea level parameters expressed as;

P = 1013.25 Pa, T = 15 deg C (deg K = deg C + 273.15), and the air density at sea level, D = 1.2250 kg/m3.

Applying the given steps below, density altitude can be calculated by known weather parameters:

a) Ambient Temperature (Degree of Fahrenheit (F) or Celsius (C))

b) Dew Point (Deg of F or C)

c) Altimeter Setting (Pressure, mb)

d) Absolute Pressure (mb), and

e) Air Density (kg/m3), using the dew point temperature according to (Eq 11);

$$\rho = \left(\frac{P_d}{R_d T}\right) + \left(\frac{P_v}{R_v T}\right) \tag{11}$$

f) Water Vapor Pressure (WVP).

Water vapor pressure is a calculation that comes across saturation vapor pressure as a polynomial developed by Herman Wobus according to (Eq 12);

$$E_S = \frac{e_{so}}{p^8} \tag{12}$$

However, following the curve fitting equation, often called Tetens' Formula, which WVP gives accurate results by applying (Eq 13);

$$E_S = c_0\, 10^{\frac{c_1 T_c}{c_2 T_c}} \tag{13}$$

particularly at higher outside air temperature, when saturation pressure becomes significant for the DA calculations.

The equations and proposed steps for density altitude calculation introduced by Shelquist (2024), are similarly demonstrated in Appendix 1 (airdensityonline, 2024) by comparing the recent (30.08.2021) and current (01.01.2024) available data weather conditions for Baku city, which indicate a variety of values in different seasonal periods which is important to consider upon implementation of UAM operations, especially altitude density.

Determination of density altitude is important to clarify prescriptive aircraft performance at a given flight level and monitor the parameters during vertical climb and descent. The measurement of the density altitude for a particular location is carried out by affecting three key atmospheric factors; air pressure, temperature, and humidity. High ambient air temperatures are less dense, therefore, by increasing altitude, the air density (according to Equation 11) is reduced accordingly. In spite of the fact that humidity does not significantly impact density altitude, the volume of water vapor in the air determines the precise calculation of density altitude according to Equation 13. High density altitude has a negative effect on aircraft aerodynamic performance, particularly during take-off and climb rates influenced by temperature; humidity mainly reduces engine thrust power as well as rotors and propeller efficiency (FAA, 2008). Density altitude is highest during the summer due to the higher temperature inherent to Azerbaijan, and in the winter weather density altitude is significantly lower in all Baku urban areas.

(B). Impact of wind speed and gust on e-VTOL aircraft operations are primary weather parameters in areas such as Baku, where wind speed and direction can be changed at any time of the day and hours. The definition of wind/gust limitation for each particular urban proposed air vehicle contributes to the selection of aircraft types for its future operations in unstable weather conditions. Requirements for wind velocity and gust are under standard rules, but analysis of the impact of turbulence, tailwind, and crosswind requires detailed investigations for aircraft with low-speed approaches and hovering landing and take-off features. Key

principles and flight rules of UAM aircraft operations in the near-term are assumed using Visual flight Rules (VFR) and instrument flight rules (IFR), and mid-term ConOps will be applied to published Radio Navigation Performance (RNP) routes and instrument procedures (Boeing, 2023). The VFR operation rule in snow conditions requires visibility of 0.5 miles (800 meters), with an ambient temperature of -4˚C and initial take-off and final approach phases at relative steady wind condition have been considered at 17 kts (31.5 km/h), (EASA, 2019). Due to its location on the Absheron Peninsula, Baku and its surroundings are opened by the coast of the Caspian Sea from three directions, while the North wind is mostly prevailing, followed by other directions. Maximum wind speed reaches 40 kmph (21.6 knots), and average speed consists of between 15 and 25 kmph (8 and 13.5 knots). Average wind gusts fluctuated between 25 kmph and up to 40 kmph (13.5-21.6 knots),

Indeed, wind characteristics are an influential factor in the design configuration and aerodynamics of the aircraft, moving air over the surface and transforming it into pressure. Measure of the force exerted on a surface by the wind, expressed as a force or wind load on the whole surface, which in the International System of Units (SI) is Newtons or Pascals (Johnson, 2020). Wu et al. (2019) conducted a detailed overview of gust loads on aircraft and concluded that the induced force influences the detrimental effect on aerodynamic performance and structural damage under increased loads. Pradeep et al. (2020), investigated optimal trajectories at wind conditions for multicopter type of e-VTOL aircraft and found that it restricts flight endurance due to the low specific energy of Lithium-ion batteries. Schweiger et al. (2023) examined the impact of wind/gust speed conditions on UAM air vehicles in the Hamburg and Munich areas and recommended considering decisions for vertiport locations and traffic flow performance.

Consequently, the determination of specific power rotor/propeller and batteries need to add the loads extracted by wind speed and gusts to the existing design performance. This can be expressed as an error coefficient or factor of wind/qusts load $(F_{(w/g)l} = W_{l})$, deemed for recalculation of e-VTOL design parameters to obtain an accurate result considering the wind load on rotor/propeller dynamic characteristic as per (Eq 14).

$$F_{(w/g)l} = \frac{1}{2}\rho V^2 A \tag{14}$$

As far as the square surface area of particular air vehicles is unknown, the precise power of rotors/propellers will remain unpredictable. Wind force will reduce the power efficiency of rotors/propellers, while reducing the battery energy density to an equivalent value. The value of equations (2-9) from the constant value will be shifted to the real value, accompanied by wind load factors.

The evaluation of the weather barriers for UAM operations introduced by Reiche et al. (2021) demonstrated the impact of wind speeds, dividing them into four categories: slow between 0 and 15 knots, and median average is 15-20 knots, high scale is 15-20 knots, and the value more than 25 knots is critical. The result found that vertical wind shear (gusts) over 35 knots will be dangerous for e-VTOL aircraft operations over megacities. Furthermore, NASA in collaboration with AvMet Applications Inc., set up a wind threshold for UAM air vehicles (Ng, 2022), classifying horizontal wind speed limitations as <15 ± 5 kts (green), <20 ± 10 kts (yellow), >25 kts, or gusts >35 kts (red).

The use of comprehensive weather conditions, including air temperature, rain, wind, cloud, icing, and precipitation is accompanied by operational restrictions on the overall air transportation system, and under these circumstances, UAM operation is not excluded as a new transportation mode. Taking into account the limitations associated with periodic variation in ambient air parameters, uncertainty remains a main challenge because of the regulatory framework, and standard procedures laid out based on actual data of e-VTOL aircraft performance as well as air navigation route characteristics at low altitude.

The smaller size e-VTOL aircrafts are more vulnerable and sensitive to weather conditions such as wind shear and gusts, air pressure and density altitude, visibility range, low altitude icing conditions and overall temperature changes. Indeed, UAM vertiport is capable of getting up-to-date weather information through sensors and transferring it to the relative operational station, ensuring reliability and safety at each stage of air vehicle flights. Recognizing the potential weather challenges, meteorological analysis is a serious matter for providing substantial UAM aircraft operations. Available historical weather data obtained from the World Weather Application Programming Interface (WWAPI, 2024) allows an assessment of the meteorological status of Baku city, in order to examine the future challenges and advantages of UAM operations, and applying advanced preventive actions.

6. Results and Discussion

To establish a successful UAM operation, efficient infrastructure with suitable characteristics is essential. The elements and relevant performance of UAM ground infrastructure and airspace management have to provide passenger and aircraft throughput at a satisfactory level in all stages of flight operations. Therefore, a properly managed relationship among the involved infrastructures contributes to setting up useful urban mobility network options. For UAM operators and flight planning management, one of the crucial approaches

may be a close collaboration among stakeholders, across the widened urban air mobility ecosystem (Kamargianni and Matyas, 2017; Pons-Prats et al., 2022). The basic on ground physical infrastructure for UAM operations is vertihubs, vertiports, and vertistops that have a relatively small footprint, allowing them to build it near urban and suburban accessible zones. In addition, requirements for communication, navigation, and surveillance (CNS) need to be developed applying highly sustainable 5G/6G wireless devices. The combination of reliable ground structures helps define the right air traffic routes for e-VTOL aircraft integrating the Air Traffic Management system as well as interoperability between air vehicles (Holden and Goel, 2016). The modeling of the UAM network applicable to the Baku metropolitan area was analyzed by considering initial determinant factors such as the urban flight destinations, vertiport placement, validity of the proposed business model, applicability of weather conditions, suitability of e-VTOL aircraft types, with the best safety features and maneuverability, as well as existing and developed rules in state regulation frameworks.

6.1 UAM Airspace Classification and Operation

Urban airspace management at low altitude driven by e-VTOL aircraft is associated with various complexities that need to be addressed across the implementation of the UAM concept in the future. The variety of air vehicle design specifications, forecasted high air traffic density, and determination of airspace class usage for particular aircraft are the reasons to develop air traffic rules and procedures (Qu et al., 2023). The designated UAM airspace operations are allowed above 400 ft, generally covering heights between 1500 and 4000 ft Above Ground Level (AGL), meanwhile the landing and take-off area comes below 400 ft (Collins et al, 2018). However, integration of UAM air vehicles into existing airspace classified within uncontrolled class G and flight operations will be performed using B, C, D, and E classes as well. UAM operators are responsible for advice on situational and weather awareness to ensure an optimized flight plan at selected classes while avoiding flights in hazardous conditions, associated with high dynamic wind variability and changes in ambient air parameters important for flights at low-altitude environments. (Boeing, 2023). The various e-VTOL air vehicles, such as multicopters, tiltwings tiltrotors, and lift+cruise vehicles designed for different ranges of flights in urban environments, require detailed knowledge of weather aspects affecting safety operations, including visibility, wind speed and gust, ice conditions at low and density altitudes. In order to provide reliability of the network schedules and to identify operational capability, real-time weather monitoring and advanced forecasting are important for air operators and fleet planning management (Schweiger et al., 2023). In the case of the necessity of adjustment mission plans, prior to the flight, it should be indicated all available information concerning that flight. This information could be contained according to FAA-CFR 14. 91.103 (FAA, 2021); aircraft performances, allowable payload, flight restrictions, ATC delay, charging problem, last minute weather changes, and most importantly density altitude, wind gust, and charging challenges. Requirements of accurate weather data necessary for UAM operations contribute to aircraft safe flights at the arranged route networks. In this context, an analysis of altitude density and wind characteristics is considered in this study, referring to previously conducted studies by Patterson et al. (2018).

6.2 Vertiport Installation and Energy Management

Designing of UAM operational networks based on business models as a passenger function transport system requires similar vertiport networks within ground infrastructure to provide landing/take-off pads, and also charging device facility capabilities. Placement of a vertiport is the primary factor, with its proximity to existing urban infrastructure (education and business centers, parks, ground and underground transportation stations) defines the efficiency of the action as having a mutually affordable connection (Choen, 1996).

Currently, modern vertiport developments are presented as a particular case (Thiemer, 2020) and in the model of conceptual design (Dezeen, 2020) introduced by several researchers however, the ground operational infrastructure should be far away from high-voltage electrical stations, or wind turbines causing airflow disturbance, which may hinder flight operations impacting electronic communication waves (Mulinazzi and Zheng, 2014). Moreover, safety assurance is the most important since the e-VTOL aircraft performs the mission in urban airspace. The definition of landing pads in often cases uses as vertistops, vertiports, and vertihubs (MVRDV, 2018; Krylova, 2020), In addition Skyports and Rooftops can be considered potential landing areas within city centers due to a lack of land spaces to ensure UAM operation (Vascik, 2019). Concerning vertiport dimensions and technical requirements, it is still an open-ended question, yet either the ICAO (2020) Annex 14, Volume II, "Heliport Planning and Design" or the EASA (2019) document CS-HPT-DSN, can be adapted, adding new standards to existing regulations. Unlike heliport planning developed for helicopters, considering ground handling services and maintenance, for the e-VTOL aircraft is necessary charging stations to meet demand of energy sources. Charging stations for full electric air vehicles at vertiports must be equipped with a powerful electrical grid system able to serve several aircraft within each interconnected parking zone, at the time. The power

grid system is a new and smart central energy generation unit having various subsystems such as controllable solid-state and local transformers, as well as stationary batteries, to ensure a stable energy supply for UAM vehicles.

A high-level electrical grid structure, consisting of electricity generated from power plants, then transferred the available energy to local distribution systems using regional transmission lines. The regional distribution center then transmits the necessary energy capacity to vertiport customers (Thipphavong, 2022). A smart distributed control unit monitors the overall energy system to balancing power fluctuations and adjust energy supply, in order to transfer the required energy demand to consumers. This provides an adequate energy demand for e-VTOL batteries, avoiding physical damage of components and increases the efficiency.

e-VTOL aircrafts, designed exclusively for electrical propulsion and energy storage systems derived special take-off and landing space requirements depending on construction dimensions. Parking places equipped with charging stations at vertiport facilities are considered a safety requirement. Methodical approach for selection of current networking and vertiport placement in this paper is based on own estimations without referring to literature or expert consensus (albeit, literature and expert opinion are absent or not available at all). However, according to the study conducted by Fadhil (2018), the vertiport placement is preferable due to its proximity and accessibility to main ground transport hubs, underground lines, and train stations. Rath and Chow (2019), argue that the location of vertiports for UAM operation is necessary close to airport access based on air travel data, although the airport itself may be most suitable area for vertihubs assignment.

Vertiports are represented as a smaller prototype of commercial airport terminals with take-off and landing areas, instead of runways, while differing by configuration. There are several studies dealing with vertiport placement and related facilities (Antcliff et al., 2016; Fadhil, 2018; Rath and Chow, 2019), as well as the definition of its various configurations (MVRDV, 2018; Krylova, 2020; Boeing, 2023), but none of them is based on practical experience (Pons-Prats et al., 2022). At the present, without analyzing society's demands and intended e-VTOL aircraft seat capacity, determining the vertiport throughput, number of take-off and landing pads (TLP), and parking areas for the assumed urban network, these are most probably restricted because of the initial applicable data sets. The mentioned factors become actual, being the commencement of UAM operations however, identification regarding vertiport size and configuration is approximately possible, referring to the current assumptions of standards and criteria as well as foreseen future perspectives, Table 3. Taking relevant time-consuming processes in UAM operations, which will be taken into account, like passenger boarding time, charging electric UAM vehicles or swapping batteries, aircraft cleaning and maintenance, as well as passenger boarding. When the demand increases and the operation is close to the saturation point, the changes in vertiport configuration can be modified according to the document issued by ICAO (2023).

The integration of the UAM network with the existing transportation system in the near perspectives reaches to create a multi-modal global urban network service, while increasing vertiport sizing and enhancing the effectiveness. Baku City, Sumgait, and Airport Shuttle could have an extra-large structure forming a hub and spoke model. While suburban vertiports could serve as spoke nodes, vertiport clusters in densely populated urban areas could function as hubs (Wu and Zhang, 2021). Synergy of airport shuttle UAM service with existing airport infrastructures can increase capacity using a minimum investment of funds (Choi and Hampton, 2020).

6.3 Battery Specifications of e-VTOL Aircraft

In order to increase the motor efficiencies of e-VTOL aircrafts, the battery specification and size need to be suited the payload required UAM mission. At the stage development of various design concept, the lithium–ion batteries are having a better technical characteristic, specified in faster rechargeability, higher energy power and density. Moreover, the sizing of an electrical battery with storage capacity for powering aircraft systems, should be configured to deliver up to 400 Wh/kg of specific energy density. Actual battery weight with a fully

Table 3. Network configurations and relevant functions

Network Locations	**Nardaran, Novkhani, Pirallahi**	**Mardakan, Hovsan, Khirdalan, Zigh**	**Airport-GYD, Baku, Sumgait, Lokbatan**
Configuration	Vertistop	Vertiport	Vertihub
Number of e-VTOL pad	1	2	3+
Parking area	1	2+	5+
Charging station	1	2+	5+
Management support	✓	✓	✓
e-VTOL servicing	✓	✓	✓
Gate infrastructure		✓	✓
Line maintenance	✓	✓	✓
Base maintenance			✓
Hangar facility			✓

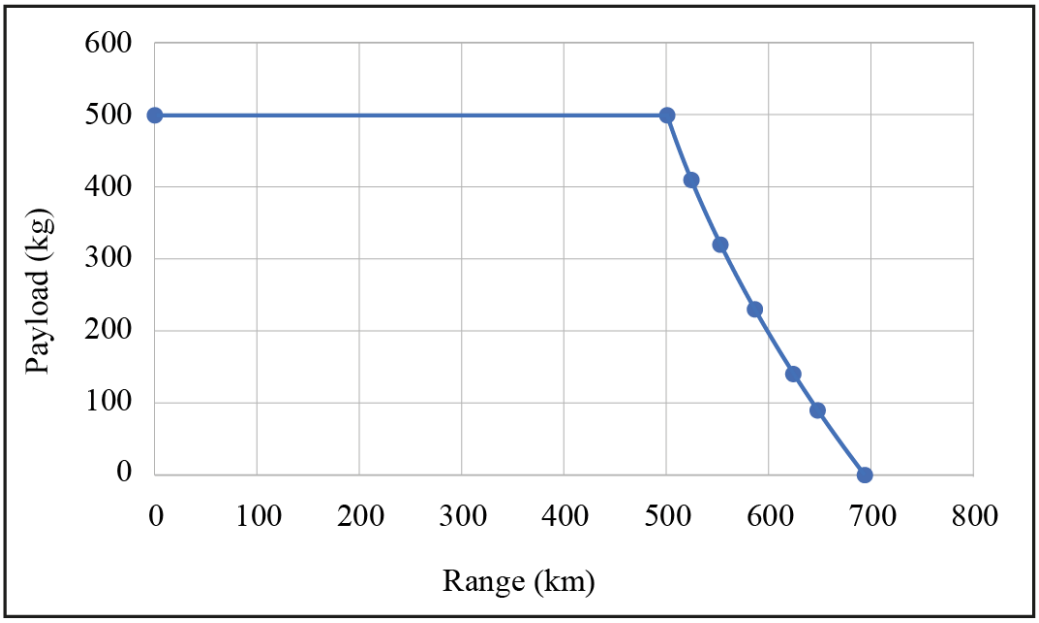

Fig. 2. The relation between payload and flight ranges (Akash et al., 2021)

occupied seat capacities per aircraft use a total energy of 741 MJ, by adding the energy required for each mission phase. Figure 2 is indicating the variation of the range, depending on the payload - number of passengers carried in the aircraft (Akash et al., 2021).

Taking into account that the battery weight is the part of the total aircraft weight, each value of specific energy density increasing by lowering battery mass, which solved using the Lithium–Sulphur battery with highest energy density equal to 600 Wh/kg (Figure 3).

The safety of electric aircraft depends on a reliability of powerplant and more important performance of an inline energy storage system providing functional link to rotor/propulsion. However, the connection between energy storage system and power capability are interrelated within the battery itself (Figure 4).

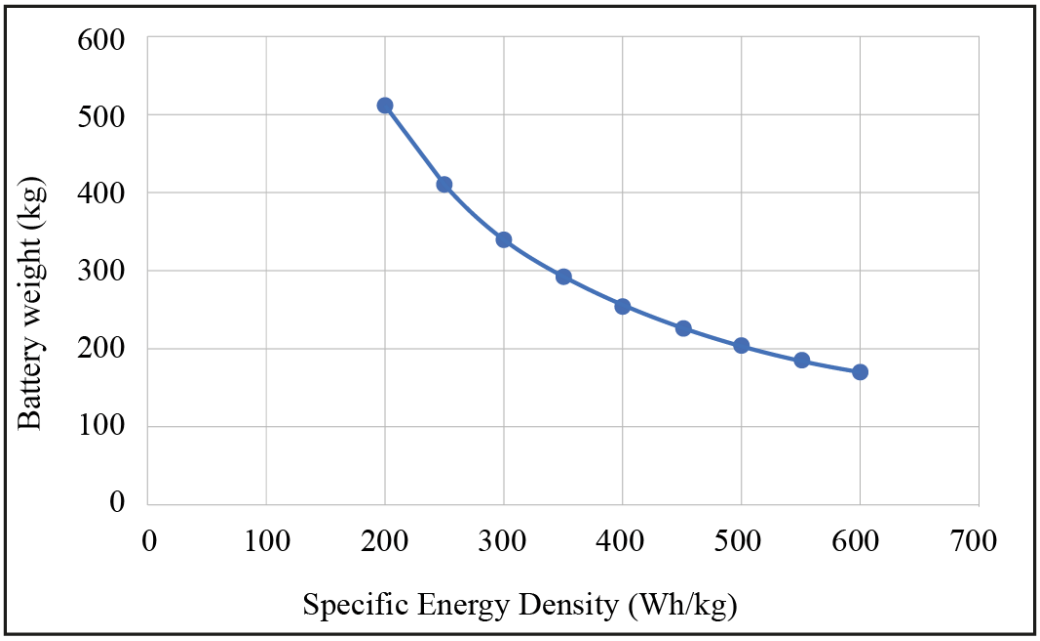

Fig. 3. The relation between battery weight and specific energy density (Akash et al., 2021)

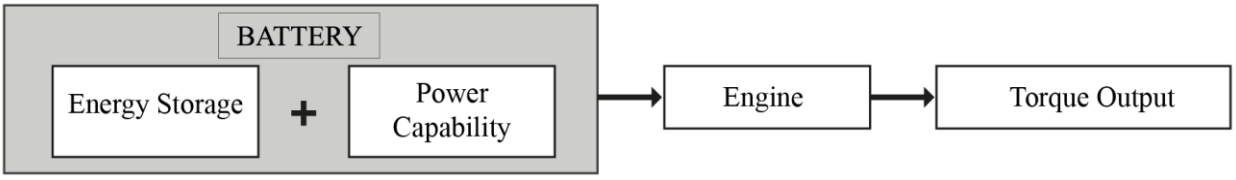

Fig.4. Schematic pathway from battery storage energy system to powertrain.

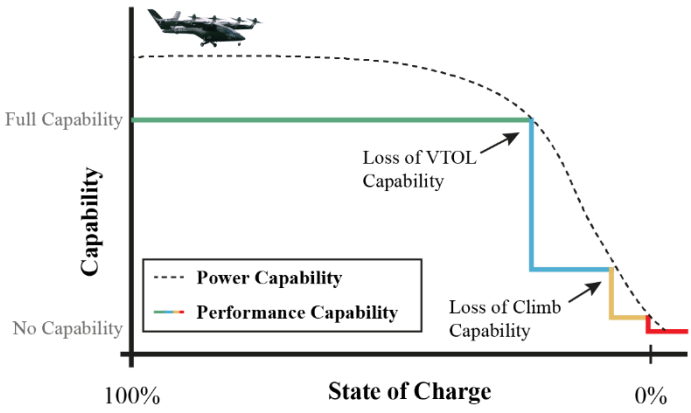

Fig.5. Energy storage system performance capability vs energy state of charge e-VTOL ((General Aviation Manufacturers Association (GAMA), 2023))

Consequently, the power capability is a function of the High Voltage Energy Storage System which include the energy state of the battery. As a battery deliver high power to powertrain system, the electric aircraft will lose some performance capability of battery by reducing power as the state of charge (SOC), Figure 5.

The State of Charge (SOC) is a metric value for estimation the remaining level of energy in the battery packs compared with the fully charged cycle, while providing the needs to be recharged. In addition, the battery is an electrochemical structure, which below 20% of discharge rate can damage its internal parts impacting on operational life cycle (Cunha et al., 2023).

Referring to study by Bills et al. (2023) generation of the EVTOL data set has developed the power profile to define the baseline battery characteristic for each mission examining charging and discharge cycle parameters as per Table 4.

During Take-off and Landing the cell is discharged at a high constant power, however landing cycle checked bit a for long time than take-off. In Cruise level the cell discharged at a lower constant power for a slightly for long duration. According to charging protocol at Charging cycles the cells are charged applying a constant current-constant voltage (CC-CV) method.

Table 4. Baseline Mission Parameters (Charge) Bills et al. (2023)

Flight mission	Parameter Definition	Results
Take-off (Hover)	54W	t=75 s
Cruise	16W	t=800 s
Landing	54W	t=105 s
Rest 1	0A	T < 27˚C
CC Charge	1C	V > 4.2
CV Charge	V=4.2	I < C/30
Rest 2	I=0	T < 35˚C

At the Rest 1 mode the cell is allowed to rest until it has cooled to a temperature below 27 °C or for at least 15 minutes and at the Rest 2 mode the cell is allowed to rest until cell temperature reaches 35 °C, then allowed to rest 15 minutes before starts to the next cycle.

6.4 UAM Service Segmentation and Business Model Application

Reviewing the UAM missions, an outcome dictates inherently to establishing suitable operational models offered by individual operators or decision makers to manage the infrastructure, taking into account the characteristics of studied area. Initially, the formation of service segmentation, in the future enables to determination of the business model, depending on the vehicle's operator capabilities. In fact, the service segment is still unchanged, while the business model can include single use or more operation functions upon owner-carrier selection.

Referring to the project "NASA Urban Air Mobility Sub-Project, " Mogford et.al. (2019) argues that air vehicle operator roles are not defined at the present however, operators are key drivers of UAM organizational processes among involved infrastructure stakeholders and, at the same time responsible persons for the airworthiness of the aircraft. Li et al., (2020) offered that future operators would be named Fleet Managers, aiming to arrange operational business models. To improve the UAM operation concept, service providers need to establish an effective partnership structure (Nneji et al., 2017), albeit according to the study by Al-Haddaet et al. (2020) the UAM operational model is still uncertain. At the first stage of operations, there are three proposed main customer segments for the future UAM market in urban environments, which are necessary to consider. Passenger carrying UAM missions will be the prevailing segment of urban transportation, next is cargo segmentation, providing door-to-door or last-minute delivery services, because of the low payload volume of e-VTOL vehicles. An emergency mission is particular, considering several use cases, including fire, search-rescue, and health care. Notably, all proposed mission operators need to perform necessary periodic maintenance services to ensure the continued airworthiness of their air vehicles. The proposed characteristics of the various actual operational models for this paper are presented in Figure 6.

Conceptual approaches for meaningful operational models with regard to passenger UAM are demonstrated in the studies Kluge et al. (2018) and Straubinger et al. (2020a). Although the interpretation of customer segmentation and business model stated differently, they have a similar aim in describing UAM operation activities in several business models.

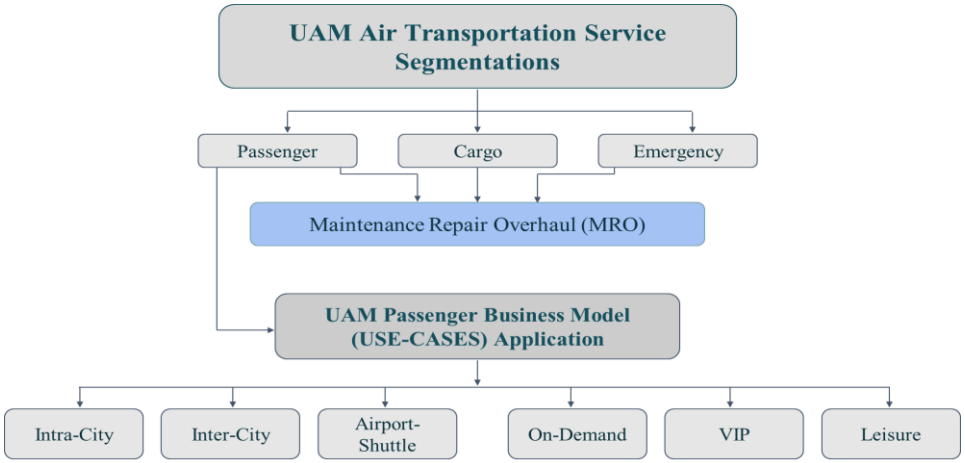

Fig.6. The proposed UAM Operation Service Segments and Business Models

In spite of many different urban air mobility missions having been proposed altogether, this emphasizes a broader definition of business models that have a strong focus on trip purposes.

The offered modes of UAM transportation vary by the purposes performed by flight destinations, classified according to business models, however the concept is still in the same meaning as air-taxi service for society (Baur et al., 2018; Dannenberger et al., 2020). The public UAM mission is intended to provide travel to and from work or on demand bases around a city, so called intra city transportation (Syed et al., 2017), rapid round-trip connectivity with the airport as an airport shuttle (Fu et al., 2019; Straubinger et al., 2021), as well as intercity operation connecting the city center to suburban and rural areas. This mode also includes regional transportation between nearby big cities using e-VTOL aircraft with long range flight capabilities (Syed et al., 2017; Volocopter, 2019). There is expectation that these flights can be set up on a scheduled basis and regularly along the same routes as an urban transportation system for optimizing air travel within an urban environment. The on-demand service model is significantly widened, where multiple individual customers are able to use a single vehicle for flights (Holden and Goel, 2016) either as an air taxi or airport shuttle as well as for emergency purposes. VIP-model is focused for customers' high income and rendered for government employees offering luxurious air transportation service in the mode of charter flights. However, leisure is not much discussed, although it is offered to leisure and tourist travelers to provide sightseeing around the region with a bird's eye view of the natural beauty and urban landscape.

Herein, the represented six business models are initially proposed for considerations of their realization upon the maturity stage of the UAM operation. There are numerous research articles attempting to establish various service model scenarios. All UAM missions can be performed under any of six business models and utilize air vehicles (air taxi), depending on destinations. A scheduled commuter intra-city or airport shuttle and an air taxi performing intercity missions are separate use cases, where each use case has the same base mission but is performed under a different business model (Patterson et al., 2018).

Ecosystem UAM involves a large number of government subjects and private stakeholders, which need mutual collaboration and agreement to develop the business. Therefore, UAM development in the near future will open a way by offering multiple business models, even if confronted with authority requirements, financial structures, and marketing problems (Pons-Prats et al., 2022). The business model, operational concept, market structures and their integration into the upcoming urban air transportation system have been proposed by several researchers, to ensure a successful UAM operation.

According to Moore (2010), the essential attractiveness of business models for users will be easy access to arrival and departure facility locations, door-to-door service, and the introduction of the on-demand mobility concept. On-demand and scheduled service concepts by Nneji et al. (2017) are considered the best solutions for commercial, private, and personal users, adding ideas to those offered by Hansman and Vascik (2016), who identified intercity and intracity use cases. Although the final functional organizational structure is not yet defined, the authors of both studies focused on the relationship between e-VTOL owners (fleet operators) and service providers as an important and dominant actor. Meanwhile, the study by Cizreliogullari et al. (2022) demonstrated that UAM operations are an air transportation ramification with a separate, equal structure consisting of four operational divisions, excluding MRO.

Reiche et al. (2018) have proposed three commercial "use cases" named, air metro, air-taxi and last-mile delivery, and the study by Baur et al. (2018) has concluded that

UAM can be valuable depending on air vehicle characteristics. Regarding UAM service segmentation, Cohen and Shaheen (2021), integrating the results of various analyses, proposed three segments and five business models of the UAM market, while emphasizing that the passenger segment will prevail over others in intensity. Similar segmentation is defined in the study conducted by Imanov (2023), while offering six business models. Furthermore, according to the findings of Al Haddad et al. (2020), the distribution and implementation of UAM are still uncertain, and the development of business models is mostly differentiated. In fact, Ernest et al. (2023) clearly describes the three most feasible use cases for passenger UAM air transportation segmentation over the near to mid-term perspectives, which are analyzed within the current paper considering only three use-cases at the initial stage appearance.

The proposed three models are applicable for the Baku metropolitan area, including intra city, suburban/district, and airport shuttle operations. Intracity service is within downtown and around, with destinations up to 50 km, meanwhile, the airport shuttle covers the same ranges and can be extended up to 150 km depending on the readiness of regional infrastructure. Inter-city assumes the journey between big cities as well as regional ones by utilizing the flight destination up to 300 km. Business model assignations and main trip characteristics are outlined in Table 5.

The purpose of all models with different functions aims to safe transportation of peoples between well-arranged networks, using a giving advantage to reduce trip times, especially in the most congested parts of the cities. e-VTOLs will become a part of multimodal transport, performing air taxi functions as a time-efficient alternative to current transportation modes, carrying a high volume of passengers on daily basis.

Table 5. UAM trip characteristics and business models

Trip characteristics	Intra-City UAM	Airport Shuttle	Inter-City UAM
Routes	Intracity, districts and suburban	Town Centers	City to City, Regional
Range	Up to 50 km	Up to 150 km	50-300 km
Average Speed	80-100 km/h	100-150 km/h	200-300 km/h
Frequency	Daily	24 hours	Daily
Network Type	Hub and Spoke	Hub and Spoke	Point-to-Point
Demand Estimation	High	High	Medium
Payload (PAX)	2-5 + Personal items	4-7 + Hand baggage	4-5 + Hand baggage

6.5 Selection of e-VTOL Aircraft Type for UAM Network Operations

Approach to aircraft selection, Stocker and Shaheen (2017) emphasized mainly, the nexus between level of automation of e-VTOL and use-cases, Bridgelall et al. (2023a), argue that, the successful deployment of eVTOL aircraft for public urban airspace prefers to use four-seat configuration battery powered air vehicles capable of autonomous operation. Straubinger et al. (2020b) demonstrated several design requirements drivers for e-VTOL aircraft that significantly impact UAM operation, however, seat capacity, flight range, and cruise speed are expressed as important top level configuration concepts. Because both systems are designed as distributed electric propulsion (DEP) concepts, which are interconnected in all electric vehicles, the current energy density and power features of e-VTOL aircraft are based on formulas; for rotors/propellers (Equations 1-6) and batteries (Equations 7-10) inherent to each flight step.

The most recent comprehensive analysis performed by Bridgelall et al. (2023b) defined the propulsion efficiency index (PEX), which serves to choose appropriate e-VTOL types. Applying three independent variables, consisting of a set of flight range, coefficient of payload, and aspect, using a linear regression model, the result found more than 90 percent of the PEX distribution level in aircraft design processes. Considering that propulsion power demand is directly proportional to battery utility consumption, this analysis also concerns changes in battery efficiency, including energy density and power. Adequately, apart from the range capability, unfavorable weather conditions, and high wind/gusts would also impact on operational performance of any e-VTOL aircraft (Bridgelall et al., 2023a).

The aircraft selection criteria depend on the established UAM flight network and operating distance. Relying on Figure 1, there are four main design concepts of UAM air vehicles: lift and cruise, multicopter, tilted wing, and rotor, with different configurations as per Table 2. According to the initially proposed networking stated in the current study, the e-VTOL aircraft within the lowest range up to 100 km capabilities are most suitable for the Baku region, as are City Airbus, EHang, Volocopter, and Cora. Usually, most big cities with suburbs cover the range within 35-50 km, including the nearest local airports. Hence, multicopters are the best inner-city air vehicles with short-distance applications enabling air taxi functions.

6.6 Designing of Urban Network Destinations For Baku Metropolitan Area

The multimodal nature of UAM operation requires integration of multiple aspects to design network mobility, involving available land surface for vertiport

placement, air navigation management, charging, communication, and service facilities, as well as affordable ground transportation to vertiports. The relationship between supply and demand in particular regions determines the optimal location of vertiports, which contribute to the modeling of air networks (NASA, 2018; Wu and Zhang, 2021). The determinants for the UAM modeling structure depicted in Figure 7, which are based on three initial input data points, as a primary component. The first includes the most congested entry gates (green pins), the second is predicted cities (red map pin), considering the identification availability of land surfaces for vertiport construction and the number of populations, the third are proposed air network connections for intracity (blue line) and airport shuttle (red line) operations using a three-dimensional (3D) Google Earth, Data Visualization Application (DVA). It should be mentioned that identification of landing pads is not considered near public-owned, commercial, and industrial areas, the top roofs of residential buildings in the downtown area, or secured zones due to land use restrictions and aircraft operational requirements, as well as to avoid negative influence on communities. Relying on regular statistical information, the most congested ground transportation occurs from four entry gate directions leading to Baku city or crossing over the center to travel to the outskirts, suburban, airport, or rural destinations.

In order to discharge the traffic, the proposed UAM network is able to significantly impact the delays on the roads, partially solving the exciting problem of residents. Lack of intensive domestic flights and train lines from South and Northern, the Enters 1 and 2 (green pin) are overloaded due to regional cargo and private transportation, with suburban and intracity travelers. The train line to the West is operational, however it's not affected by the decreasing traffic solution in two directions, because the western highway has a in both directions. Meanwhile, the ground transportation infrastructure remains complicated on the ways from the Eastern side of nearby districts and suburbs, uniting all destinations at entries 3 and 4 (green pin). The average radius of the Baku metropolitan area consists of approximately 30 km from the city center within maximum distance to Sumgait (35.6 km) and Pirallahi district (39.8km), and with a minimum distance to Zigh (7.4 km) and the central stadium (9.5 km) near Enter 3. Three geographic locations from the West of Baku covered Sumgait, Khirdalan, and Lokbatan providing an excellent opportunity to enable the significant contribution of the establishment of regional networking UAM operations for middle and long-ranges, including Eastern Zangezur economic territory. Taking into account proposed urban network destinations, the installation of vertiports will differ depending on daily operational capabilities, interest and the number of populations willing to use the offered intracity air transportation service by applying brand new technological achievements.

In recent years, there have been numerous publications to study the advancement of the new UAM concept based on e-VTOL aircraft. The prediction from industry stakeholders is relatively positive, as these air vehicles are able to provide safer, noiseless, and more efficient air transportation service in low altitude airspace (Xu, 2020). Both organizations, NASA, and FAA, emphasize studying UAM aircraft characteristics, network design, and market feasibility continuously (Gibson, 2017) in order to update situations in current progress.

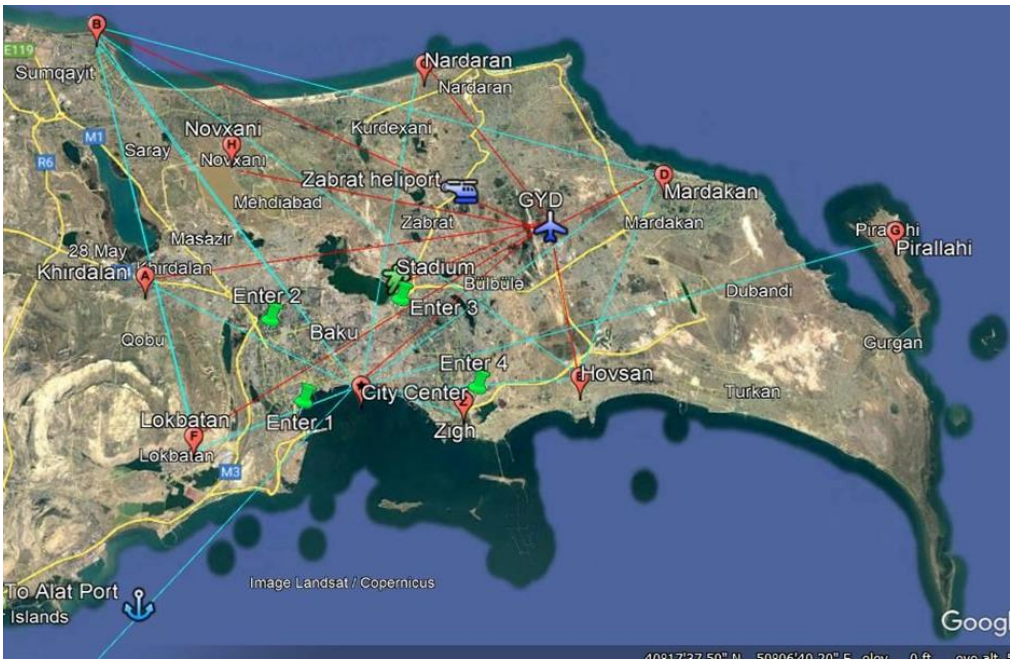

Fig.7. Proposed UAM networking for Baku metropolitan area

6.7 Regulatory Framework Necessary to Establish with Administrative Authorities

The intended project to deploy UAM services requires the definition of applicable standards and regulations to ensure safety operation, and sustainable integration within the overall transportation system of big cities. To provide common knowledge and skills concerning UAM air transportation within and between urban areas relevant regulatory frameworks are necessary for each infrastructure activity. The regulatory framework is different across countries and significantly varies depending on the specific regional conditions. To the author knowledge, there are not any documents yet, concerning the UAM concept issued by Azerbaijan authorities. However, public service representatives should consider adapting necessary regulatory documents, referring to previous or basic recommendations issued by international aviation organizations. Effective integration of UAM operations in the Baku metropolitan area and urban environment through the coordination and engagement of civil aviation representatives as an organization developing regulations and standards.

7. Conclusion

Urban Air Mobility e-VTOL aircraft manufacturers, involved organizations, and stakeholders are attempting to deploy the concept beginning in 2025 and in 2026 expected to be globally (urbanairmobilitynews, 2023). However, many experts assume that in 2030 UAM air transportation will become more widespread (Chomsky, 2023) other than following years. There are signs from different countries as the USA, Japan, Germany, France, China, Korea and Singapore enforcing to the initial preparatory stage of implementation and certification. As a new mode of urban air transportation, eVTOL aircraft will provide mitigation of traffic congestion on the roads, safe and noiseless operation, as well as zero-emission, because of full electric powertrains with a distributed propulsion system.This study presents a comprehensive scenario for improving intra-city mobility criteria, and the use of eVTOL aircraft in the public airspace of the Baku metropolitan area, considering passenger segmentation use cases, network planning, vertiport and navigation infrastructure requirements, weather conditions, and suitable aircraft selection. Despite the analysis, there are still significant limitations to finding detailed references to published data, associated lack of regulatory framework issued on behalf of aviation authorities. The challenges that need to be overcome, rely on government policy requirements, introducing changes in urban planning for vertiport installations, rules of air traffic management over urban airspace, providing reliable wireless equipment to ensure communication, navigation, surveillance (CNS), and society acceptance.

Notwithstanding the limitations and challenges, this paper has practical and theoretical implications for policy decision makers. The findings provide a practical perspective for urban planners and involved single companies, which may be useful guidelines at the initial stages of UAM services and obtaining significant information about e-VTOL aircraft and its design configurations to overcome arising barriers in the implementation processes. The study not consider financial evaluations regarding infrastructure management, the establishment of regulatory documents and the air vehicle prices. The theoretical contribution of this paper is that the industry needs more research to fully capture the initial and future implications for Azerbaijan and all regions. Therefore, it enables local scientists to explore different relevant topics concerning the overall UAM operational concept, infrastructure management, and financial analysis. Consequently, it can motivate aviation stakeholders to investigate a UAM market, conduct a safety assessment, and to consider the feasibility of the potential investment opportunity, cost estimation for insurance and maintenance, as well as be used to explore in future work. Furthermore, this study supposes that e-VTOL aircraft to be reliable in autonomous operation mode over urban environments, performing air mobility missions, and will see higher demand for expansion in this sphere of application. Particularly, short-range multicopters largely suit air taxi functions around residential areas of big cities and nearby suburbs.

Application of e-VTOL aircraft enabling UAM missions associated with new configuration architecture can have an added-value benefit of expanding higher speed and improved cruise efficiency, as well as reasonable operating and maintenance costs. The energy expenses will be much less than the fuel price, in addition electric propulsion components contain fewer moving parts and lubrication points, which are significant resource and cost savings (Patterson et al., 2018). The various design configurations of UAM vehicles, upgraded with electrical propulsion and reliable battery storage capabilities, contributed the exclusion of complex flight control actuators, mechanical transmission, the use of fossil fuels and many others in progress of effective use the urban air transportation mission in the largest megalopolises (Rezende and Barros, 2018). Successful largest companies such as; Boeing, Airbus, Volocopter, Wisk, Lilium, and others, after performing test flights, prepare their machines for certifications, which look forward to entry into service nearly in 2025-2026. Moreover, the presented UAM aircraft have many types, while keeping similarities in distributed electric propulsion systems in all-battery configurations. Ongoing upgrading processes in the development of

UAM air vehicles are expected to achieve the required reliability to meet future user demands, enable high safety performance, and obtain society's perceiving (Pons-Prats et al., 2022).

Nomenclature

BSP_{hover} : Battery Specific Power for hover

BSP_{cr} : Battery Specific Power for Cruise

R_{trip} : Distance for trip

SE_{trip} : Distance for trip

SP_{char} : Specific Power for charge

t_{char} : Time for charge

V_{cr} : Cruise speed

L/D : Lift to Drug ratio

ω_{bat} : Battery weight fraction

η_h : Hover efficiency

η_c : System efficiency

g : Gravitational constant

σ : Disk loading

ρ_{air} : Aircraft configuration (load factor)

P_d : Pressure of dry air (Pa)

P_v : Water vapor pressure (Pa)

R_d : Specific gas constant for dry air J/ (kg.K)

R_v : Specific gas constant for water vapor J/(kg. K)

A : Surface are (sg.m)

F : Force

T, T_c : Air temperature degree C

V : Wind speed

E_S : Saturation pressure of water vapor (mb)

P : Standard pressure at sea level 10.13 (Pa)

(w/g) : Wind/gusts

e_{so} : Constan equal to c_0 = 6.1078

c_1, c_2 : Lift coefficient

ρ : Air density (kg/m3)

ρA : Area density

W_l : Wind load (Newton, N)

References

Adu-Gyamfi, B.A.; Good, C. (2022). Electric aviation: A review of concepts and enabling technologies. Transp. Eng, 9, 100134.

Airdensityonline. (2024). Baku City Circuit, Available at: https://airdensityonline.com/track-results/Baku_City_Circuit/, Accessed 02.01.2024

Akash, A., Raj, V. S. J., Sushmitha, R., Prateek, B., Aditya, S., & Sreehari, V. M. (2021). Design and analysis of VTOL operated intercity electrical vehicle for urban air mobility. Electronics, 11(1), 20.

Al Haddad, C., Chaniotakis, E., Straubinger, A., Plötner, K., & Antoniou, C. (2020). Factors affecting the adoption and use of urban air mobility. Transportation Research Part A: Policy and Practice, 132, 696–712. doi:10.1016/j.tra.2019.12.020.

Alharasees, O., Adali, O. H., & Kale, U. (2022). Comprehensive Review on Aviation Operator's Total Loads. 2022 New Trends in Aviation Development (NTAD), 15-20.

Alharasees, O., Jazzar, A., Kale, U., & Rohacs, D. (2023). Aviation communication: the effect of critical factors on the rate of misunderstandings. Aircraft engineering and aerospace technology, 95(3), 379-388.

Antcliff, K. R., Moore, M. D., & Goodrich, K. H. (2016). Silicon Valley as an early adopter for on-demand civil VTOL operations. In 16th AIAA Aviation Technology, Integration, and Operations Conference (p. 3466).

Arxcom. (2024). https://www.arxkom.gov.az/en/bakinin-bas-plani?plan=coxmerkezli-seher-ve-demoqrafiya (English version is available), Accessed 13.01.2024.

Bacchini, A., and Enrico Cestino, E. (2019). "Electric VTOL Configurations Comparison", Aerospace, https://doi:10.3390/aerospace6030026.

Balakrishnan, K., Polastre, J., Mooberry, J., Golding, R., Sachs, P. (2018). The roadmap for the safe integration of autonomous aircraft, Available at: https://www.airbusutm.com/uam-resources-airbus-blueprint, Accessed 03.01.2024

Baur, S., Schickram, S., Homulenko, A., Martinez, N., & Dyskin, A. (2018). Urban air mobility: The rise of a new mode of transportation. Roland Berger.

Bills, A., Sripad, S., Fredericks, L., Guttenberg, M., Charles, D., Frank, E., & Viswanathan, V. (2023). A battery dataset for electric vertical takeoff and landing aircraft. Scientific Data, 10.

Boeing. (2023). Concept of Operations for Uncrewed

Urban Air Mobility, Version 2.0.

Bridgelall, R., White, S., & Tolliver, D. (2023a). Integrating Electric Vertical Takeoff and Landing Aircraft into Public Airspace: A Scenario Study. Future Transportation, 3(3), 1029-1045.

Bridgelall, R., Askarzadeh, T., & Tolliver, D. D. (2023b). Introducing an efficiency index to evaluate eVTOL designs. Technological Forecasting and Social Change, 191, 122539.

Butterworth-Hayes, P., and Stevenson, B. (2019). The Uber Air vision of urban air mobility faces multiple, complex regulatory challenges, Available at: https://www.unmannedairspace.info/latest-news-and-information/the-uber-air-vision-of-urban-air-mobility-faces-multiple-complex-regulatory-challenges/, Accessed 24.01.2024

Cizreliogullari, M. N., Barut, P., Imanov, T. (2022). Future Air Transportatıon Ramification: Urban Air Mobility (UAM) Concept. Prizren Social Science Journal, Vol.6, Issue 2, May-August 2022. https://doi.org/10.32936/pssj.v6i2.335.

Cohen, A., and Shaheen, S., (2021). Urban air mobility: Opportunities and obstacles. In: Vickerman, R. (Ed.), International Encyclopedia of Transportation. Elsevier, Oxford, pp. 702–709, URL https://www.sciencedirect.com/science/article/pii/B978008102671710764X.

Choi, W., and Hampton, S. (2020). Scenario-based strategic planning for future civil vertical take-off and landing (VTOL) transport. J. Aviation/Aerospace Educ. Res. 29 (1), 1–31.

Chomsky, R. (2023). Exploring the Future of Urban Air Mobility (UAM): Key Concepts and Innovative Technologies, Available at: https://sustainablereview.com/exploring-the-future-of-urban-air-mobility-uam-key-concepts-and-innovative-technologies/, Accessed 26.05.2024

Collins, C. A., Roberson, G. T., & Hale, S. A. (2018). FAA 14 CFR Part 107 for Commercial UAS and UAS as Agriculture Field Equipment: A Review for Agriculture Safety Standards. In 2018 ASABE Annual International Meeting (p. 1). American Society of Agricultural and Biological Engineers.

Cunha, D., Wheeler, B., Silver, I., & Andre, G. (2023). Electric Aircraft Battery Performance: Examining Full Discharge Under Two Conditions. International Journal of Aviation Science and Technology, Volume 4, Issue 1

Dannenberger, N., Schmid-Loertzer, V., Liliann Fischer, Schwarzbach, V., Kellermann, R., Biehle. (2020). Traffic solution or technical hype? Representative population survey on delivery drones and air taxis in Germany

Darvishpoor, S., Roshanian, J., Raissi, A., Hassanalian, M. (2020) Configurations, flight mechanisms, and applications of unmanned aerial systems: A review, Progress in Aerospace Sciences. 121 (2020) 100694. https://doi.org/10.1016/j.paerosci.2020.100694.

Dezeen (2020). ShoP and Gensler reveal designs for UBER air Skyports. Available at: https://www.dezeen.com/2019/06/12/uber-air-skyports-shop-architects-gensler/, Accessed 14.01.2024

Di Vito, V., Dziugiel, B., Melo, S., ten Thije, J., Duca, G., Liberacki, A., ... & Witkowska-Koniecz, A. (2023). Operational Concepts for Urban Air Mobility deployment in the next decades. In Journal of Physics: Conference Series (Vol. 2526, No. 1, p. 012098). IOP Publishing.

Duranton, G., & Turner, M. A. (2011). The fundamental law of road congestion: Evidence from US cities. American Economic Review, 101(6), pp. 2616-2652.

EASA. (2019). CS-HPT-DSN Issue 1, Heliport Design, 23 May 2019.

EASA. (2022). Second Publication of Means of Compliance with the Special Condition VTOL Issue 2. Available at: https://www.easa.europa.eu/en/downloads/136697/en, Accessed 21.01.2024.

Ekici, S., Yalin, G., Altuntas, O. and Karakoc, T.H. (2013), "Calculation of HC, CO and NOx from civil aviation in Turkey in 2012", International Journal of Environment and Pollution, Vol. 53 Nos 3/4, pp. 232-244.

Ernest, N. S., Tripoli. U., González, J., Arbery. M. (2023). Advanced air mobility: winning business models for passenger flight, Available at: https://www.es.kearney.com/transportation-travel/article/-/insights/advanced-air-mobility-winning-business-models-for-passenger-flight, Accessed 15.01.2024.

FAA. (2008). Density altitude, FAA–P–8740–2, Available at: https://www.faasafety.gov/files/gslac/library/documents/2011/Aug/56396/FAA P-8740-02 Density Altitude[hi-res], Accessed 22.01.2024

FAA. (2021). Federal Aviation Administration. 14 CFR part 91.103. Available at: https://www.ecfr.gov, Accessed 15.01.2024.

FAA. (2023). Urban Air Mobility (UAM) Concept of Operations: Version 2.0, Available at: https://www.faa.gov/air-taxis/uam_blueprint,

Accessed 04.01.2024.

Fadhil, D.N. (2018). A GIS-Based Analysis for Selecting Ground Infrastructure Locations for Urban Air Mobility. Master' thesis. Technical University of Munich, Munich, Germany.

Fard, M. T., He, J., Huang, H., & Cao, Y. (2022). Aircraft distributed electric propulsion technologies-a review. IEEE Transactions on Transportation Electrification. Volume: 8, Issue: 4, DOI: 10.1109/TTE.2022.3197332

Fu, M., Rothfeld, R., Antoniou, C. (2019). Exploring preferences for transportation modes in an urban air mobility environment: Munich case study. Transp. Res. Rec. 2673(10), 427–442.

GAMA. (2023). Managing Range and Endurance of Battery-Electric Aircraft, Version 1.0, Available at: https://gama.aero/wp-content/uploads/Managing-Range-and-Endurance-of-Battery-Electric-Aircraft_v1-1.pdf, Accessed 26.05.2024

Gudmundsson, S. (2013). General aviation aircraft design, 1st ed: Applied Methods and Procedures. Butterworth-Heinemann. Oxford, UK, https://doi.org/10.1016/C2011-0-06824-2.

Hansman, J., and Vascik, P., (2016). Operational aspects of aircraft-based on-demand mobility aircraft-based on-demand mobility. 2nd on-demand mobility and emerging aviation technology road mapping workshop 156.

Hirschberg, M. (2019). Stand on the Shoulders of Giants. Vertiflite, Available at: http://evtol.news/2019/01/02/stand-on-the-shoulders-of-giants/, Accessed 13.11.2023

Holden, J., & Goel, N. (2016). Uber elevate: Fast-forwarding to a future of on-demand urban air transportation. Uber Technologies. Inc., San Francisco, CA. Available at: https://evtol.news/__media/PDFs/UberElevateWhitePaperOct2016.pdf, Accessed 11.01.2024

Hymel, K. (2019). If you build it, they will drive: Measuring induced demand for vehicle travel in urban areas. Transport policy, 76, 57-66.

Jazzar, A., Alharasees, O., & Kale, U. (2022). Assessment of aviation operators' efficacy in highly automated systems. Aircraft engineering and aerospace technology, 95(2), 302-311.

Johnson, L. (2020). How to Calculate Wind Loads from Wind Speeds, Available at: sciencing.com, https://sciencing.com/calculate-wind-load-large-flat-surface-12079539.html, Accessed 25.01.2024.

Johnson, W. (2012). Helicopter theory. Courier Corporation. Available at: https://books.google.com.cy/books, Accessed 07.01.2024.

ICAO. (2020). Annex 14 - Aerodromes - Volume II – Heliports, 5th Edition, July 2020.

ICAO. (2023). Airport Planning Manual, Update of PART 1 MASTER PLANNING Doc 9184, 3rd Edition, 2023, Section 2, Chapter 7. Available at: https://store.icao.int/en/airport-planning-manual-master-planning-doc-9184-part-1, Accessed 10.01.2024.

Imanov, T., (2023). Initial Appearances and Urban Air Mobility Transportation System Network in Northern Cyprus, In book: International Research and Reviews in Social, Human and Administrative Science (pp.37-64), Publisher: Serüven Publishing.

Kamargianni, M., & Matyas, M. (2017). The business ecosystem of mobility-as-a-service. In transportation research board (Vol. 96). Transportation Research Board.

Karakoc, T.H., Ozerdem, M.B., Sogut, M.Z., Colpan, C.O., Altuntas, O. and Açıkkalp, E. (Eds) (2016), Sustainable Aviation: Energy and Environmental Issues, Springer.

Kale, U., Alharasees, O., Rohacs, J., & Rohacs, D. (2022). Aviation operators (pilots, ATCOs) decision-making process. Aircraft Engineering and Aerospace Technology, 95(3), 442-451.

Kasliwal, A., Furbush, N. J., Gawron, J. H., McBride, J. R., Wallington, T. J., De Kleine, R. D., Kim, H. C., Keoleian, G. A. (2019). Role of flying cars in sustainable mobility. Nature communications, 10(1):1555.

Kluge, U., Paul, A., Ureta, H., Ploetner, K.O. (2018). Profiling future air transport passengers in Europe. In: European Commission (ed.) 7th Transport Research Arena TRA 2018, Vienna, Austria.

Kraenzler, M., Schmitt, M., & Stumpf, E. (2019). Conceptual design study on electrical vertical take-off and landing aircraft for urban air mobility applications. In AIAA Aviation 2019 Forum (p. 3124).

Krylova, M. (2020). UAM infrastructure, Available at: https://mariakrylova.com/portfolio/uam-infrastructure/, Accessed 14.01.2024

Mattingly, J. D., Heiser, W. H., Daley, D. H. (2002). Aircraft Engine Design, American Institute of Aeronautics and Astronautics: Available at: https://books.google.com.cy/books, Accessed 08.01.2024

Melton, J., Kontinos, D., Grabbe, S., Alonso, J., Sinsay, J.,

& Tracey, B. (2014). Combined electric aircraft and airspace management design for metro-regional public transportation. NASA/TM, 216626, 2014.

Moore, M. D. (2010) "Aviation Frontiers - On Demand Aircraft,"10th AIAA Aviation Technology, Integration, and Operations (ATIO) Conference, Fort Worth, Texas, 13–15 September 2010, AIAA-2010-9343.

Mulinazzi, T. E., & Zheng, Z. C. (2014). Wind Farm Turbulence Impacts on General Aviation Airports in Kansas, K-TRAN: KU-13-6. Topeka, KS: University of Kansas.

MVRDV. (2018). Airbus UAM. Available at: https://www.mvrdv.com/projects/421/airbus-uam, Accessed, 17.01.2024

NASA. (2018). Urban air mobility (UAM) market study. Washington, DC: Available at: https://escholarship.org/uc/item/0fz0x1s2, Accessed 19.01.2024

NASA. (2020). UAM Vision Concept of Operations (ConOps) UAM Maturity Level (UML) 4, Version 1.0, Available at: https://ntrs.nasa.gov/citations/20205011091, Accessed 04.01.2024.

National Institute of Aerospace (NIA). (2017). NASA Strategic Framework for On-Demand Air Mobility, Available at: http://www.nianet.org/ODM/roadmap.htm, Accessed 04.01.2024

Newman, S. J. (2007). Principles of Helicopter Aerodynamics–Second edition JG Leishman Cambridge University Press, The Edinburgh Building, Shaftesbury Road, Cambridge, CB2 2RU, UK. 2006. 826pp. ISBN 0-521-85860-7. The Aeronautical Journal, 111(1126), 825-826.

Ng, H. K. (2022). Collaborative Weather Research and Development for Urban Air Mobility. In FPAW 2022 Spring Meeting.

Nneji, V. C., Stimpson, A., Cummings, M. (Missy), & Goodrich, K. H. (2017). Exploring Concepts of Operations for On-Demand Passenger Air Transportation. 17th AIAA Aviation Technology, Integration, and Operations Conference. doi:10.2514/6.2017-3085.

Palaia, G., Abu Salem, K., Cipolla, V., Binante, V., & Zanetti, D. (2021a). A conceptual design methodology for e-VTOL aircraft for urban air mobility. Applied Sciences, 11(22), 10815.

Palaia, G., Zanetti, D., Salem, K. A., Cipolla, V., & Binante, V. (2021b). THEA-CODE: a design tool for the conceptual design of hybrid-electric aircraft with conventional or unconventional airframe configurations. Mechanics & Industry, 22, 19.

Patterson, M. D., German, B. J., and Moore, M. D. (2012) "Performance Analysis and Design of On-Demand Electric Aircraft Concepts," 12th AIAA Aviation Technology, Integration, and Operations (ATIO) Conference and 14th AIAA/ISSMO Multidisciplinary Analysis and Optimization Conference, Indianapolis, IN, Sept 17–19 2012, AIAA-2012-5474.

Patterson, M. D., Antcliff, K. R., & Kohlman, L. W. (2018). A proposed approach to studying urban air mobility missions including an initial exploration of mission requirements. In Annual Forum and Technology Display (No. NF1676L-28586).

Pons-Prats, J., Zivojinovic, T., Kuljanin, J. (2022). On the understanding of the current status of urban air Mobility development and its future prospects: Commuting in a flying vehicle as a new paradigm. Transportation Research Part E 166, 102868. doi.org/10.1016/j.tre.2022.102868.

Pradeep, P., Lauderdale, T. A., Chatterji, G. B., Sheth, K., Lai, C. F., Sridhar, B., ... & Erzberger, H. (2020). Wind-optimal trajectories for multirotor eVTOL aircraft on UAM missions. In AIAA Aviation 2020 Forum (p. 3271).

Presidential Library. (2019). Capital Population, Available at: https://bakucity.preslib.az/en/page/qPf6G5CZ1H, Accessed 13.01.2024.

Rath, S., & Chow, J. Y. (2019). Air taxi skyport location problem for airport access. arXiv preprint arXiv:1904.01497. https://doi.org/10.48550/arXiv.1904.01497.

Reiche, C., Cohen, A.P., Fernando, C. (2021). An Initial Assessment of the Potential Weather Barriers of Urban Air Mobility. IEEE Trans. Intell. Transp. Syst, 22, 6018–6027.

Reiche, C., Goyal, R., Cohen, A., Serrao, J.D., Kimmel, Sh., Fernando, Ch., Shaheen, S. (2018). Urban Air Mobility Market Study, https://escholarship.org/uc/item/0fz0x1s2. DOI:10.7922/G2ZS2TRG.

Rezende, R. N., Barros, J. E., (2018). General Aviation 2025 – A supercomputer with wings. Conference paper, https://www.researchgate.net/publication/326262874.

Schwartz, O. (2023). Magic Flying Carpets – Legend, Fact or Pure Fiction? Available at: https://nazmiyalantiquerugs.com/blog/magic-flying-carpet-rug-aladdin/, Accessed 03.01.2024

Schweiger, K., Schmitz, R., & Knabe, F. (2023). Impact of

Wind on eVTOL Operations and Implications for Vertiport Airside Traffic Flows: A Case Study of Hamburg and Munich. Drones, 7(7), 464.

Shamiyeh, M., Rothfeld, R., & Hornung, M. (2018). A performance benchmark of recent personal air vehicle concepts for urban air mobility. In Proceedings of the 31st Congress of the International Council of the Aeronautical Sciences, Belo Horizonte, Brazil (Vol. 14, p. 10).

Shelquist, R. (2024). Density Altitude Calculator-using dew point, Available at: https://wahiduddin.net/calc/calc_da.htm, Accessed 15.01.2024

Stocker, A., & Shaheen, S. (2017). Shared automated vehicles: Review of business models. International Transport Forum Discussion Paper. Available at: https://www.econstor.eu/handle/10419/194044, Accessed 04.01.2024.

Straubinger, A., Kluge, U., Fu, M., Al Haddad, C., Ploetner, K.O., Antoniou, C. (2020a). Identifying demand and acceptance drivers for user friendly urban air mobility introduction. In: Müller, B., Meyer, G. (eds.) Lecture Notes in Mobility, pp. 117–134. Springer, Berlin.

Straubinger, A., Rothfeld, R., Shamiyeh, M., Büchter, K. D., Kaiser, J., & Plötner, K. O. (2020b). An overview of current research and developments in urban air mobility–Setting the scene for UAM introduction. Journal of Air Transport Management, 87, 101852.

Straubinger, A., Michelmann, J., & Biehle, T. (2021). Business model options for passenger urban air mobility. CEAS Aeronautical Journal, 12(2), 361-380.

Syed, N., Rye, M., Ade, M., Trani, A., Hinze, N., Swingle, H., Smith, J. C., Marien, T., and Dollyhigh, S. (2017). "ODM Commuter Aircraft Demand Estimation," 17th AIAA Aviation Technology, Integration, and Operations Conference, AIAA AVIATION Forum, 2017, AIAA 2017-3082.

Thiemer, D. (2020). eVTOL vertiports design and operations, Available at: https://www.airsight.de/projects/item/evtol-vertiports-design-and-operations/, Accessed 14.11.2024.

Thipphavong, D. P. (2022). Analysis of Electrical Grid Capacity by Interconnection for Urban Air Mobility. In AIAA Aviation 2022 Forum (p. 3316).

Uber. (2016) "Fast-Forwarding to a Future of On-Demand Urban Air Transportation," White Paper, Available at: https://evtol.news/__media/PDFs/UberElevateWhitePaperOct2016.pdf, Accessed 04.01.2024.

Ugwueze, O., Statheros, T., Horri, N., Bromfield, M. A., & Simo, J. (2023). An Efficient and Robust Sizing Method for eVTOL Aircraft Configurations in Conceptual Design. Aerospace, 10(3), 311.

Urbanairmobilitynews. (2023). The global timetable for AAM and UAM launch and development, Available at: https://www.urbanairmobilitynews.com/sponsored-editorial-right-column/the-global-timetable-for-aam-and-uam-launch-and development, Accessed 26.05.2024

Vascik, P. D., & Hansman, R. J. (2019). Development of vertiport capacity envelopes and analysis of their sensitivity to topological and operational factors. In AIAA Scitech 2019 Forum (p. 0526).

Vertical Flight Society. (2023). eVTOL Aircraft Directory, Available at: https://evtol.news/aircraft, Accessed 30.12.2023

Volocopter. (2019). Mobility of the Future: Fraport and Volocopter Are Developing Airport Infrastructure and Passenger Processes for Air Taxi Services, Available at: https://www.volocopter.com/en/newsroom/mobility-of, Accessed 11.01.2024

WPR. (2024). Baku Population 2024, Available at: https://worldpopulationreview.com/world-cities/baku-population, Accessed 13.01.2024.

WWAPI. (2024). Metropolitan Area (bak) Annual Weather Averages Baku, Available at: https://www.worldweatheronline.com/v2/weather-averages.aspx?q=bak, Accessed 21.01.2024

Wu, Z., & Zhang, Y. (2021). Integrated network design and demand forecast for on-demand urban air mobility. Engineering, 7(4), 473-487.

Wu, Z., Cao, Y., & Ismail, M. (2019). Gust loads on aircraft. The Aeronautical Journal, 123(1266), 1216-1274.

Xu, E. (2020). The future of transportation: White paper on urban air mobility systems. EHang: Guangzhou, China.

Yang, X. G., Liu, T., Ge, S., Rountree, E., Wang, C. Y (2021). Challenges and key requirements of batteries for electric vertical takeoff and landing aircraft. Joule, 5(7):1644-59.

Yu, X., Sandhu, N.S., Yang, Z., Zheng, M. (2020) Suitability of energy sources for automotive application—A review. Appl. Energy, 271, 115169.

Zhao, S., Guo, Z., Yan, K., Wan, S., He, F., Sun, B., Wang, G. (2021). Towards high-energy-density lithium-ion batteries: Strategies for developing high-capacity lithium-rich cathode materials. Energy Storage Mater, 34, 716–734.

Yazar, I., Kiyak, E., Caliskan, F. and Karakoc, T.H. (2018), "Simulation-based dynamic model and speed controller design of a small-scale turbojet engine", Aircraft Engineering and Aerospace Technology, Vol. 90 No. 2.

Appendix 1. Weather for Baku City Circuit (airdensityonline, 2024)

Time	Temp	Hum	Uncorrected Barometer	Dew Point	Grains	Wind	Air Density	Density Altitude
Aug 30 12:00 am	79 deg F	72%	29.90 Hg	69 deg F	107.4	NE 6 mph	94.07 %	2077 ft.
Aug 30 1:00 am	78 deg F	75%	29.89 Hg	70 deg F	108.3	NW 6 mph	94.22 %	2024 ft.
Aug 30 2:00 am	77 deg F	77%	29.90 Hg	69 deg F	107.5	NW 7 mph	94.42 %	1952 ft.
Aug 30 3:00 am	76 deg F	78%	29.90 Hg	69 deg F	105.3	NW 8 mph	94.64 %	1873 ft.
Aug 30 4:00 am	77 deg F	79%	29.88 Hg	70 deg F	110.4	NW 7 mph	94.31 %	1991 ft.
Aug 30 5:00 am	77 deg F	80%	29.88 Hg	70 deg F	111.9	N 7 mph	94.28 %	2002 ft.
Aug 30 6:00 am	77 deg F	78%	29.89 Hg	70 deg F	108.9	N 7 mph	94.38 %	1967 ft.
Aug 30 7:00 am	78 deg F	77%	29.90 Hg	70 deg F	111.2	N 7 mph	94.19 %	2036 ft.
Aug 30 8:00 am	80 deg F	73%	29.91 Hg	71 deg F	112.6	NE 6 mph	93.85 %	2159 ft.
Aug 30 9:00 am	83 deg F	67%	29.92 Hg	71 deg F	113.9	NE 5 mph	93.33 %	2346 ft.
Aug 30 10:00 am	85 deg F	61%	29.93 Hg	70 deg F	110.5	NE 7 mph	93.09 %	2430 ft.
Aug 30 11:00 am	87 deg F	56%	29.93 Hg	69 deg F	108.0	NE 7 mph	92.79 %	2539 ft.
Aug 30 12:00 pm	89 deg F	51%	29.92 Hg	69 deg F	104.8	SE 8 mph	92.49 %	2647 ft.
Aug 30 1:00 pm	90 deg F	46%	29.91 Hg	67 deg F	97.4	SE 9 mph	92.44 %	2666 ft.
Aug 30 2:00 pm	91 deg F	43%	29.90 Hg	65 deg F	93.9	SE 10 mph	92.33 %	2707 ft.
Aug 30 3:00 pm	91 deg F	41%	29.89 Hg	64 deg F	89.5	SE 10 mph	92.38 %	2687 ft.
Aug 30 4:00 pm	90 deg F	42%	29.89 Hg	64 deg F	88.8	SE 10 mph	92.55 %	2627 ft.
Aug 30 5:00 pm	88 deg F	48%	29.89 Hg	66 deg F	95.4	SE 9 mph	92.77 %	2548 ft.
Aug 30 6:00 pm	87 deg F	52%	29.89 Hg	67 deg F	100.3	SE 9 mph	92.83 %	2527 ft.
Aug 30 7:00 pm	85 deg F	57%	29.88 Hg	68 deg F	103.2	SE 8 mph	93.09 %	2432 ft.
Aug 30 8:00 pm	84 deg F	61%	29.90 Hg	69 deg F	107.0	SE 7 mph	93.23 %	2379 ft.
Aug 30 9:00 pm	82 deg F	65%	29.92 Hg	69 deg F	106.8	SE 6 mph	93.64 %	2233 ft.
Aug 30 10:00 pm	81 deg F	67%	29.92 Hg	69 deg F	106.6	SE 6 mph	93.83 %	2166 ft.
Aug 30 11:00 pm	80 deg F	70%	29.92 Hg	69 deg F	107.8	E 6 mph	93.98 %	2109 ft.

Time	Temp	Hum	Uncor Bar	Dew Point	Grains	Wind Speed	Wind Dir	Air Density	Density Altitude
Jan 01 12:00 am	44 deg F	72%	30.10 Hg	36 deg F	30.3	17 mph	NW(332)	103.083 %	-1043 ft.
Jan 01 1:00 am	44 deg F	69%	30.11 Hg	35 deg F	29.0	22 mph	NW(336)	103.151 %	-1066 ft.
Jan 01 2:00 am	45 deg F	68%	30.12 Hg	35 deg F	29.7	25 mph	NW(339)	102.962 %	-1003 ft.
Jan 01 3:00 am	46 deg F	68%	30.13 Hg	36 deg F	30.9	25 mph	NW(339)	102.773 %	-939 ft.
Jan 01 4:00 am	46 deg F	68%	30.14 Hg	36 deg F	30.9	23 mph	NW(339)	102.796 %	-947 ft.
Jan 01 5:00 am	47 deg F	68%	30.15 Hg	37 deg F	32.0	23 mph	NW(342)	102.607 %	-884 ft.
Jan 01 6:00 am	47 deg F	69%	30.17 Hg	37 deg F	32.5	24 mph	NW(347)	102.648 %	-897 ft.
Jan 01 7:00 am	48 deg F	70%	30.19 Hg	39 deg F	34.2	25 mph	NW(353)	102.496 %	-846 ft.
Jan 01 8:00 am	48 deg F	70%	30.22 Hg	39 deg F	34.2	24 mph	N(356)	102.582 %	-875 ft.
Jan 01 9:00 am	49 deg F	70%	30.25 Hg	40 deg F	35.5	23 mph	N(356)	102.440 %	-828 ft.
Jan 01 10:00 am	51 deg F	68%	30.27 Hg	41 deg F	37.1	18 mph	NW(353)	102.076 %	-705 ft.
Jan 01 11:00 am	53 deg F	64%	30.29 Hg	41 deg F	37.6	16 mph	NW(353)	101.740 %	-592 ft.
Jan 01 12:00 pm	55 deg F	60%	30.29 Hg	41 deg F	37.9	17 mph	NW(354)	101.332 %	-454 ft.
Jan 01 1:00 pm	56 deg F	57%	30.29 Hg	41 deg F	37.3	18 mph	N(0)	101.141 %	-389 ft.
Jan 01 2:00 pm	56 deg F	56%	30.28 Hg	40 deg F	36.7	16 mph	NE(6)	101.140 %	-389 ft.
Jan 01 3:00 pm	56 deg F	56%	30.29 Hg	40 deg F	36.7	14 mph	NE(14)	101.169 %	-398 ft.
Jan 01 4:00 pm	54 deg F	61%	30.30 Hg	41 deg F	37.1	11 mph	NE(24)	101.576 %	-536 ft.
Jan 01 5:00 pm	52 deg F	68%	30.31 Hg	42 deg F	38.5	9 mph	NE(33)	101.979 %	-672 ft.
Jan 01 6:00 pm	49 deg F	76%	30.32 Hg	42 deg F	38.4	7 mph	NE(30)	102.620 %	-888 ft.
Jan 01 7:00 pm	47 deg F	82%	30.33 Hg	42 deg F	38.5	6 mph	NE(18)	103.072 %	-1040 ft.
Jan 01 8:00 pm	46 deg F	86%	30.34 Hg	42 deg F	38.8	5 mph	N(5)	103.307 %	-1118 ft.
Jan 01 9:00 pm	45 deg F	88%	30.35 Hg	42 deg F	38.2	4 mph	NW(347)	103.541 %	-1196 ft.
Jan 01 10:00 pm	45 deg F	87%	30.35 Hg	41 deg F	37.8	4 mph	NW(314)	103.562 %	-1203 ft.
Jan 01 11:00 pm	45 deg F	87%	30.35 Hg	41 deg F	37.8	3 mph	SW(218)	103.544 %	-1197 ft.